Doctoral Dissertation (Shinshu University)

Synthesis and properties of shape memory water-borne epoxy and its nanocomposites

September 2015

DONG YUBING

ABSTRACT

Shape memory polymers (SMPs), which have attracted considerable attention in recent years and will come to play a significant role in all areas of human life because of their scientific and technological significance, are a new class of stimuli-responsive materials that can maintain a temporary shape and subsequently recover their original shape by external stimuli, such as heat, water, pH, light, electric field, and magnetic field. As smart materials, SMPs can be potential applied in aerospace structures, biomedical devices, sensors, textiles, dry adhesives, self-healing applications, and so on. Many recent studies have proven the favorable shape memory (SM) properties of epoxies. Shape memory epoxies (SMEPs) merit a special reference among the diverse SMPs such as polyurethane, cross-linked polyethylene, styrene rubbers and acrylate systems as they are unique thermosetting SMP systems with excellent thermal, thermo-physical and mechanical properties along with ease of processability into engineering components. Unfortunately, the processes involved in developing epoxy are very environmentally unfriendly, complex, and expensive. A vast majority of these products are still formulated with organic solvents. However, as environmental regulation become stricter, the requirement for the industries to switch to more ecological and safer systems is constantly growing. This thesis focuses on the development and investigation of SMEP and SMEP nanocomposites which prepared via latex technology.

The most significant results achieved in this dissertation are given as follows:

(1) We reported a facile and environmental-friendly method to prepare SM epoxy materials. In the first strategy, we synthesized epoxy-graft-polyoxyethylene octyl phenyl ether (EP-g-TX100), which is a novel reactive copolymer emulsifier for preparing of water-borne epoxy (WEP). The chemical structure and emulsifying ability of EP-g-TX100 were systematically characterized by Fourier transform infrared spectroscopy (FTIR), nuclear magnetic resonance spectroscopy (NMR), field emission scanning electron microscopy (FE-SEM), transmission electron microscopy (TEM). In

the second strategy, we synthesized WEP via phase-inversion technology. After that, the freeze-drying and hot-press molding technology was applied to preparing the samples. The results show that the as-synthesized emulsifier EP-g-TX100 exhibits the expected structure, can covalently react with the curing agent through the side chains, and has excellent emulsifying ability for epoxy in water. WEP particle has an average diameter of 137 nm, with particles ranging from 50 nm to 300 nm. Furthermore, the final epoxy products show excellent SM property.

(2) Carbon nanotube (CNT)/WEP SM nanocomposites were successfully synthesized via freeze-drying and hot-press molding. CNTs were mixed directly with a WEP. CNT/WEP nanocomposites were obtained from these mixtures by freeze-drying and compressing under a pressure of 10 MPa at 120 °C for 2 h. The morphology and mechanical properties of the nanocomposites were investigated by TEM, SEM, dynamic mechanical analysis (DMA) and tensile testing. The SM properties of the nanocomposites were evaluated by fold-deploy SM testing. The effects of filler content and recovery temperature on the SM properties were revealed through systematic variation. Results confirmed that CNTs were homogenously dispersed and incorporated into the WEP matrices. Thus, significant improvements in the mechanical and SM properties of the nanocomposites were achieved. Moreover, CNT/WEP SM foams were prepared. CNTs were first dispersed in WEP by intensive stirring and then mixed with curing agent and blowing agent at room temperature. CNT/WEP SM foams were obtained from these mixtures via freeze-drying and foaming under a vacuum at 100 °C. The SM properties of the foams were evaluated together with other physical properties. Compression and thermo-mechanical cycle tests were performed to measure the effects of the CNTs on the mechanical performance of the foams. The foams had a high shape recovery and fixity ratio of more than 90% even after several thermo-mechanical cycles with the addition of 1.0 wt% CNTs. The CNTs significantly enhanced the strength of the WEP SM foams.

(3) In-situ grown silica/WEP SM nanocomposites were successfully synthsized by hydrolysis of tetraethoxysilane (TEOS) within the WEP and prepared via freeze-drying and hot-press molding method. The silane coupling agent 3-triethoxysilylpropylamine

(KH550) was introduced to improve the interfacial properties between the in-situ generated silica particle and epoxy matrix. The morphology structure and the effect of the content of the in-situ formed silica on the mechanical and SM properties of the silica/WEP composites were studied. The experimental results indicated that the silica particles were homogenously dispersed and well incorporated into the epoxy matrix. Significant improvements were achieved in the mechanical property of the organic-inorganic hybrid materials. The silica/WEP composites exhibited high shape recovery and fixity ratio approximately 100% even after 10 thermo-mechanical cycles. Moreover, silica/WEP SM foams were synthesized and prepared without extra blowing agent. Silica was synthesized by hydrolysis of TEOS. Silica/WEP foams were obtained from the TEOS solution and WEP mixtures after freeze-drying and foaming in the presence of residual moisture as the blowing agent under a vacuum at 110 °C. The morphologies of the resulting foams were evaluated by SEM and TEM. Compression and thermo-mechanical cycle tests were performed to measure the mechanical and SM properties of the foams. The experimental results indicated that the micrograph and mechanical properties of the foams were closely related to the freeze-drying time. The final foams have excellent SM properties even after several thermo-mechanical cycles. The properties obtained in the epoxy foams may offer new opportunities for their use in future structural applications.

WEPs, as novel versatile environmentally-friendly materials, are being attached great importance in engineering field and mainly used in coatings, metal primers, epoxy cement concrete, glass fiber sizing, and wood adhesives, etc., and additional function of SM will be a good aspect for extending their further applications. Furthermore, our strategy for obtaining SM epoxy materials will pave the way for designing and developing the functional SM effect polymers. The proposed method is applicable to various host polymers and does not require organic solvents.

ACHIEVEMENT

LIST OF PUBLICATIONS

Journal Publications

1. **Yubing Dong,** Qing-Qing Ni, Lili Li, Yaqin Fu. Novel vapor-grown carbon nanofiber/epoxy shape memory nanocomposites prepared via latex technology. *Materials Letters*, 2014, 132: 206-209.
2. **Yubing Dong**, Qing-Qing Ni, Yaqin Fu. Preparation and characterization of water-borne epoxy shape memory composites containing silica. *Composites Part A*, 2015, 72: 1-10.
3. **Yubing Dong,** Qing-Qing Ni. Effect of vapor-grown carbon nanofibers and in-situ hydrolyzed SiO_2 on the mechanical and shape memory properties of water-borne epoxy composites. *Polymer Composites*, 2015, 36(9): 1712-1720.
4. **Yubing Dong,** Qing-Qing Ni, In-situ grown silica/waterborne shape memory epoxy composite foams prepared without extra blowing agent. *Journal of Applied Polymer Science*, 2015,132(39): 1-11.
5. **Yubing Dong,** Juan Ding, Jing Wang, Xiang Fu, Huimin Hu, Shan Li, Hongbing Yang, Congsheng Xu, Mingliang Du, Yaqin Fu. *Composites Science and Technology*, 2013, 76: 8-13.
6. **Yubing Dong**, Rui Wang, Shan Li, Hongbing Yang, Mingliang Du, Yaqin Fu. *Journal of Colloid and Interface Science*, 2013, 391: 8-15.

Conference

1. **Yubing Dong,** Qing-Qing Ni. CNT/epoxy shape memory nanocomposites prepared via latex technology, 14th International Symposium on Fiber Science and Technology (ISF), p46 (2014, 10).
2. **Yubing Dong,** Qing-Qing Ni. Synthesis and properties of shape memory water-borne epoxy composites, 日本複合材料合同会議 JCCM-3, p8 (2015, 3).

ACKNOWLEDGMENTS

It is my pleasure to thank the many people who made the completion of this thesis possible. I could not have reached the end of the long journey without their support and encouragement.

First of all, I would like to thank my supervisor, Prof. Qing-Qing Ni for his continued guidance and encouragement throughout my time in Shinshu University.

I would also like to appreciate my committee members, Prof. Yasushi Murakami, Prof. Yasuo Gotoh, Prof. Toshiaki Natsuki, and Prof. Jianhui Qiu, for their valuable comments and suggestions on my research.

I would like to thank all past and present members of the Qing-Qing Ni group especially Mr. Ran Li, and Yi Wang. I would like to thank all my friends I’ve studied with between 2013 and 2015 at Shinshu University.

My special thanks go to Prof. Yaqin Fu and Yaofeng Zhu at Zhejiang Sci-Tech University not only for their professional guidance but also for their personal advice and assistance which have significantly boosted my research.

Finally, I would like to thank my parents, as well as my sister, and my wife. I’d also like to thank my parents both for all the encouragement and advice a son could want. This thesis would not have been possible without their assistance love, dedication, and encouragement.

September, 2015

Ueda, Japan

CONTENTS

1General introduction 1

1.1 Introduction 1

1.2 Structure and mechanism of SMPs 1

1.3 Synthesis of SMPs 4

1.3.1 Polyurethane SMPs 5

1.3.2 Styrene SMPs 5

1.3.3 Epoxy SMPs 6

1.3.4 Some novel SMPs 7

1.4 SMPs Characterization 8

1.5 SMP composites (SMPCs) 9

1.5.1 Carbon fiber reinforced SMPCs 9

1.5.2 Iron- or nickel reinforced SMPCs 10

1.5.3 Silica reinforced SMPCs 11

1.5.4 Clay reinforced SMPCs 12

1.6 Application of SMPs and SMPCs 13

1.6.1 Deployable structures 13

1.6.2 Morphing structures 14

1.6.3 Biomedical applications 15

1.6.4 Other applications 17

1.7 Outline of this dissertation 18

References 19

2 Preparation of shape memory epoxy materials via latex technology 25

2.1 Introduction 25

2.2 Experimental 26

2.2.1 Materials 26

2.2.2 Synthesis of EP-g-TX100 27

2.2.3 Preparation of water-borne epoxy (WEP) 27

2.2.4 Preparation of WEP films 28

2.2.5 Characterization 29
2.3 Results and discussion 31
2.3.1 Synthesis and characterization of EP-g-TX100 31
2.3.2 Morphology and structure of WEP 33
2.3.3 SM property of WEP 35
2.4 Conclusions 41
Reference 42

3 Preparation and properties of CNT/WEP shape memory nanocomposites 43

3.1 CNT/WEP shape memory nanocomposites 43
3.1.1 Introduction 43
3.1.2 Experimental 45
3.1.2.1 Materials 45
3.1.2.2 Preparation of CNT/EP-g-TX100 dispersions 45
3.1.2.3 Preparation of CNT/WEP SM nanocomposites 46
3.1.2.4 Characterization 46
3.1.3 Results and discussion 47
3.1.3.1 EP-g-TX100 as a dispersant for CNTs in aqueous 47
3.1.3.2 Morphology and mechanical properties of CNT/WEP nanocomposites 53
3.1.3.3 Dynamic mechanical properties 55
3.1.3.4 SM properties of CNT/WEP SM nanocomposites 57
3.1.4 Conclusions 60
3.2 SM CNT/WEP composite foams 61
3.2.1 Introduction 61
3.2.2 Experimental 62
3.2.2.1 Materials 62
3.2.2.2 Synthesis of SM CNT/WEP composite foams 63
3.2.2.3 Characterization 63
3.2.3 Results and discussion 64
3.2.3.1 Epoxy foam Micrograph 64
3.2.3.2 Compression results 65
3.2.3.3 Thermo-mechanical cycle test 66

3.2.3.4 Electrical conductivity of the CNT/WEP foams 69
3.2.4 Conclusions 70
Reference 71

4 Preparation and properties of silica/WEP shape memory nanocomposites 74

4.1 Silica/WEP shape memory nanocomposites 74
4.1.1 Introduction 74
4.1.2 Experimental 76
4.1.2.1 Materials 76
4.1.2.2 Synthesis of the silica/WEP composites 76
4.1.2.3 Characterization 77
4.1.3 Results and discussion 78
4.1.3.1 Morphology and structure 78
4.1.3.2 Dynamic mechanical properties 82
4.1.3.3 Mechanical properties 84
4.1.3.4 Shaper memory properties 85
4.1.4 Conclusions 91
4.2 SM silica/WEP composite foams 92
4.2.1 Introduction 92
4.2.2 Experimental 93
4.2.2.1 Materials 93
4.2.2.2 Synthesis of SM silica/WEP composite foams 94
4.2.2.3 Characterization 95
4.2.3 Results and discussion 96
4.2.3.1 Micrograph of the silica/WEP foams 96
4.2.3.2 DMA tests 98
4.2.3.3 Compression characterization 100
4.2.3.4 SM behaviors of the silica/WEP composite foams 101
4.2.4 Conclusions 107
Reference 108

5 Conclusions 111

CHAPTER ONE

General Introduction

1 General introduction

1.1 Introduction

Shape memory polymers (SMPs) represent a technologically important class of stimuli-responsive materials for which the response lies in the shape change. More specifically, the definition of an SMP is a polymer can be deformed and subsequently fixed into a temporary shape, which would remain stable unless it is exposed to an appropriate external stimulus (e.g., temperature [1], electric field [2], light [3], magnetic field [4], pH [5], ultrasound [6], water [7], specific antigen–antibody interactions [8], enzymes [9], and glucose [10]) that triggers the polymer to recover to its original (or permanent) shape. Accordingly, the associated behavior of SMP is called polymer shape memory effect (SME) [11]. The term “shape memory” was first proposed by Vernon H in 1941 [12]. However, the importance of SMPs was not recognized until the 1960s, when cross-link polyethylene was used for making heat-shrinkable tubes and films. During the past decades, with the rapid development and wide investigation of SMPs, their features are more and more prominent. SMPs have stimulated research interest from both academia and industries [13-15].

1.2 Structure and mechanism of SMPs

Shape memory behavior can be exploited and demonstrated in various polymer systems that are significantly different in molecular structure and morphology. The SMP systems include ultra-high molecular weight polyethylene [16] and cross-linked polyethylene/polypropylene [17], natural rubber [18], polyurethane [19], polymethyl methacrylate [20], Polydioxanone-co-polyethylene glycol [21], epoxies [22], polymannitol sebacate/cellulose [23], low cross-link density polyimides [24],

polyaspartimide urea [25], polybutadiene/acrylonitrile [26], poly(ether ether ketone) [27], poly (3-hydroxyalkanoate)s [28], copolymers composed of dodecanedioic acid or sebacic acid monomers [29], and bile acid-based polyesters [30]. Have been developed to exhibit SME, but their shape memory or mechanical properties are not highly desirable and require further optimization.

Several types of structures and programming models have been proposed to illustrate the mechanism of SMEs. Meng et al. reported that a stable polymer network and a reversible switching transition of the polymer are the two prerequites for the SME (see Fig. 1.1) [31]. The stable network of SMPs determines the original shape, which can be formed by molecule entanglement, crystalline phase, chemical cross-linking, or interpenetrated network [32, 33]. The lock in the network represents the reversible switching transition responsible for fixing the temporary shape, which can be crystallization/melting transition [34, 35], vitrification/glass transition [36, 37], liquid crystal anisotropic or isotropic transition [38, 39], reversible molecule cross-linking, and supramolecular association and disassociation. Typical reversible molecule cross-linking reactions, include photo dimerization [40, 41], Dielse-Alder reaction [42, 43], and oxidation/redox reaction of mercapto group [44]. Typical switching transition per supramolecular association/disassociation includes hydrogen bonding [45, 46], self-assembly metaleligand coordination [47, 48], and self-assembly of β–CD [49, 50]. In addition to the above reversible switches, other stimuli which can significantly change the mobility of the SMP may also trigger the SME, such as water, solvent, ions, pressure, light, pH [1-10].

All of the above-mentioned SMP models substantially contribute to determining the theoretical configuration of thermally sensitive SMPs, whereas the diversification of the molecular structure design provides the opportunity to develop SMPs with stimulus sensitivities other than thermal induction. As shown in Fig. 1.2, two types of structures and programming models were proposed for athermal sensitive SMPs. One model is designed to create a SEM of light-sensitive SMPs, in which the chromophores are covalently grafted onto a cross-linked polymer network. The light-sensitive can be achieved through efficient, photo-reversible cycloaddtion reactions between

chromophore molecules [13]. Another athermal water-sensitive SMP system was made from a nanocomposite containing nanocellulose whiskers dispersed in an elastomer matrix. The reversible formation and disruption of a percolation network of nanocellulose whiskers in an elastomer matrix features an unprecedentedly fast switching SME that is sensitive to water [51].

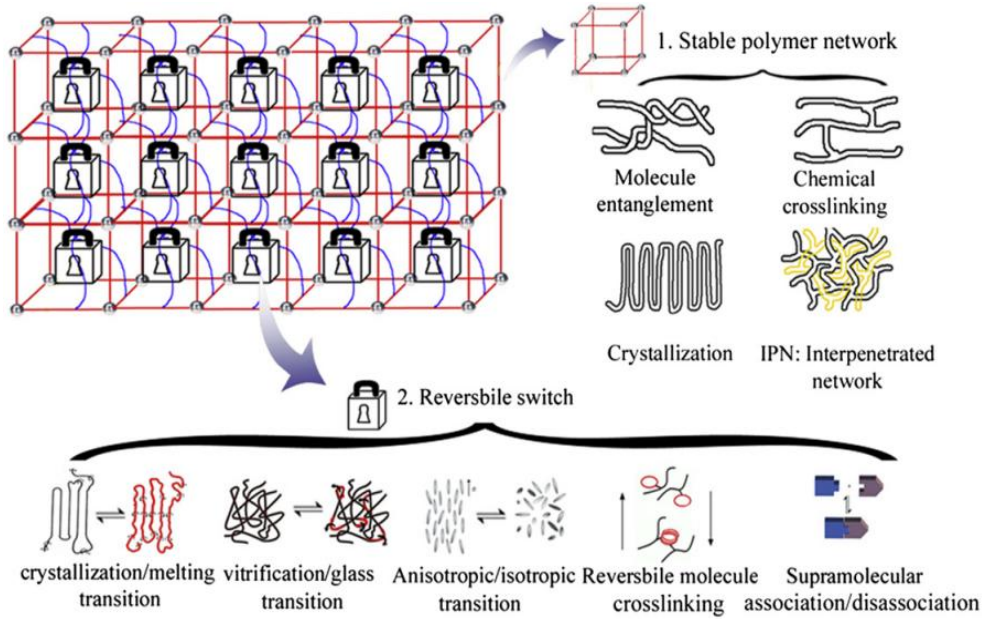

Figure 1.1 Various molecular structures of SMPs [31].

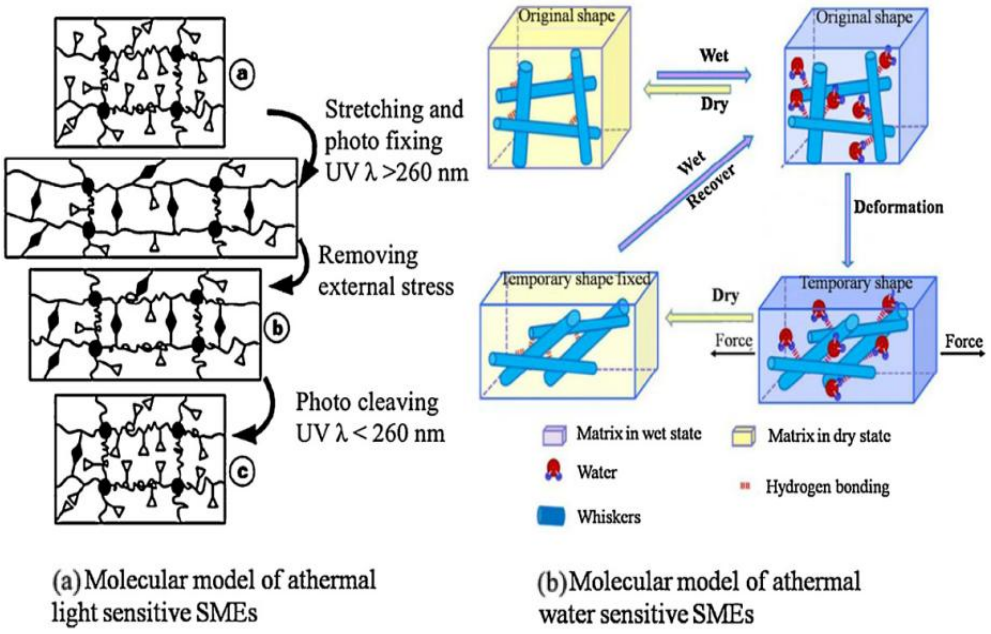

Figure 1.2 Molecular models of light and water-sensitive SMEs [13, 51].

1.3 Synthesis of SMPs

More than twenty types of SMPs have been synthesized and widely researched in the recent years. The physically cross-linked SMPs include linear polymers [52], branched polymers [53] or a polymer complex [54]. The SME of linear polymer is due to the phase separation and the domain orientation. The typical physically cross-linked SMP is linear block copolymers, such as polyurethanes. In polyesterurethanes, oligourethane segments are the hard elastic segments, while polyester serves as the switching segment [55]. The phase separation and the domain orientation of poly(e-caprolactone) based polyesterurethanes can be determined by Raman spectroscopy [56]. A similar effect is found for copolyester based ionomers obtained by the bulk polymerization of adipic acid and mixed monomers (bis(poly(oxyethylene)) sulfonated dimethyl fumarate and 1,4-butanediol) [57]. The polycarbonate segment is synthesised by the copolymerization of ethylene oxide in the presence of CO_2 catalyzed by a polymer supported bimetallic catalyst, which yields an aliphatic polycarbonate diol. This macrodiol is further processed by the prepolymer method into polyurethane SMP [58]. Covalent net-points can be obtained by cross-linking of linear or branched polymers as well as polymerization and polycondensation of one or several monomers, whereby at least one has to be at least tri-functional [59]. Depending on the synthesis strategy, cross-links can be created during synthesis or by post-processing. The shape recovery is triggered and controlled by the transvinylene content [60]. The other synthesis routes to obtain polymer networks involve the copolymerization of monofunctional monomers with low-molecular weight or oligomeric difunctional cross-linkers. The copolymerization of monofunctional monomers of low molecular weight with oligomeric difunctional cross-linkers enables the creation of AB copolymer networks with increased toughness and elasticity at room temperature [61]. To date, many kinds of SMPs have been developed through chemical cross-linking, such as cross-linked polystyrene, epoxy, poly(vinyl chloride), polyethylene [17]. The synthesis of other types of SMPs, such as polyolefines [62, 63], poly(vinyl butyral) [64], polysiloxanes [65], poly((meth)acrylates) [66], natural rubber/polycaprolactone [67],

polyethylenes [68], poly(ethylene oxide-ethylene terephtalate) copolymers [69], polycyclooctene [70], Castor oil-PEG-polyurethane [71], semicrystalline elastomers [72], and Poly-3-hydroxyalkanoates-co-polyethylene glycol methacrylate copolymers [73].

1.3.1 Polyurethane SMPs

Since the development of the shape memory segmented polyurethane (SMPU) copolymer by Hayashi of Mitsubishi Heavy Industry, extensive studies on this material have been carried out [74]. SMPU consists of a two-phase structure: a hard segment and soft segment. The hard segments are formed either from a long chain macro diol with a higher thermal transition temperature, or from diisocyanates and chain extenders. Typically, the linear polyurethane can be usually synthesised using the following process: through the reaction of difunctional, hydroxy-terminated oligoesters and ethers with an excess of a low molecular weight diisocyanate, the isocyanate-terminated prepolymers can be obtained [75]. The basic structure of the diisocyanate can be either aromatic or aliphatic; each type of diisocyanate has a different ability to form a semi-crystalline hard segment. Then low molecular weight diols or diamines are incorporated as chain extenders to further couple these pre-polymers. In this way, the linear, phase-segregated polyurethane or polyurethane–urea block copolymers are formed.

1.3.2 Styrene SMPs

Styrene-based SMP must have two-phases or exhibit a cross-linked structure to exhibit SME. The variety of methods to polymerize styrene and the wide availability of possible comonomers enable these necessary features. Styrene can be polymerized by anionic, cationic, or free controlled radical polymerization methods. In this way, a huge variety of network architectures may be designed by the proper choice of mechanism, initiator and comonomers. Through cationic polymerization, random copolymer networks formed from renewable natural oils with a high degree of unsaturation, like

soy bean oils, copolymerized with styrene and divinylbenzene are obtained [76]. Styrene-based SMPs have been prepared through the cationic copolymerization of the following candidate materials: regular soybean oil, low saturation soybean oil and conjugated soybean oil with various alkene comonomers including styrene and divinylbenzene, norbornadiene, or dicyclopentadiene (comonomers used as cross-linking agents) initiated by boron trifluoride diethyl etherate or related modified initiators [77]. By controlling the cross-link densities and the rigidity of the polymer backbones, the SMP shows a tunable T_g, mechanical properties, and a good SME. In addition, the materials show good reprogramming properties upon numerous shape recovery cycles and excellent shape fixity and recovery ratios. The advantage of the soybean oil polymers lies in the high degree of chemical control over the shape memory characteristics. It makes these SM materials particularly promising in applications. Leng et al. have synthesized SMP based on styrene copolymer networks with different degrees of cross-linking [59]. The SMP, with T_g in the range from 35 to 55 °C, experienced good shape recovery performance. Moreover, the T_g can be adjusted through the alternation of the gel content of the copolymer; the T_g increased with increasing gel content. The largest reversible strain of the SMP reached as high as 100% and the reversible strain of the copolymer decreased with increasing gel content.

1.3.3 Epoxy SMPs

SM behaviors can be observed in several polymers, including polyurethane-based polymers [78], styrene-based polymers, epoxies [79] and others. SM epoxy resins (SMEPs) merit a special reference among the diverse SMPs such as polyurethane, polynorbonene, cross-linked polyethylene, styrene rubbers and acrylate systems as they are unique thermosetting SMP systems with excellent thermal, thermophysical and mechanical properties along with ease of processability into engineering components. As epoxy polymers find extensive use as adhesives, coating, structural material, etc., additional function of shape memory will be a good aspect for extending their further applications. A series of SMEP were prepared by using the same epoxy, diglycidyl ether

bisphenol A by varying the content of curing agents 4, 4-methylenedianiline and m-phenylenediamine [80]. Oxazolidone chemistry was exploited for the preparation of SMEP by reacting diepoxide with tolylene diisocyanate to form isocyanatetelechelic oligomeric polyoxazolidone [81]. Many challenging applications require high failure strain and good mechanical stability. SMEP holds good mechanical attributes but has poor elongation in general. By using aromatic/aliphatic epoxy in combination with aliphatic diamine as curing agent, it is possible to achieve high strain and low rubbery modulus [82]. Leng et al. have synthesized the epoxy SMEP, from an epoxy, a hardener and another linear epoxy monomer [83]. The epoxy was mixed with the hardener at a 1:1 weight ratio. An active linear epoxy monomer was copolymerized with the polymer matrix to tailor the network. The monomer is composed of a long linear chain of C-O bonds and two epoxy groups at the chain ends. With an increase in the linear monomer content, the T_g ranges from 37 to 96 °C, and a decrease in the rubber modulus is obtained from dynamic mechanical analysis.

1.3.4 Some novel SMPs

Many SMPs with multiple-shape memory effect (MSME) have been developed [84-87] because of the significant applications such as packaging and robot. Different from dual-shape SMPs which can only remember its single original permanent shape, multiple-shape memory polymer (MSMP) can remember one or more shapes in addition to its original permanent shape. MSMP composites either have more than one reversible switching transition or have a single broad switching transition acting as the switching transitions [88-90]. Moreover, two-way SMPs change their shape upon suitable stimulation without the requirement for pre-deformation [91-93]. They may recover their original shape by changing the amplitude or direction of the stimulation. Two-way SME has been studied systematically on liquid crystalline elastomers. The ordering of mesogenic moieties and the elastic properties of liquid crystalline elastomers enable the two-way SME of liquid crystal elastomer. Thermal-active semicrystalline polymers with one single semicrystalline phase [94-96], or with two semicrystalline phases [97] can

also show two-way SME under constant stress. The underlying two-way shape memory mechanism is that cooling induced crystallization of semicrystalline polymer films results in elongation under a tensile load; subsequent heating to melt the network yields contraction.

1.4 SMPs Characterization

The main characterization techniques and the corresponding chemical, thermal and mechanical parameters are discussed here. These include Fourier transform infrared spectroscopy (FTIR), optical microscopy, scanning electron microscopy (SEM), transmission electron microscopy (TEM), electrical conductivity measurements, and temperature distribution measurements detected by infrared camera, thermo-gravimetric analysis (TGA), differential scanning calorimetry (DSC), dynamic mechanical analysis (DMA), atomic force microscopy (AFM), and mechanical properties testing.

FTIR is a measurement technique for collecting infrared spectra and is a powerful tool for identifying types of chemical bonds (i.e., functional groups). The wavelength of light absorbed is characteristic of the chemical bond, which can be distinguished in this annotated spectrum. By interpreting the infrared absorption spectrum, the chemical bonds can be determined [98]. SEM and TEM can be used to observe the surface morphology of SMPs or SMPs composites [99, 100]. Some types of electrically conductive fillers may be incorporated into SMPs to fabricate conductive SMP composites. In order to evaluate the electro-active performance, many researchers have used a variety of methods to measure the electrical conductivity [101]. TGA is employed to investigate thermal stability by evaluating the change in mass as a function of temperature. TGA is a very useful tool for a first, simple and fast evaluation of the thermal stability properties before planning their SME [102]. For SMPs, in most cases, DSC is used to determine the critical glass transition temperature (T_g) during the transition process, which is often defined as the median point of the glass transition range in the heating ramp [99]. DMA is used to monitor the thermal and dynamic mechanical properties of the SMPs and their composites. These data of SMPs allow the

calculation of the complex modulus (e.g., storage modulus and loss modulus), damping or tan delta as well as viscosity data. DMA allows the rapid scanning of the modulus and viscosity of an SMP as a function of temperature or frequency [103]. The mechanical properties of SMPs under varying temperature conditions are important parameters to evaluate the thermal, mechanical and shape memory performance. The relevant tests include tension tests [104], compression tests [105], three point bending tests, relaxation tests, creep tests, and nanoscale indentations by AFM [106].

1.5 SMP composites (SMPCs)

Although outstanding in many aspects as compared with SM alloys (SMAs), SMPs have intrinsic low mechanical strength and shape recovery stress. These problems have largely restricted the applications of SMPs. Reinforcing fillers are able to improve the mechanical performance and shape recovery stress of SMPs through physical blending, in-situ polymerization and chemical cross-linking [107-110]. Most of the fillers can significantly improve the elastic modulus and recovery stress of SMPs. Fillers which can have chemical bonding with SMP chains are more effective in improving the shape memory performance and the mechanical properties of SMPs. Fillers performing the function of cross-linking agents not only reinforce the SMP, but also improve the shape memory properties. Fillers can improve the thermal and electrical conductivity of the polymers and have positive effect on the SME of SMPs [111, 112].

1.5.1 Carbon fiber reinforced SMPCs

One of the main objectives of incorporating carbon nanofibers (CNFs) or carbon nanotubes (CNTs) into SMP is to achieve electroactive SME by Joule heating in intrinsic thermal-responsive SMPs [113, 114]. The biggest challenge of CNT/SMP composites is to disperse the CNTs uniformly in SMP matrix. Many methods have been used such as melt mixing [115], melt mixing followed by in-situ polymerization [116], extrusion and casting [117], solution mixing assisted with ultrasonic distribution [118], and chemical functionalization of CNTs followed by cross-linking reaction. Chemical

functionalization of CNTs is one of the most effective methods because chemical functionalization can increase the compatibility between the CNTs and the SMP matrix. For example, Raja et al. [119] functionalized CNTs and prepared biodegradable SMPU/poly (lactic acid) (PLA)/CNT nanocomposites. The functionalized CNTs lead to the best reinforcing effect. Moreover, after the chemical treatment, the born -OH groups in CNTs may react with the SMP matrix such as the isocynate of SMPU monomers to form an additional cross-linking network to improve the SM properties. Ni et al. investigated an SMPU filled with CNTs [120]. The results indicate that CNT/SMPU nanocomposites exhibit a good SME and their recovery stress with only 3.3% weight fraction of CNTs will reach almost twice of that bulk SMP.

Furthermore, CNTs significantly enhanced the mechanical and thermal properties, imparted unique electrical properties as well as improved the shape memory behavior of the polymer matrix [121, 122]. CNTs have an anisotropic nature enabling a percolative behavior at low volume fractions in the SMP matrix. The nanosize CNTs and their exceptional electrical and mechanical properties provided an excellent opportunity to improve the thermal management and structural reinforcement of a polymer matrix. Conductive SMPCs containing CNTs provided actuation of SME by applying electric current rather than heating by raising the environmental temperature. It was found that SMPCs containing CNTs could be used as electro-active actuators for controlling micro-aerial vehicles [123]. Fabrics made of carbon fibers have high elastic modulus and high strength, and can remarkably increase the mechanical strength of SMPs [124]. These composites, in the fiber (axial) direction, can bear much higher mechanical load, while in the transverse directions the SME can be mostly maintained [125].

1.5.2 Iron- or nickel reinforced SMPCs

Magnetic particles, such as iron, nickel, and some of their alloys, are called ferromagnetic materials. These materials exhibit a strong attraction to magnetic fields and are able to retain their magnetic properties after the external field has been removed. The domains of ferromagnetic material are nearly randomly organized in unmagnetized

state and the net magnetic field for the part as a whole is zero. When a magnetizing force is applied, the domains become aligned to produce a strong magnetic field within the part. The ferromagnetic particles can generate heat in an alternating magnetic field via hysteresis loss, eddy current, and/or additional mechanisms based on the different kinds of magnetic particles and their sizes. The particles interact with the external magnetic field via a Zeeman term, and with SMP matrix via elastic deformation, as well as with each other via the demagnetization field [126]. When the programmed SMP composite with a certain ferromagnetic particle content was exposed to an alternating magnetic field, the temperature of the material increased. If the temperature exceeded the T_g (or T_m) of SMP matrix, the original permanent shape could be recovered [127, 128]. This indirect, non-contact heating method could be used to trigger the SME if the SMP could not be actuated by direct heating methods through increasing environmental temperature. Magnetic materials with suitable Curie temperature (T_C) could significantly reduce the danger of overheating in biomedical applications as the ferromagnetic material worked as a thermostat. Adjusting the applied magnetic field strength, frequency, and T_C one could control the amount of heat generated for different potential applications.

1.5.3 Silica reinforced SMPCs

Among the numerous additives currently, silica is another commonly used because of its chemical stability, favorable morphology, availability, and low price. Lee et al. functionalized silica with allyl isocyanate groups and made silica/water-borne polyurethane nanocomposites using UV [129]. It was demonstrated that the functionalized silica particles had the function of both reinforcing fillers and stress relaxation retarders. Wang et al. used polycaprolactone grafted-silica to improve polycaprolactone SM effects [130]. The silica/SMP exhibited excellent mechanical strength, high strain and good shape memory properties due to the introduction of silica as a cross-linking agent. Jang et al. reported that the SME is retained in reinforced SMPU/silica hybrids [131]. Kim et al. synthesized PU–silic a nanocomposites via

sol–gel reactions between the surface silanol groups of fumed silica and aminopropyltriethoxysilane terminated PU with a broad range of silica contents with two different molecular weights of PU. It was found that the silica particles that were incorporated into the polymer chains were well dispersed in the PU matrix and acted as multifunctional cross-links and reinforcing fillers, in addition, the silica particles augmented the initial and rubbery moduli, yield, and break strengths, as well as the glass transition temperature. The resultant silica/SMPU composites exhibited excellent mechanical and SM properties [132].

1.5.4 Clay reinforced SMPCs

The recent research of exfoliated nanoclay/SMP focused on modification of exfoliated nanoclay to enable its reaction with the SMP matrix. The modified organic-exfoliated nanoclay can significantly improve the shape recovery ratios, shape recovery stress and mechanical properties. The nanoclay may play its role as an additional hard phase contributing to shape memory properties [133]. For example, Cao and Jana employed the $-H_2CH_2OH$ group of the quaternary ammonium ions in organ-clay to react with isocyanine -NCO [134]. This reaction adds an additional network contributing to the SME. Chung et al. used surface-modified monmorillonite to chemically bond to SMPU [135]. The modified monmorillonit has methyl tallow bis-2-hydroxyethyl ammonium group which can be chemically bonded with polyurethane. In addition to reinforcement research, SMPCs research has been focused on SMPCs with athermal stimuli-active effect, SMPCs with novel SME, and SMPCs with new functions. Heat treatment of the nanoclay can improve the compatibility of the clay with the SMP matrix. The loss of moisture and most surface hydroxyl groups as a result of the heat treatment can provide a better interfacial bonding between the SMP and clay interface. Xu et al. heat treated a nanofabric type clay attapulgite at 850 ^{o}C to reinforce SMPU. The mechanical properties and SME of the nanocomposites were remarkably improved [136].

1.6 Application of SMPs and SMPCs

As a novel kind of smart materials, SMPs currently cover a broad range of application areas ranging from outer space to automobiles. Recently, they are being developed and qualified especially for deployable components and structures in aerospace [137]. In addition, SMPs also present additional potential in the areas of biomedical devices [138, 139], sensors [140], textiles [141], dry adhesives [142], self-healing applications [143] and actuators [144].

1.6.1 Deployable structures

For the traditional aerospace deployable devices, the change of structural configuration in orbit is accomplished through the use of a mechanical hinge, stored energy devices or motor driven tools. There are some intrinsic drawbacks for the traditional deployment devices, such as complex assembling process, massive mechanisms, large volumes and undesired effects during deployment. In contrast, the deployment devices fabricated using SMPs and their composites may overcome certain inherent disadvantages. Santo et al. reported two new SMC self-deployable structures: a composite cross and a composite frame containing a thin aluminum sheet [145]. The former structure represents a possible deploying configuration for a structural sheet whereas the latter is a conceptual study of a solar sail. The experimental results showed that such structures can successfully self-deploy following the desired design constraints without noticeable damages, as shown in Fig. 1.3.

Figure 1.3 Shape memory test of the SMC frame [145].

1.6.2 Morphing structures

A large and growing body of literature has investigated shape memory materials, comprising alloys, ceramics, and polymers, due to the potential associated with the SME. SMAs have been widely employed for actuation purposes in the large shape adaptation context [146, 147]. Nevertheless, it is SMPs which have attracted the most attention with respect to variable stiffness applications in morphing. This is based on the large reversible strain capacity they offer, combined with the additional property enhancement capability when reinforced to form shape or elastic memory composites. When viewed from the morphing perspective, the superiority of SMPs compared to SMAs lies in smaller density, larger reversible strains, ease of adaptation of their thermo-mechanical characteristics to suit particular needs, responsiveness to other than thermal stimulants. Further advantages of SMPs include reduced material, manufacturing, and processing cost accompanied by fabrication flexibility. On the other hand, the realisable actuation forces are much lower than in the case of SMAs since the corresponding stresses lie at a maximum of a few MPa for SMPs in contrast to at least 10 MPa for SMAs [148]. This, however, is of no primary importance in the variable stiffness context. Nevertheless, aspects such as the danger of micro-scale damage to SMPs in the event of insufficient programming temperature as well as uncertain long-term durability and reliability should not be neglected [148].

Flight vehicles are envisioned to be multi-functional so that they can perform more missions during a single flight, such as an efficient cruising and a high maneuverability mode. When the airplane moves towards other portions of the flight envelope, its performance and efficiency may deteriorate rapidly. To solve this problem, researchers have proposed to radically change the shape of the aircraft during flight. By applying this kind of technology, both the efficiency and flight envelope can be improved. This is because different shapes correspond to different trade-offs between beneficial characteristics, such as speed, low energy consumption and maneuverability. For instance, Lockheed Martin has proposed a z-shape morphing vehicle concept and verified its flight properties through ground and wind tunnel tests of unmanned air

vehicles (UAV) [149], as illustrated in Fig. 1.4.

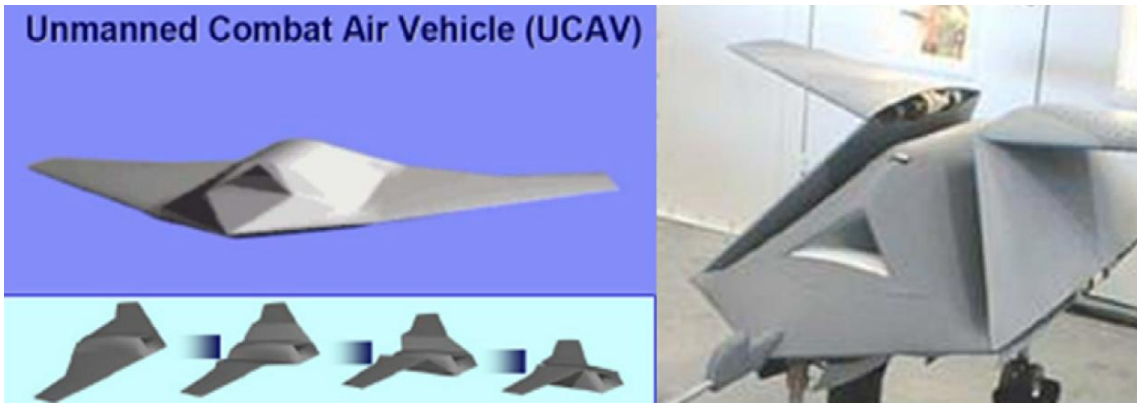

Figure 1.4 Z-shaped morphing wings produced by Lockheed Martin [149].

1.6.3 Biomedical applications

SMPs can remember a primary shape and can return to this primary shape from a deformed secondary shape when given an appropriate stimulus. This property allows them to be delivered in a compact form via minimally invasive surgeries in humans, and deployed to achieve complex final shapes. SMPs show extensive interest in used for biomaterials and bioinspiration [150, 151].

Recently, Wache et al. have conducted a feasibility study and preliminary development on a polymer vascular stent with an SMP as the drug delivery system. The field of applications of this polymer stent was demonstrated in pre-trials [152]. The use of the SMP stent as a drug delivery system leads to significant reduction of restenosis and thrombosis. An improved biological tolerance in general is expected when using biocompatible SMP materials. The exciting SMPs can move from one shape to another in response to a stimulus. Thus, SMPs are dual-SM materials. A triple-SMP was recently reported in [153]. As shown in Fig. 1.5, the SMP is able to change from an initial shape (A) to a second shape (B) and finally deform to a third shape (C). It may be inserted into the body, expanded at a target site, and be removed at a later point in time which may be necessary even with degradable materials.

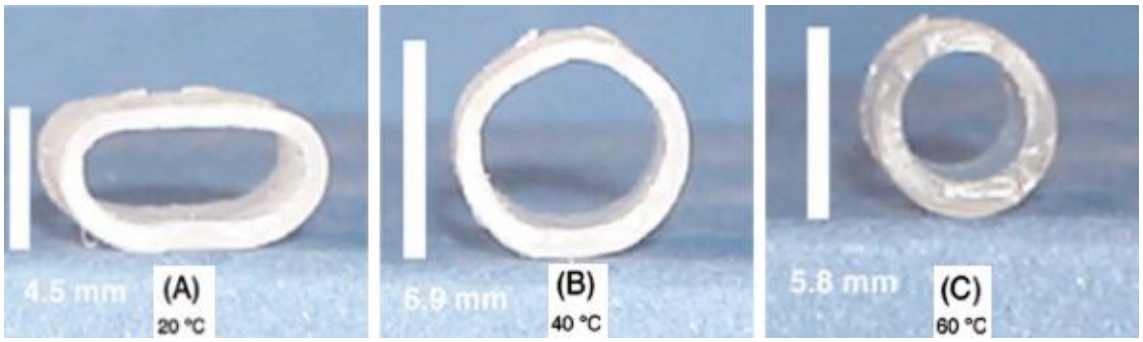

Figure 1.5 Through increasing the temperature from 20 °C (A) to 40 °C (B) an initial shape change was induced followed by a second shape change through increasing the temperature to 60 °C (C) [153].

Small et al. developed a prototype device for endovascular embolization of fusiform (non-necked) aneurysms based on thermally activated SMP [154]. The device consisted of two main components: (1) an SMP stent and (2) an SMP embolicfoam attached to the outside of the stent. The device was compressed over a light diffusing fiber for photothermal actuation. The embolic foam component filled the aneurysm lumen while the stent maintained a patent flow channel in the parent artery in an in vitro model (Fig. 1.6).

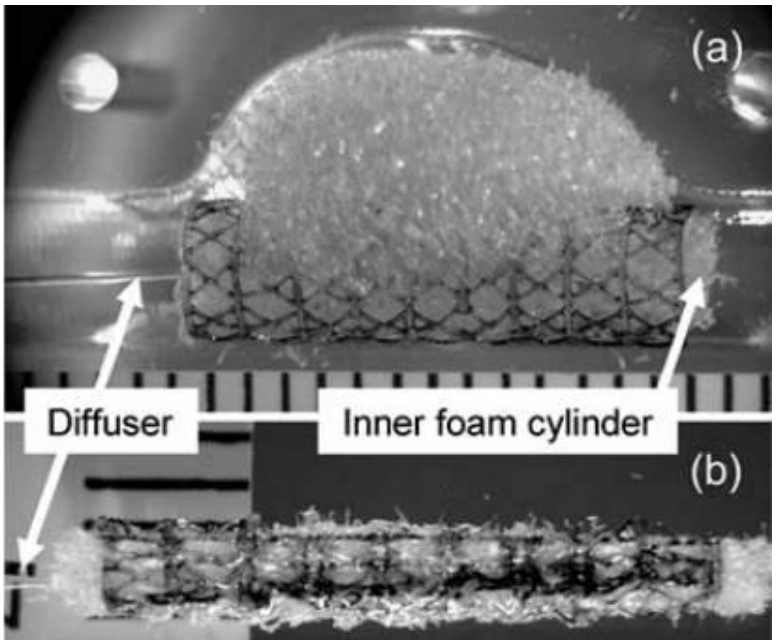

Figure 1.6 SMP stent-foam devices with removable inner foam cylinder and laser light diffuser (a) before and (b) after collapsing for delivery. The device is shown in the bottom mold of the fusiform aneurysm model in (a) [154].

Thermally activated SMP-based mechanical clot extraction devices to treat ischemic stroke was reported by Maitland et al. These devices were designed to be delivered through a catheter and penetrate the clot in a narrow form, and then actuate into a clot-grabbing form for clot extraction [155]. Maitland et al. demonstrated photothermal actuation of corkscrew-shaped and umbrella-shaped devices by coupling light from a diode laser operating at a wavelength of 810 nm into the SMP device [155]. The thermo-responsive SMPU sheds light for the possibility to fabricate micro/nano devices for surgery or operation at the cellular level. Ikuta and Hayato have developed many polymer micro-machines, which are similar to the size of cells or even smaller and can be triggered for operation by a laser beam outside the cell [156]. This suture can be applied loosely in its temporary shape under elongated stress. When the temperature is raised above T_g, the suture will shrink and then tighten the knot, in which case it will apply an optimal force. The biocompatibility and degradation products should be considered. These sutures should be degradable and show gradual mass loss during degradation. The hydrolyzable ester bonds are introduced into the polymers so that they would cleave under physiological conditions. In this way, the degradation kinetics could be controlled through the composition and relative mass content of the precursor macrodiols [157].

1.6.4 Other applications

Referenced form [158], there is a list of potential application for SMPs: (1) Fashion design; (2) Household Items, pillow, curtain and insoles; (3) Toys; (4) Packaging of thermal sensitive products, sensors, drug, and food air delivery systems; (5) Tents and camping equipment, life jacket, floating wheels, water and snow skis, surf and snow boards; (6) Thermally insulated deployable shelters, hubs, prefabricated walls, access denial barriers, automatic disassembly of electronic products, reusable SMP mandrel; and (8) Self-peeling dry adhesive.

1.7 Outline of this dissertation

In our study, in order to develop an excellent SM epoxy material via environmental-friendly latex method, we synthesized a water-borne epoxy (WEP) via phase-inversion technology. We found that WEP has excellent SM property, besides a mechanical strength and SM fixity ratio lower than those of common (solvent-based) SM epoxy. CNTs and in-situ grown nanosilicas were applied to improve the mechanical and SM properties of the WEP. On the other hand, we also discussed the effect of nanofiller and cell structure on the mechanical and SM properties of the WEP SM nanocomposites foams. The additional function of SM of WEP will be a good aspect for extending their further applications.

The thesis is comprised of five subsequent chapters, experimental methods, results and conclusions of three main studies and development of the WEP and its nanocomposites design for SM materials.

In chapter 1 presents an overview the SMPs and their nanocomposites, including the structures, properties, synthesis, and their application.

In chapter 2 reports a facile and environmental-friendly method to prepare high performance shape memory epoxy materials form WEP.

In chapter 3, on the base of WEP, we successfully synthesized and systemically characterized carbon nanotube (CNT)/WEP SM nanocomposites and SM foams, respectively.

In chapter 4 focuses on the further investigation of the silica/WEP SM nanocomposites and SM foams, respectively.

Finally, Chapter 5 summarizes the results of all the work described in this thesis.

References

[1] H. Luo, Z. Li, and G. Yi, *Mater. Lett.*, 140(2015)71.

[2] F. Du, W. Yang, and C. Y. Tang, *Composites: Part B*, 68(2015)170.

[3] J. S. Sodhi, P. R. Cruz, and I. J. Rao, *Int. J. Eng. Sci.*, 89(2015)1.

[4] Y. Cai, J. Jiang, and B. Zhang, *J. Appl. Polym. Sci.*, 127(2013)49.

[5] W. W. Guo, D. Seliktar, and I. Willner, *Adv. Mater.*, 27(2015)73.

[6] G. Q. Li, G. Fei, H. Xia, and Y. Zhao, *J. Mater. Chem.*, 22(2012)7692.

[7] Y. Zhu, J. L. Hu, L. Deng, *Soft Matter*, 8(2012)2509.

[8] T. Miyata, N. Asami, and T. Uragami, *Nature*, 1999(399)766.

[9] M. R. Lee, K. H. Baek, and I. Shin, *Angew. Chem. Int. Edn.*, 43(2004)1675.

[10] Y. C. Chung, D. K. Nguyen, and B. C. Chun, *Fiber Polym.*, 11(2010)952.

[11] T. Xie, *Polymer*, 52(2011)4985.

[12] J. L. Hu, Y. Zhu, H. H. Huang, J. Lu, *Prog. Polym. Sci.*, 37(2012)1720.

[13] A. Lendlein, R. Langer, *Nature*, 434(2005)879.

[14] A. Lendlein, R. Langer, *Science*, 296(2002)1673.

[15] T. Xie, *Nature*, 464(2010)267.

[16] A. Maksimkin, S. Kaloshkin, and M. Zadorozhnyy, *J. Alloys Comp.*, 586(2014)214.

[17] J. Zhao, M. Chen, and X. Zhao, *ACS Appl. Mater. Interface*, 5(2013)5550.

[18] B. Heuwers, A. Beckel, and A. Krieger, *Macromol. Chem. Phys.*, 214(2013)912.

[19] M. Ahmad, B. Xu, and M. Miraft, *Appl. Sci.*, 2(2012)535.

[20] T. Liu, J. Li, and Y. Peng, *Soft Matter*, 7(2011)1641.

[21] Y. Niu, P. Zhang, and Y. Wang, *Polym. Chem.*, 3(2012)2508.

[22] K. Kumar, R. Biju, and Na, Reghunadhan, *React. Funct. Polym.*, 73(2013)421.

[23] A. Sonseca, and C. Weder, *J. Polym. Sci. Part A Polym. Chem.*, 52(2014)3123.

[24] H. Koerner, R. J. Strong, and K. M. Lee, *Polymer*, 54(2013)391.

[25] J. A. Shumaker, A. J. W. Mcclung, and J. W. Baur, *Polymer*, 53(2012)4637.

[26] F. Xie, L. Huang, and J. S. Leng, *Polymer*, 55(2014)5873.

[27] X. L. Wu, Z. Ding, and K. Y. Sun, *J. Appl. Polym. Sci.*, 131(2014)39844.

[28] Y. B. Kim, and Y. H. Rhee, *Macromol. Rapid Commun.*, 26(2005)1070.

[29] B. C. Guo, Y. W. Chen, and J. Q. Zhao, *Biomacromolecules*, 12(2011)1312.

[30] J. E. Gautrot, and X. X. Zhu, *Macromolecules*, 42(2009)7324.

[31] H. Meng, G. Li, *Polymer*, 54(2013)2199.

[32] W. Voit, T. Ware, and R. R. Dasari, *Adv. Funct. Mater.*, 20(2010)162.

[33] Z. Yu, Y. Liu, and M. Fan, *J. Polym. Sci. Part B:Polym. Phy.*, 48(2010)951.

[34] F. L. Ji, J. L. Hu, and T. C. Li, *Polymer*, 48(2007)5133.

[35] Y. Zhu, J. L.Hu, and H. M. Liem, *J. Appl. Polym. Sci.*, 100(2006)4603.

[36] K. M. Lee, H. Koerner, and R. A. Vaia, *Soft Matter*, 7(2011)4318.

[37] G. Li, A. King, and T. Xu, *J. Mater. Civ. Eng.*, 25(2013)393.

[38] S. K. Ahn, P. Deshmukh, and R. M. Kasi, *ACS Nano*, 5(2011)3085.

[39] K. M. Lee, H. Koerner, and R. A. Vaia, *Soft Matter*, 7(2011)4318.

[40] J. S. Sodhi, and I. J. Rao, *Int. J. Eng. Sci.*, 48(2010)1576.

[41] L. B. Wu, C. L. Jin, and X. Y. Sun, *Biomacromolecules*, 12(2011)235.

[42] T. Defize, R. Riva, and M. Alexandre, *Macro. Chem. Phys.*, 213(2012)187.

[43] J. Zhang, Y. Niu, and K. Yang, *Polym. Chem.*, 3(2012)1390.

[44] D. Aoki, Y. Teramoto, and Y. Nishio, *Biomacromolecules*, 8(2007)3749.

[45] J. Li, C. L. Lewis, and M. Anthamatten, *Macromolecules*, 44(2011)5336.

[46] S. Chen, J. Hu, and L.Chan, *Polymer*, 51(2010)240.

[47] J. R. Kumpfer, S. J. Rowan, *J. Am.Chem. Soc.*, 133(2011)12866.

[48] X. Yan, D. Xu, and X. Chi, *Adv. Mater.*, 24(2012)362.

[49] J. Chen, M. Liu, and H. Liu, *Chem. Eng. J.*, 159(2010)247.

[50] X. J. Han, Z. Q. Dong, and Y. F. Wang, *Macro. Rapid. Commu.*, 33(2012)1055.

[51] Y. Zhu, J. L. Hu, and G. D. Ye, *Soft matter*, 8(2012)2509.

[52] S. B. Lee, B. C. Chun, and Y. C. Chung, *Macromolecules*, 34(2001)6431.

[53] T. Takahashi, N. Hayashi, and S. Hayashi, *J. Appl. Polym. Sci*., 60(1996)1061.

[54] Y. P. Cao, Y. Guan, and J. Du, *J. Mater. Chem.*, 12(2002)2957.

[55] Z. L. Ma, W. G. Zhao, and Y. F. Liu, *J. Appl. Polym. Sci.*, 63(1997)1511.

[56] H. Liem, and L. Y. Yeung, *J. Appl. Polym. Sci.*, 105(2007)765.

[57] S. I. Han, B. H. Gu, and K. H. Nam, *Polymer*, 48(2007)1830.

[58] S. Xu, and M. Zhang, *J, Appl. Polym. Sci.*, 104(2007)3818.

[59] J. S. Leng, H. B. Lv, and S. Y. Du, *MRS Bull LLC.*, 34(2009)848.

[60] J. Kunzelman, T. Chung, and P. T. Mather, *J. Mater. Chem.*, 18(2008)1082.

[61] C. P. Buckley, C. Prisacariu, and A. Caraculacu, *Polymer*, 48(2007)1388.

[62] M. C. Choi, J. Y. Jung, and Y. W. Chang, *Polym. Bull.*, 71(2014)625.

[63] M. Kashif, Y. W. Chang, *Eur. Polym. J.*, 66(2015)273.

[64] Y. K. Bai, Y. Chen, and T. Wang, *J. Mater. Chem. A*, 2(2014)9169.

[65] D. Zhang, and M. A. Grunlan, *J. Polym. Sci. Pol. Chem.*, 49(2011)754.

[66] N. Xu, M. Jiang, and C. F. Xiao, *Polym-plast. Technol.*, 53(2014)7725.

[67] W. C. Chen, S. M. Lai, and M. Y. Chang, *J. Macromol. Sci. B*, 53(2014)645.

[68] L. Ma, J. Zhao, and R. C. Hedden, *Polymer*, 56(2015)490.

[69] M. Bonfil, A. Sirkecioglu, and F. Uras, *J. Appl. Polym. Sci.*, 131(2014)40590.

[70] Z. Wang, J. Zhao, and M. Chen, *ACS Appl. Mater. Interfaces*, 6(2014)20051.

[71] Y. Guo, X. Gao, and Y. Luo, *J. Polym. Sci. Part B: Polym. Phys.*, 53(2015)860.

[72] J. Zhou, A. Sara, and S. S. Sheiko, *Macromolecules*, 47(2014)1768.

[73] A. M. Gumel, M. Suffian, and M. Annuar, *J. Appl. Polym. Sci.*, 131(2014)41149.

[74] H. Khonakdar, S. Jafari, and H. Abedini, *Macromol. Theory Simul.*, 16(2007)43.

[75] S. J. Chen, and Y. J. Liu, *J. Polym. Sci. Part B: Polym. Phys.*, 45(2007)444.

[76] F. Li, and R. C. Larock, *J. Appl. Polym. Sci.*, 80(2001)658.

[77] F. Li, M.V. Hanson, R. C. Larock, *Polymer*, 42(2001)1567.

[78] H. Tobushi, S. Hayashi, and K. Hoshio, *Smart Mater. Struct.*, 15(2006)1033.

[79] G. Q. Liu, C. L. Guan, and H. S. Xia, *Macromol. Rapid Commun.*, 27(2006)1100.

[80] W. B. Song, L.Y. Wang, Z. D. Wang, *Mat. Sci. Eng. A*, 529(2011)34.

[81] D. J. Merline, C. P. R. Nair, and C. Gouri, *Eur. Polym. J.*, 43(2007)3629.

[82] I. A. Rousseau, T. Xie, *J. Mater. Chem.*, 20(2010)3431.

[83] J. S. Leng, X. L. Wu, and Y. J. Liu, *Smart Mater. Struct.*, 18(2009)9503.

[84] Z. He, N. Satarkar, T. Xie, and J. Z. Hilt, *Adv. Mater.*, 23(2011)3192.

[85] L. Wang, X. Yang, and S. Zhou, *Polym. Chem.*, 4(2013)4461.

[86] Y. Luo, Y. Guo, and X. Gao, *Adv. Mater.*, 25(2013)743.

[87] R. R. Kohlmeyer, M. Lor, and J. Chen, *Nano Lett.*, 12(2012)2757.

[88] S. K. Ahn, R. M. Kasi, *Adv. Funct. Mater.*, 21(2011)4543.

[89] H. Radusch, I. Kolesov, and U. Gohs, *Macro. Mater. Eng.*, 297(2012)1225.

[90] K. Yu, T. Xie, and J. Leng, *Soft Matter*, 8(2012)5687.

[91] H. Tamagawa, *Mater. Lett.*, 64(2010)749.

[92] J. Li, W. R. Rodgers, and T. Xie, *Polymer*, 52(2011)5320.

[93] S. V. Ahir, A. R. Tajbakhsh, and E. M. Terentjev, *Adv. Funct. Mater.*, 16(2006)556.

[94] S. J. Hong, W. R .Yu, and J. H.Youk, *Smart Mater. Struct.*, 19(2010)35022.

[95] S. Pandini, S. Passera, and M. Messori, *Polymer*, 53(2012)1915.

[96] J. J. Li, W. R. Rodgers, and Xie T, *Polymer*, 52(2011)5320.

[97] J. Zotzmann, M. Behl, and A. Lendlein, *Adv. Mater.*, 22(2010)3424.

[98] Y. Han, X. Yuan, and S. Li, *Adv. Funct. Mater.*, 24(2014)4996.

[99] K. Yu, Y. J. Liu, and J. S. Leng, *J. Intel. Mater. Syst. Str.*, 22(2011)2147.

[100] Y. Wu, J. Hu, and B. Kumar, *J. Mater. Chem. A*, 3(2015)97.

[101] S. Chen, S. Chen and Z. Ge, *Polym. Composite.*, 36(2015)439.

[102] F. Xie, L. Huang, and J. Leng, *Polymer*, 55(2014)5873.

[103] K. Yua, Q. Ge, and H. J. Qi, *Polymer*, 55(2014)235938.

[104] G. Scaleta, F. Auricchioa, and E. Bonettib, *Int. J. Plasticity*, 67(2015)127.

[105] G. Ellson, M. D. Prima, and T. Ware, *Smart Mater. Struct.*, 24(2015)55001.

[106] M. Ebara, M. Akimoto, and T. Aoyag, *Polymer*, 55(2014)5961.

[107] J. Nji, G. Q. Li, *Smart Mater. Struct.*, 19(2010)35007

[108] S. S. Mahapatra, M. S. Ramasamy, and J. W. Cho, *RSC Adv.*, 4(2014)15146.

[109] Y. Liu, Y. Li, G. Yang, and S. Zhou, *ACS Appl. Mater. Interfaces*, 7(2015)4118.

[110] M. John, G. Q. Li, *Smart Mater. Struct.*, 19(2010)75013.

[111] H. Luo, Z. Li, and Y. Wang, *Mater. Lett.*,140(2015)71.

[112] S. S. Mahapatra, and J. W.Cho, *Sensor. Actuat. B Chem.*, 193(2014)384.

[113] K. Yu, Y. Liu, and J. Leng, *RSC Adv.*, 4(2014)2961.

[114] H. Luo, Z. Li, and G. Yi, *Mater. Lett.*,137(2014)385.

[115] J. Chen, Z. Zhang, and Y. Wang, *Mater. Design*, 69(2015)105.

[116] Y. Bai, Y. Zhang, and T. Wang, *J. Mater. Sci.*, 48(2013)2207.

[117] T. Richardson, M. Mosiewicki, and M. Auad, *Polym. Composite.*, 32(2011)455.

[118] F. Du, E. Yea, and C. Tang, *Compos. Part B. Eng.*, 68 (2015)170.

[119] M. Raja, S. H. Ryu, and A. M. Shanmugharaj, *Eur. Polym. J.*, 49(2013)3492.

[120] Q. Q. Ni, C. Zhang, and T. Kimura, *Compos. Struct.*, 81(2007)176.

[121] Z. Tang, D. Sun, and B. Guo, *Compo. Sci. Technol.*, 75(2013)15.

[122] Z. Tang, H. Kang, Q. Wei, and B. Guo, *Carbon*, 64(2013)487.

[123] H. Paik, N. S. Goo, and J. W. Cho, *Smart Mater. Struct.*, 15(2006)1476.

[124] T. Ohki, Q. Q. Ni, N. Ohsako, M. Iwamoto, *Compos. Part A*, 35(2004)1065.

[125] C. S. Zhang, Q. Q. Ni, *Compos. Struct.*, 78(2007)153.

[126] S. Conti, M. Lenz, and M. Rumpf, *J. Mech. Phys. Solids*, 55(2007)1462.

[127] M. Heuchel, M. Y. Razzaq, and A. Lendlein, *Polymer*, 65(2015)215.

[128] S. Glock, L. P. Canal, and V. Michaud, *Compo. Sci. Technol.*, 114(2015)110.

[129] S. K. Lee, S. H. Yoon, and B. K. Kim, *J. Polym. Sci. Polym. Chem.*, 49(2010)634.

[130] Y. M. Zhang, Q. H. and T. M. Wang, *J. Mater. Chem.*, 21(2011)9073.

[131] M. K. Jang, A. Hartwig, and B. K. Kim, *J. Mater. Chem.*, 19(2009)1166.

[132] C. Y. Bae, H. C. Park, B. K. Kim, *High Perform. Polym*., 23(2011)7518.

[133] H. T. Zhou, J. Hu, and S. J. Chen, *J. Appli. Polym. Sci.*, 109(2008)406.

[134] J. J. Mcdowell, N. S. Zacharia, G. A. Ozin, *J. Am. Chem. Soc.*, 132(2010)3236.

[135] H. T. Zhuo, J. Hu, S. J. Chen, *Express Polym. Lett.*, 5(2011)182.

[136] J. N. Zhang, Y. M. Ma, and L. Jiang, *Mater. Lett.*, 65(2011)3639.

[137] L. Santoa, F. Quadrinia, and A. Accetturaa, *Procedia Eng.*, 88(2014)42.

[138] A. Lendlein, R. Langer, *Science*, 7(2002)1673.

[139] S. Sharifi, M. Behl, and A. Leddlein, *Biomaterials*, 34(2013)8105.

[140] H. B. Lu, J. S. Leng, and S. Y. Du, *Compos. Sci. Technol.*, 71(2011)1427.

[141] J. L. Hu, S. J. Chen, *J. Mater. Chem.*, 20(2010)3346.

[142] C. M. Chen, C. L. and T. Xie, *Adv. Funct. Mater.*, 23(2013)3813.

[143] Y. Li, S. S. Chen, and J. Q. Sun, *Adv. Mater.*, 24(2012)4578.

[144] J. J. Songa, H. H. Changa, and H. E. Naguib, *Eur. Polym. J.*, 67(2015)186.

[145] L. Santo, F. Quadrini, and A. Accettura, *Procedia Engineering*, 88(2014)42.

[146] F. T. Calkins, J. H. Mabe, *J. Mech. Design*, 132(2010)111012.

[147] C. Bil, K. Massey, and E. J. Abdullah, *J. Intel. Mat. Syst. Str.*, 24(2013)879.

[148] L. Sun, W. M. Huang, and Z. Ding, *Mater. Design.*, 33(2012)577.

[149] Y. Liu, H. Du, and J. Leng, *Smart Mater. Struct.*, 23(2014)23001

[150] M. C. Serrano, G. A. Ameer, *Macromol. Biosci.*, 12(2012)1156.

[151] J. J. Songa, H. H. Changa, and H. E. Naguib, *Macromol. Biosci.*, 56(2015)82.

[152] H. M. Wache, and D. J. Tartakowska, *J. Mater. Sci. Mater. Med.*, 14(2003)109.

[153] I. Bellin, S. Kelch, and A. Lendlein, *PNAS*, 103(2006)18043.

[154] W. Small, and T. S. Wilson, *IEEE Trans. Biomed. Eng.*, 54(2007)1157.

[155] D. J. Maitland, M. F. Metzger, and T. S. Wilson, *Lasers Surg. Med.*, 30(2002)1.

[156] M. S. Ikuta, K. Hayato, *Appl. Phys. Lett.*, 82(2003)133.

[157] W. Small, T. S. Wilson, and D. J. Maitland, *Opt. Express*, 13(2005)1.

[158] H. Meng, G. Li, *Polymer*, 54(2013)2199.

CHAPTER TWO

Preparation of shape memory epoxy materials via latex technology

2 Preparation of shape memory epoxy materials via latex technology

In the present study, in order to develop an excellent shape memory epoxy (SMEP) material prepared via environmental-friendly method, we synthesized a water-borne epoxy (WEP) via phase-inversion technology. Epoxy-graft-polyoxyethylene octyl phenyl ether (EP-g-TX100), which is a reactive copolymer emulsifier that covalently reacts with the curing agent through the side chains, is investigated for preparing of WEP. WEP particles had an average diameter of 137 nm, with particles ranging from 50 nm to 300 nm. Then, the freeze-drying and hot-press molding technology was applied to preparing the epoxy material which shows excellent SM properties. Our strategy for obtaining SMEP will pave the way for designing and developing the functional SME polymers. Our proposed method is applicable to various host polymers and does not require organic solvents. Thus, the current simple and environmental friendly approach may be used to synthesize SM materials as temperature sensor materials.

2.1 Introduction

Shape memory polymers (SMPs), which have attracted considerable attention in recent years and will come to play a significant role in all areas of human life because of their scientific and technological significance, are a new class of stimuli-responsive materials that can maintain a temporary shape and subsequently recover their original shape by external stimuli, such as heat [1-3], water [4], pH [5], light [6], electric field [7], and magnetic field [9]. As smart materials, SMPs can be potential applied in aerospace structures [10], biomedical devices [11, 12], sensors [13], textiles [14], dry adhesives [15], self-healing applications [16], and so on.

Epoxies are widely employed in many non-shape memory (SM) applications, such as coatings, adhesives, civil engineering, and electronics, due to their high strength, good thermal stability, and excellent chemical resistance. Many recent studies have proven the favorable SM properties of epoxies [1, 17]. The shape recovery ratio and elastic modulus of epoxies range from 98% to 100% and from 2 GPa to 4.5 GPa, respectively [1]. In addition, epoxies exhibit good thermal stability and chemical resistance. Unfortunately, the processes of epoxies are very environmentally unfriendly, complex, and expensive. A vast majority of these products are still formulated with organic solvents. However, as environmental regulation become stricter, the requirement for the industries to switch to more ecological and safer systems is constantly growing.

Water-borne epoxies (WEPs), as novel versatile environmentally-friendly materials, which are being attached great importance in engineering field and mainly used in concrete coatings, metal primers, epoxy cement concrete, glass fiber sizing, and wood adhesives [18]. In the present study, in order to develop an excellent SMEP material prepared via environmental-friendly method, we synthesized a WEP via phase-inversion technology. With WEP, the freeze-drying and hot-press molding technologies were applied to preparing the epoxy material which shows excellent SM properties.

2.2 Experimental

2.2.1 Materials

The nonionic surfactant, polyoxyethylene octyl phenyl ether (TX100, supplied by Aladdin Industry, USA), which has a critical micelle concentration value of 0.2 mM to 0.9 mM at 25 °C, was used. The commercially available epoxy (diglycidyl ether of bisphenol A, DGEBA) E-44 (epoxy equivalent~213-244; supplied by Wuxi Resin Factory, China), 2, 4-toluene diisocyanate (TDI, supplied by Bayer, Germany), and deuterated chloroform were obtained from commercial sources and used as received. A commercially available room-temperature curing agent (AB-HGF®, Zhejiang Anbang

New Material Development Co., Ltd, China) was obtained from commercial sources and used as received. All dispersion experiments were performed with deionized (DI) water.

2.2.2 Synthesis of EP-g-TX100

In this experiment, DGEBA (3.720 g, 8 mmol) was added into a three necked-flask and stirred at 80 to 90 °C under vacuum (-0.08 MPa) for 30 min to eliminate moisture. After the mixture was cooled at 50 °C for 10 min, TDI (0.870 g, 5 mmol) was added dropwise into the flask under vigorous mixing. The mixture was then warmed to 70 °C and stirred for 8 h under a nitrogen atmosphere. The grafting reaction occurred between the pendant hydroxyl groups of epoxy resin and the isocyanate groups of TDI [19]. When the grafting reaction was completed, TX100 (3.900 g, 6 mmol) was added dropwise to the reaction system, and the mixture was agitated for another 16 h under a nitrogen atmosphere. After the reaction was completed, the mixture was filtered and washed several times with DI water. The resulting product was dried at 80 °C under vacuum for 24 h. The copolymer (5.685 g) was obtained with a yield of 67 %. This copolymer contains three structural segments: an epoxy moiety, a TDI moiety and a TX100 segment. The reaction is shown in Fig. 2.1.

2.2.3 Preparation of water-borne epoxy (WEP)

WEP was synthesized from epoxy/EP-g-TX100/water using the phase-inversion technique, as shown in Fig. 2.2. The emulsifier EP-g-TX100 (10 g) and epoxy (90 g) were added into a 500 mL three necked-flask, warmed to 70 °C, and stirred to homogeneity. The mixture was then poured into a 1000 mL stainless steel cup and stirred at 10 °C using an ice bath maintain a low emulsification temperature. The shearing speed was 3000 r/min. DI water was added drop-wise until phase inversion occurred. Enough water was added to produce an emulsion with 50% solid weight.

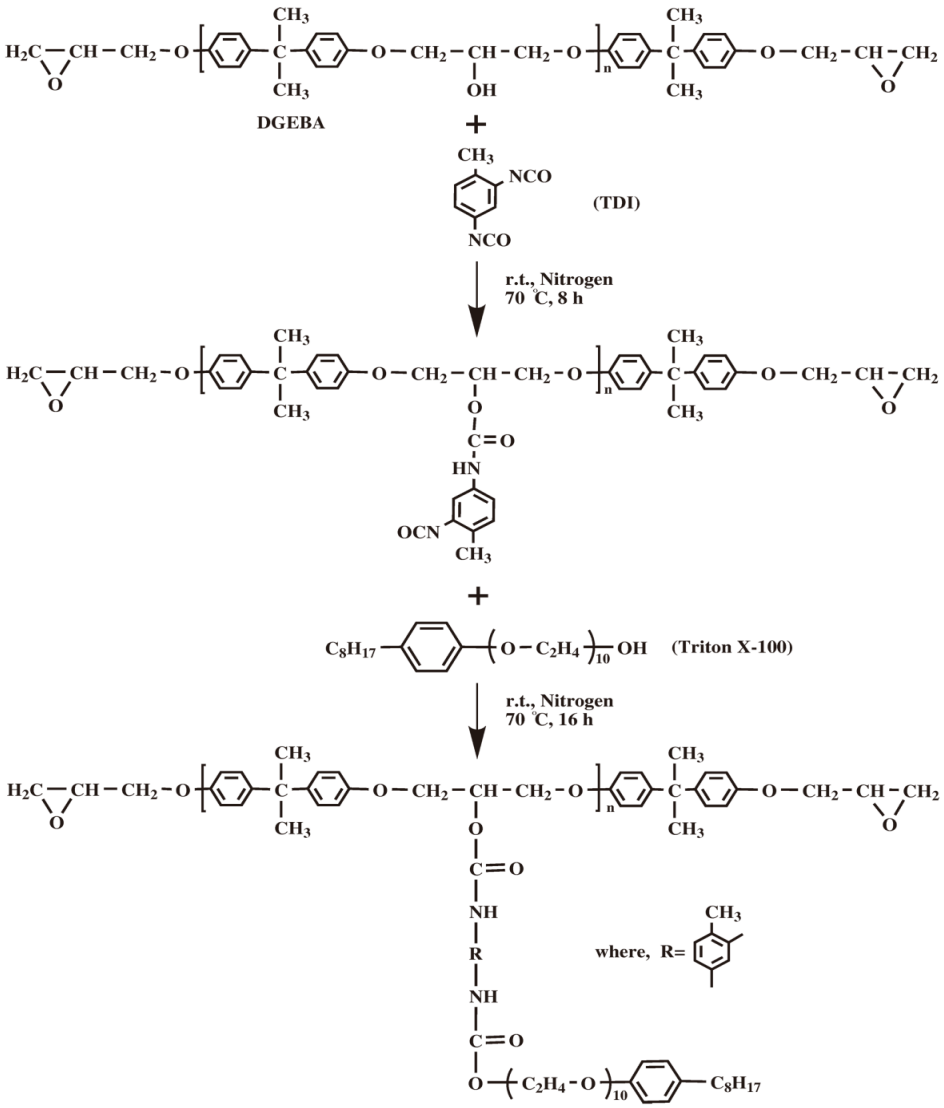

Figure 2.1 Synthesis of WEP emulsifier (EP-g-TX100).

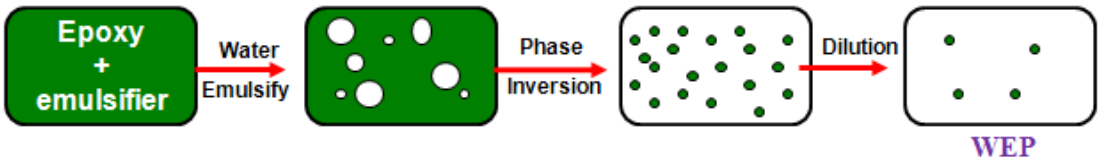

Figure 2.2 Synthesis of WEP.

2.2.4 Preparation of WEP films

The curing agent was added the WEP. The weight ratio of the WEP to the cuing agent was 4:1. Second, the mixture was frozen in liquid nitrogen for 5 min, and the aqueous solvent was removed using a Labconco Free Zone freeze-dryer operated at 0.1

mbar and -55 °C for 7 d. Finally, the resulting composite powder was compressed into films at 120 °C for 2 h under a pressure of 10 MPa.

2.2.5 Characterization

Fourier transform infrared spectroscopy (FTIR) spectra of pure epoxy, TX100, EP-g-TX100, and cured EP-g-TX100 were recorded on a Nicolet 5700 attenuated total reflection FTIR (ATR-FTIR) instrument (Thermo Electron Corp., USA) with a resolution of 4 cm^{-1}. The ^{1}HNMR measurements were performed on an AVANCE AV 400 MHz Digital FT-NMR spectrometer operating at 400 MHz using deuterated chloroform ($CDCl_3$) as a solvent at 25 °C. WEP was observed under a field emission scanning electron microscopy (Ultra 55, Zeiss, Germany). High vacuum conditions were applied and a secondary electron detector was used for image acquisition. SEM micrograph of the WEP particles were frozen in liquid nitrogen and the aqueous solvent was removed using a Labconco FreeZone freeze-dryer operated at 0.1 mbar and -20 °C for 48 h. The samples were determined via a DMA Q800 (TA Instrument, America) at a frequency of 1 Hz, and then heated from 0 to 100 °C at a rate of 5 °C/min. The test was conducted under strain control, with a strain of 0.1% and a preload of 0.01 N.

SM properties of WEP were evaluated using the fold-deploy SM test. Specimens with an original length of L_o were heated to T_{high} above the T_g in hot water. The specimens were then bent into a "U" shape circling a central axis, this length is the distance between the two ends of the specimens (L_b). After heating, the specimens were cooled to 25 °C while being held with a constant external force for 10 min. The specimens shrank immediately after the release of the load at 25 °C. The length increased from L_b to L_f. As the specimens were heated from 25 °C to T_{high}, they underwent shape recovery and the length between the two ends increased to L_r. The SM testing process is shown in Fig. 2.3; here, L_o is the original length, L_b is the length after bending at T_{high} (55, 65 and 75 °C) and cooling to 25 °C, L_f is the length at 25 °C after the release of the load, and L_r is the final recovered length. The values of the shape recovery ratio (R_r) and shape fixity ratio (R_f) are defined by Eq. (2.1).

$$R_f = \frac{L_o - L_f}{L_o - L_b} \times 100\%, \quad and \quad R_r = \frac{L_r - L_b}{L_o - L_b} \times 100\% \qquad \text{Eq.}(2.1)$$

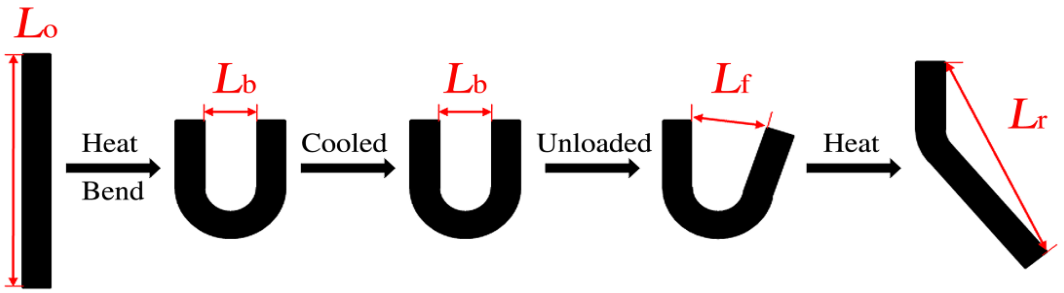

Figure 2.3 Schematic of the shape recovery performance test.

The shape memory properties of the specimens were further confirmed by the thermo-mechanical cycles which were performed using a TMA/SS6100 (Hitachi High-Tech Science Co., Japan). In step 1, the samples were heated to a high degree and then deformed by force from 0 to 450 mN at a rate 100 mN/min. In step 2, the samples were cooled to the room temperature under constant force (450 mN) to fix the deformation shape. In step 3, the force was unloaded to 0 N. In the final step, the samples was reheated the high temperature, and an additional isothermal step was included to ensure the recovery shape a high temperature. Shape fixity and recovery ratios are two important parameters for determing, and evaluating SMP characteristics, as defined by Eq. (2.2). The shape recovery and fixity ratios are determined in terms of the strain, where N is the number of thermo-mechanical cycles, R_f is the shape fixity ratio, R_r is the shape recovery ratio, ε_m is the pre-deformation strain, ε_u is the temporary strain fixed and ε_p is the permanent strain.

$$R_f(N) = \frac{\varepsilon_u(N)}{\varepsilon_m}, \quad and \quad R_r(N) = \frac{\varepsilon_m - \varepsilon_p(N)}{\varepsilon_m - \varepsilon_p(N-1)} \qquad \text{Eq.}(2.2)$$

Recovery stress tests were conducted using a TMA/SS6100. In step 1, the samples were heated to a high degree and then deformed by force from 0 to 100 and 300 mN at a rate 100 mN/min. In step 2, the samples were cooled to the room temperature under constant force to fix the deformation shape. In step 3, the force was unloaded to 0 N. In the final step, the samples were reheated from room temperature to 110 °C under a constant strain condition and the recovery stress was measured.

2.3 Results and discussion

2.3.1 Synthesis and characterization of EP-g-TX100

The formation of the EP-g-TX100 polymer network is shown in Fig. 2.1. The structures of the synthesized EP-g-TX100 were determined from the attenuated total reflectance (ATR)-FTIR spectra. Fig. 2.4, shows a new stretching vibration absorption peak of the C=O group at 1730 cm^{-1} and a bending vibration absorption peak of the N-H group at 1535 cm^{-1} in curve (c) and (d), respectively, these peaks confirm that a grafting reaction occurred between the hydroxyl groups of the epoxy resin (or TX100) and the isocyanate groups of TDI [19]. The stretching vibration absorption peak of the epoxy group at 915 cm^{-1} can also be observed in curve (c), indicating that the epoxy groups. The signal of epoxy at 915 cm^{-1} vanishes when excessive concentrations of the curing agent were added to EP-g-TX100. This disappearance suggests that a curing reaction occurred between EP-g-TX100 and the curing agent (Fig. 2.4d).

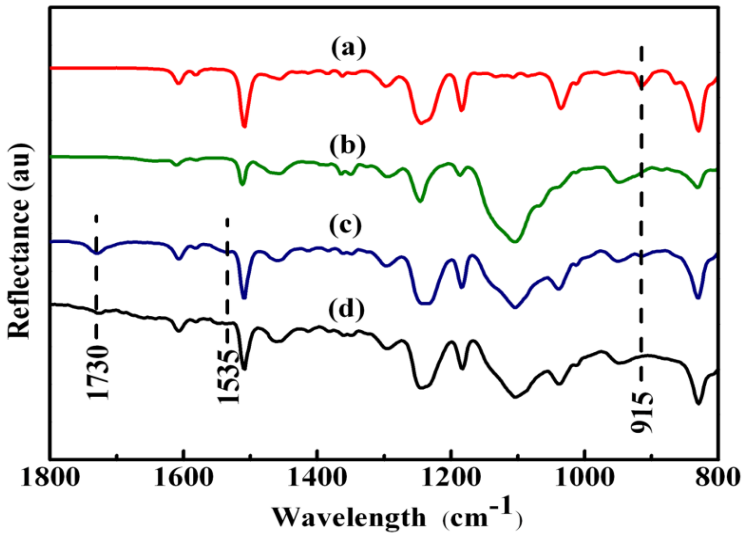

Figure 2.4 ATR-FTIR curves of (a) pristine epoxy, (b) Triton X-100, (c) EP-g-TX100, and (d) cured EP-g-TX100.

The structures of the synthesized EP-g-TX100 were further confirmed via ^{1}HNMR spectroscopy. The complete assignment of the proton signals is shown in Fig. 2.5. In the ^{1}HNMR spectrums of (A) pristine epoxy and (B) EP-g-TX100, the sharp resonance

centered at 3.64 ppm (peak a) is attributed to methylene protons of PEO [20]. Furthermore, resonance signals at 1.89 ppm (peak b) are assigned to the NH protons of -OCONH- groups [19]. The peaks at 6.82 ppm (peak c) and 7.14 ppm (peak d) are attributed to the aromatic protons of the bisphenol A moiety of epoxy resin. Moreover, the peak at 1.63 ppm (peak g) corresponds to the methyl protons. The glycidyl terminal group is characterized by five peaks in the range of δ=2.74 ppm to 4.66 ppm range (ranges e and f) [21]. These results indicate that the as-synthesized EP-g-TX100 exhibits the expected structure.

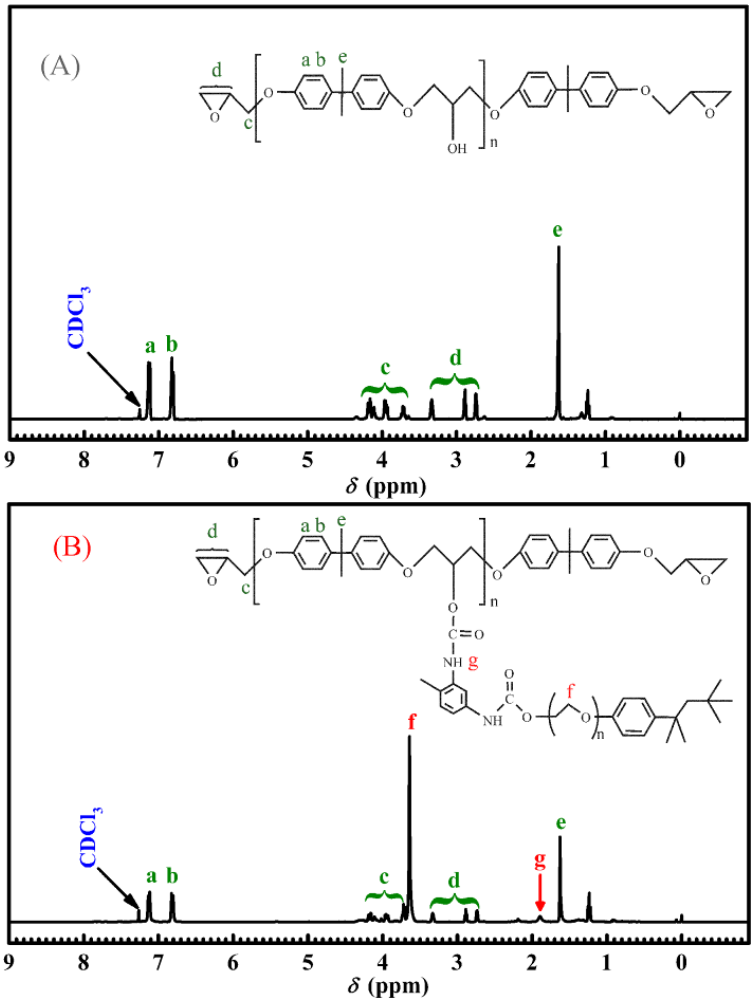

Figure 2.5 ^{1}HNMR spectra of (A) pristine epoxy and (B) EP-g-TX100.

Fig. 2.1 shows the formation and structure of the emulsifier EP-g-TX100. EP-g-TX100 molecular is composed of three parts: epoxy, TDI, and TX100. The non-ionic surfactant, TX100 (Hydrophile-Lipophile Balance (HLB) =13.5) [22], it is an

excellent and wildly used surfactant for oil/water (O/W) emulsion, because of its special structure: one end is polar hydrophilic group and the other end is non-polar hydrophobic group. TX100 can reduce the emulsion particle coalescence, and it can also protect the particles from the intense shear-induced aggregation [23]. However, TX100 has an average molecular weight of 650 g/mol. Thus, it acts as a plasticizer to the polymer matrix. In addition, TX100 can migrate to the filler-polymer interface during and/or after the composite processing. A high TX100 concentration in the interphase region acts as a weak boundary layer and reduces the strength of the filler-polymer adhesive. Gerin concluded that the driving force for surfactant migration is the thermodynamic reduction of the surface free energies [24]. After curing with the epoxy curing agent, the epoxy modified TX100 (EP-g-TX100) can be fixed to the epoxy 3-D network structure, because of EP-g-TX100 has two epoxy groups which can be covalently reacts with epoxy curing agent. On the other hand, general, the HLB value of a non-ionic surfactant as the emulsifier for O/W system is between 8 and 18, and the closer of the HLB value between emulsifier and oil (or polymer) is better. According to Eq. (2.3) [25], where f_i is the mass (or weight) fraction of the surfactant i, the HLB value of EP-g-TX100 is approximately 10.1, which is lower than HLB value of TX100. In other words, TX100 dangled epoxy EP-g-TX100 is potential emulsifier with an excellent emulsification adaptability, efficiency and compatibility with epoxy in epoxy/water system.

$$\mathrm{HLB} = \mathrm{HLB_i} \times f_i \qquad \text{Eq.(2.3)}$$

2.3.2 Morphology and structure of WEP

The images of the WEP prepared via phase-inversion technology are shown in Fig. 2.6A-C. The WEP particles had an average diameter of 137 nm, with particles ranging from 50 nm to 300 nm (see Fig. 2.6D), as determined by particle-size analysis (Delsa Nano C, Beckman Coulter, USA). The sample for SEM was frozen in liquid nitrogen, and the aqueous solvent was removed using a Labconco FreeZone freeze-dryer operated at 0.1 mbar and -20 °C for 48 h. According to the SEM and TEM results, a schematic of

the epoxy/EP-g-TX100 emulsion illustrating the various species present in colloidal length scale is shown in Fig. 2.6E. Micelles are formed since the emulsifier concentration is above the critical micelle concentration (CMC). High shear produces both emulsifier micelles and emulsifier-stabilized epoxy droplets. The interfacial layer of emulsion droplet was composed of emulsifier EP-g-TX100, and the epoxy was encapsulated in the droplet. The emulsifier causes a lowering of the interfacial tension and provides the droplet steric and electro static repulsion to stabilize it against coalescence.

WEP system is an inhomogeneous two-phase system that consists of water as continuous phase and resin emulsion droplets as dispersed phase. Water evaporates after applying WEP under atmospheric conditions. When most of the water is evaporated, the emulsion droplets come into contact and form a close pack of spheres, with the residual water (with most of the hardener dissolved in it) filling the gaps in between. Then, as the first stage of the coalescence process the WEP droplets form hexagons before merging to a supposedly homogeneous, continuous phase. When the state of dense packing and, even more so, when the hexagonal state is reached, hardener molecules penetrate the WEP droplets and react with the epoxy. Meanwhile, most of the residual water and any added coalescing solvents diffuse into the film surface and evaporate [26]，as shown in Fig. 2.7. However, the curing mechanism of the WEP after freeze-drying has a slight difference from the process under atmospheric conditions. During mixing of the WEP and curing agent, the water content of the system was approximately 50%. When frozen in liquid nitrogen (-196 °C) and freeze-dried at a low temperature of -55 °C, the WEP and curing agent system was in ice form. After water in ice form sublimated, epoxy and hardener composite powder was obtained. The powder become sticky when exposed to air, because WEP is made from liquid epoxy, which starts to melt at room temperature. A pressure of 5 MPa was applied to pack the powder and decrease the distance between the epoxy and curing agent. In addition, the last post-curing step was performed at 120 °C for 12 h to ensure curing completion. The molecular weight, viscosity and T_g of the epoxy molecules increased during the curing processing, resulting in harder droplets that are not prone to good coalescence [18].

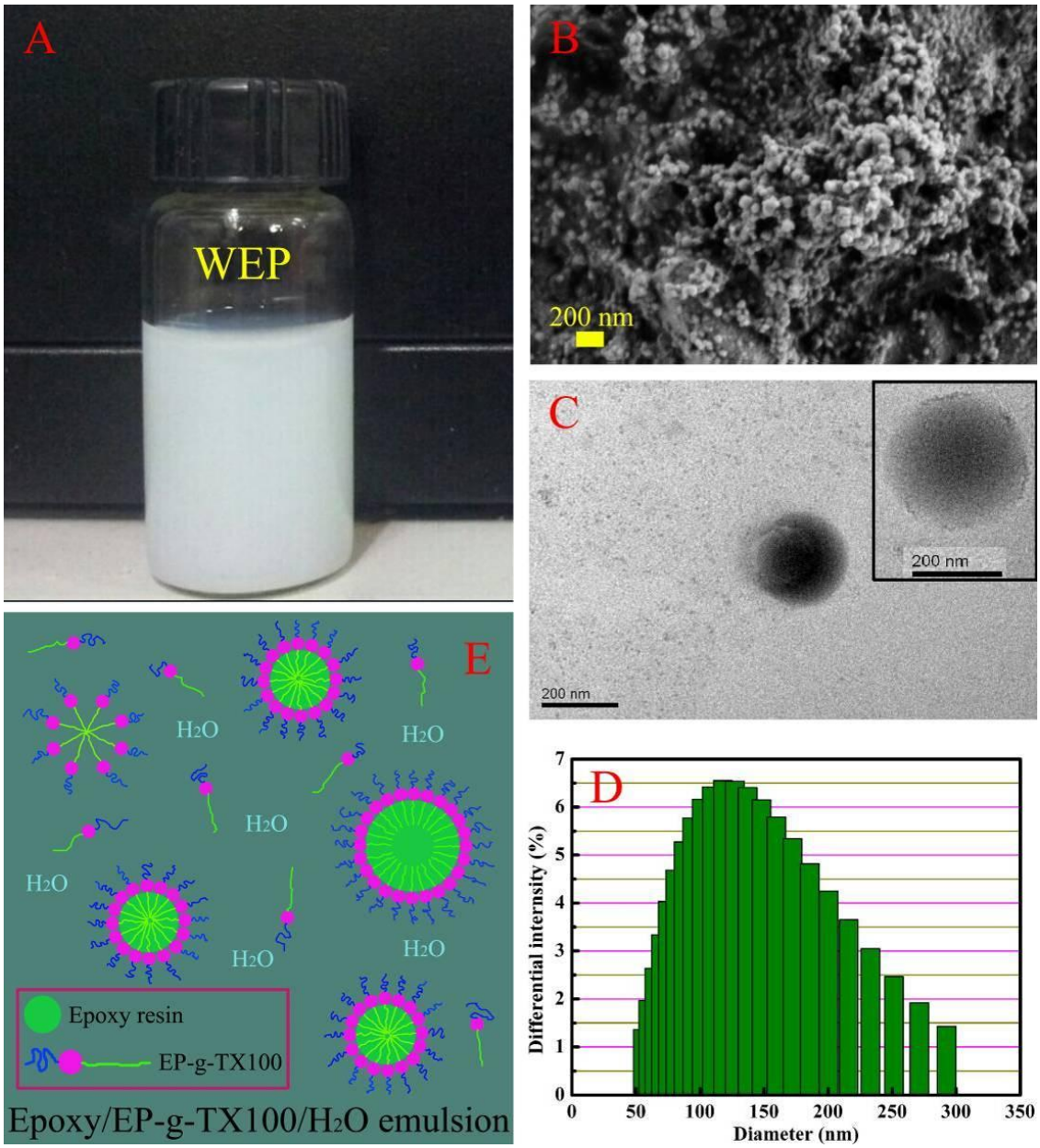

Figure 2.6 (A) Photographs of the water-borne epoxy (WEP); (B) SEM micrograph of WEP particles; (C) TEM micrograph of WEP particles; (D) The particle size distribution of WEP; and (E) Schematic representation of the main components present in WEP.

2.3.3 SM property of WEP

SM property of WEP tested via fold-deploy method at 55, 65, and 75 °C (all above T_g, as shown in Fig. 2.8) is shown in Table 2.1. The SME of epoxy is driven by entropy among the polymer chains between the cross-linked molecules. Below the SM transition

temperature (T_{trans}), polymer chains between network points cannot undergo conformational changes and are locked into shape unless a suitably large mechanical force is applied. However, the chains can undergo rotational conformation changes at relatively lower stresses when heated to their T_{trans}. Above the T_{trans}, the polymer chains begin to align as the polymer deforms, thereby increasing the energy stored in the material as the entropy of the chains decreases. Upon cooling in the deformed shape, the polymer chains can no longer freely rotate. When the material is heated above its T_{trans} without constraint, the polymer chains recover the stored energy by returning to the initial high-entropy configuration, and return to their initial shape [26].

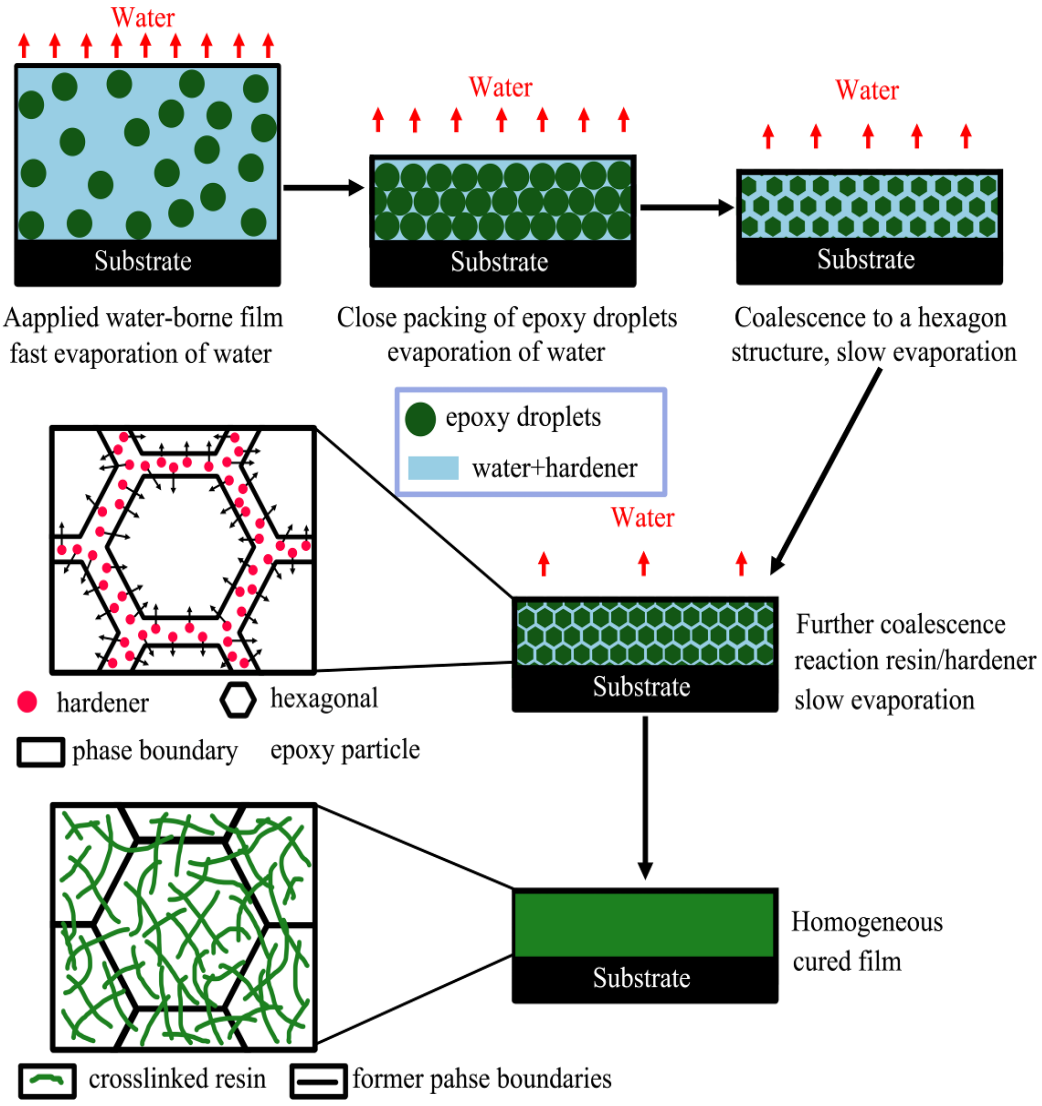

Figure 2.7 Film formation of the WEP and hardener system.

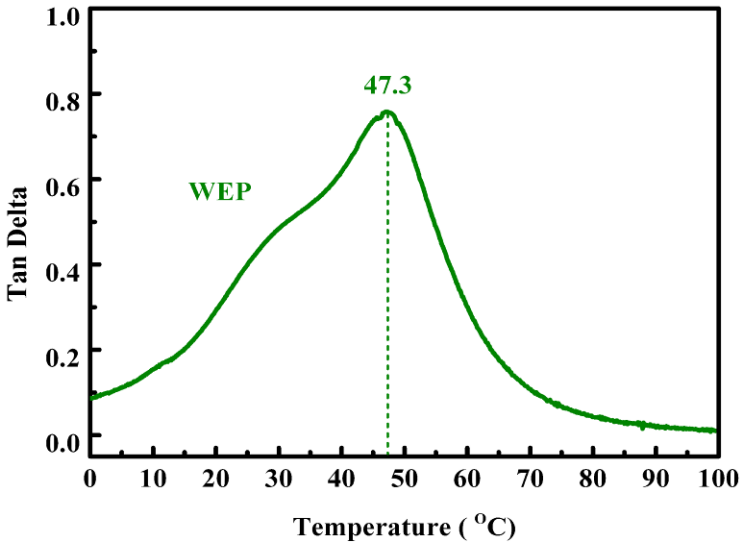

Figure 2.8 Tan delta of WEP.

Table 2.1 Shape memory property results of WEP got form fold-deploy method.

Sample	Shape recovery ratio (%)			Fixity ratio (%) (25 °C, 24 h)
	(55 °C)	(65 °C)	(75 °C)	
Neat WEP	99.30	99.90	100.0	95.55

SM properties of WEP were also investigated by TMA/SS6100. The results of the SM fixity and recovery ratios are shown in Fig. 2.9 and 2.10 and Table 2.2. Shape fixity and recovery carried out near and above the glass transition temperature (T_f =T_r=52 °C, T_f =T_r=65 °C, and T_f =T_r=80 °C), with R_f and R_r above 97% in all cases. Consecutive shape memory cycling experiments (T_f =T_r=52 °C, T_f =T_r=65 °C, and T_f =T_r=80 °C) show that shape memory performance is highly reproducible (Figure 2.10). Fig. 2.10 (A_1, B_1, and C_1) shows the stress–strain-temperature diagrams of WEP at three different temperatures. Three cycles have an excellent repeatability at different temperatures. Furthermore, in the first cycle, the shape recovery ratios over 90% of the epoxy reinforced with silica. WEP has a shape recovery ratio of more than 99% after the second cycle. The ratio tends to be a constant 100% with increased cycle numbers. This phenomenon is called “training” effect [27]. Fig. 2.11 shows that the recovery stresses of WEP at different deforming iso-strains, and the recovery stress increase with the iso-strain. The recovery stresses are 0.19 and 0.60 MPa at iso-strain 4.6% and 17.3%, respectively. The shape recovery behavior of WEP is shown in Fig. 2.12.

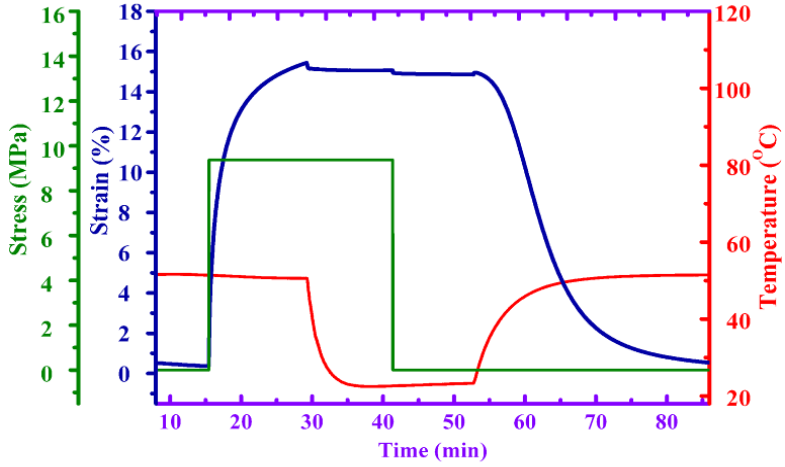

A

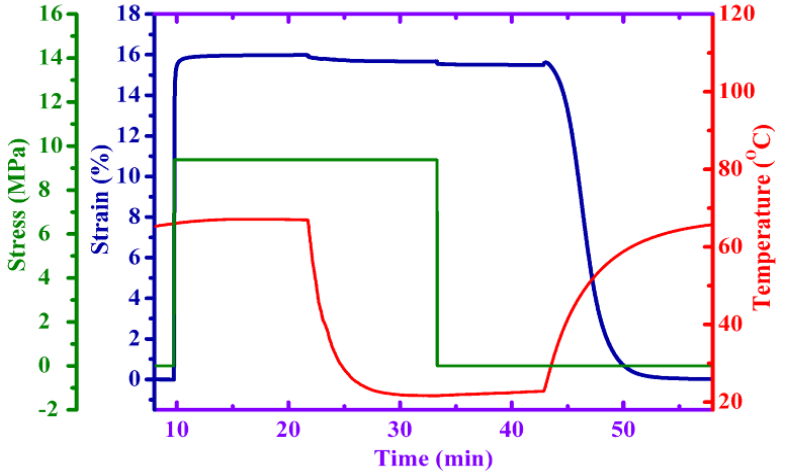

B

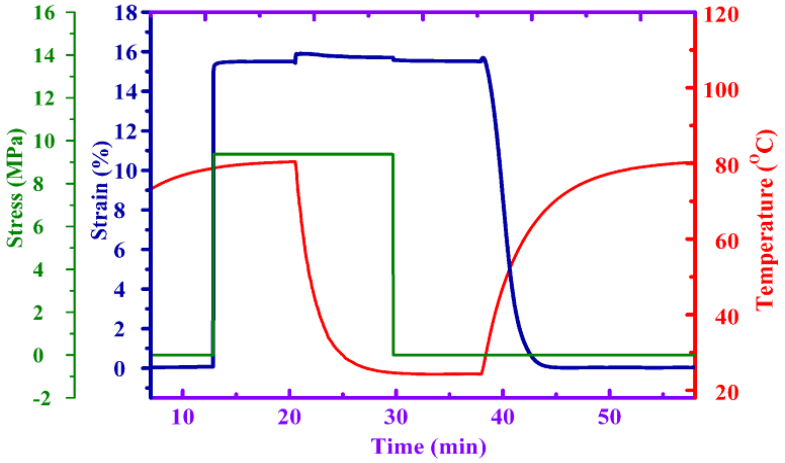

C

Figure 2.9 Dual-shape memory cycle at T T_f =T_r=52 °C (A), 65 °C (B) and 80 °C (C).

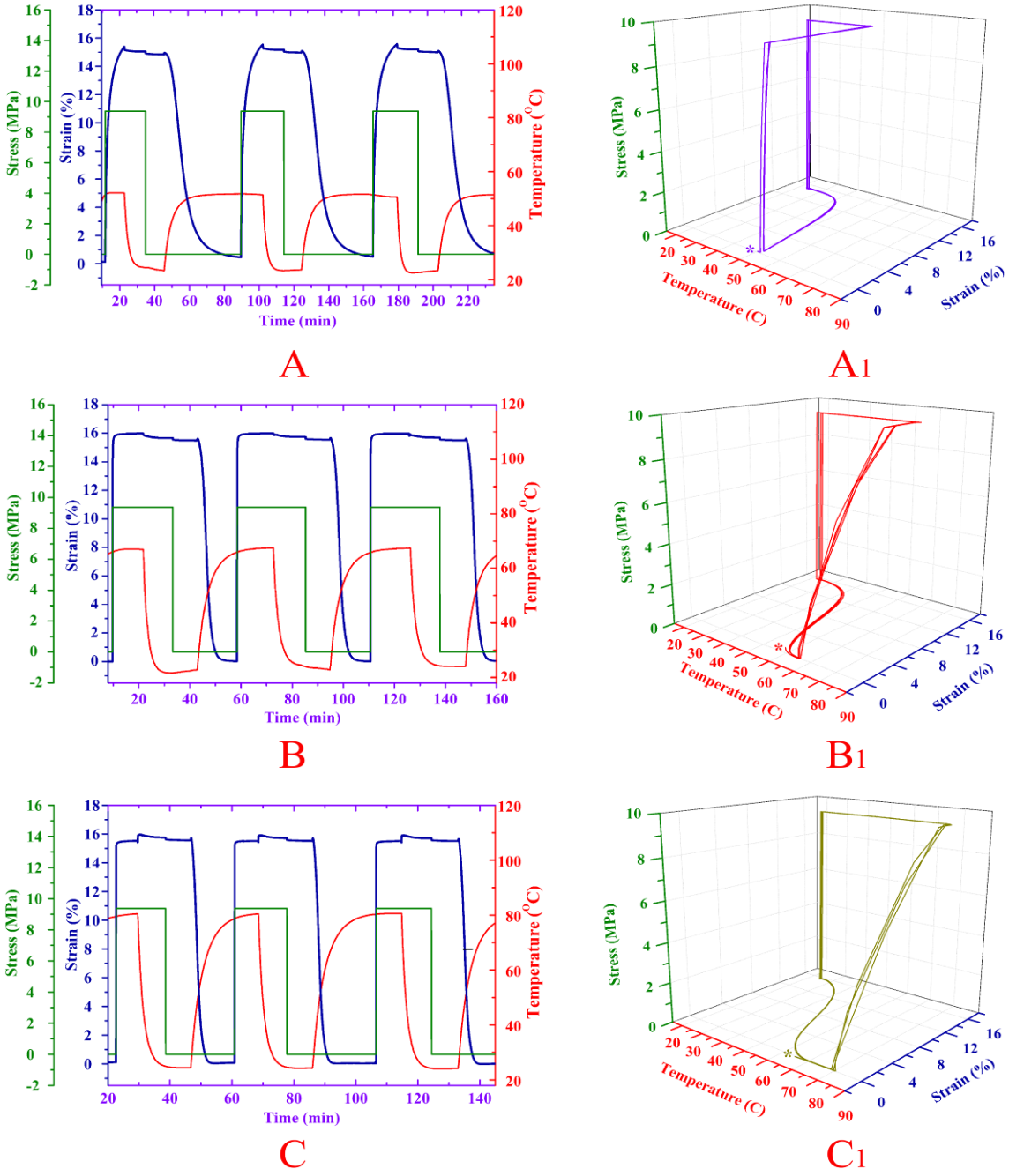

Figure 2.10 Consecutive dual-shape memory cycling of WEP: (A and A_1) T_f =T_r=52 °C, (B and B_1) T_f =T_r=65 °C, and (C and C_1) T_f =T_r=80 °C.

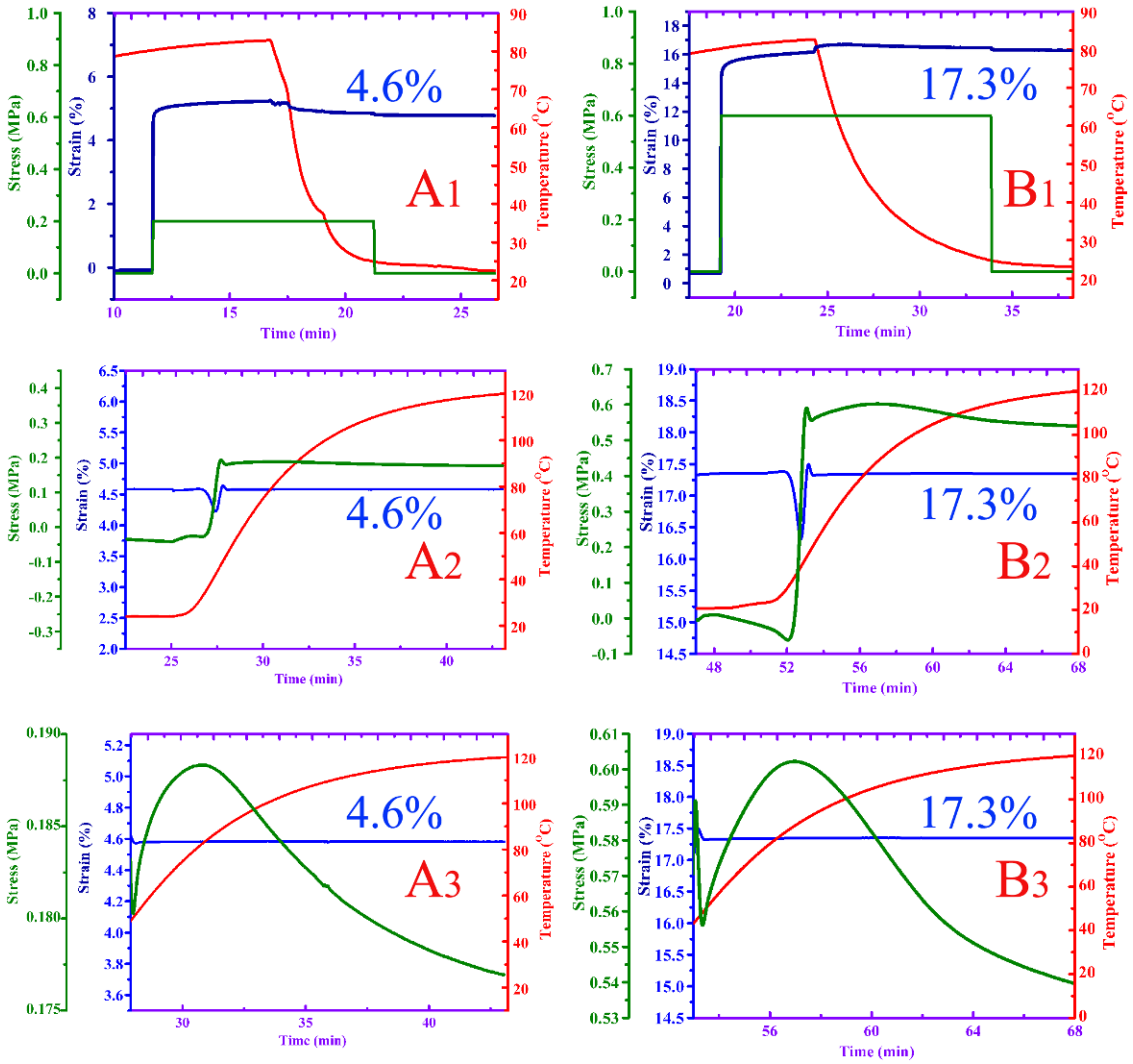

Figure 2.11 Stress generated during iso-strain recovery of WEP deformed at iso-strains: (A_1 and B_1) fixing processing, (A_2 and B_2) shape memory recovery force form room tempreature to 120 °C, and (A_3 and B_3) shape memory recovery force near and above T_g .

Table 2.2 Shape memory property results of WEP got form TMA test.

Cycle number	Shape recovery ratio (%)			Fixity ratio (%)		
	(52 °C)	(65 °C)	(80 °C)	(52 °C)	(65 °C)	(80 °C)
1	97.3	99.9	100	99.1	99.3	99.2
2	99.6	100	100	99.1	99.3	99.2
3	98.9	100	100	99.1	99.3	99.2

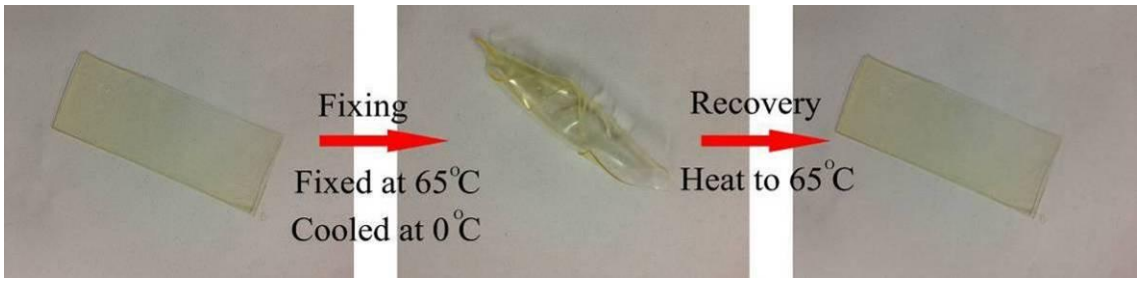

Figure 2.12 Illustration of the SME of WEP.

2.4 Conclusions

This study designed and successfully synthesized EP-g-TX100, which is a reactive copolymer that covalently reacts with the curing agent through the side chains, as proven via proved by FTIR and HNMR, respectively. In addition, EP-g-TX100 was shown highly effective in preparing of epoxy emulsion. With WEP, the freeze-drying and hot-press molding technology was applied to preparing the epoxy material which shows excellent SM property. WEP exhibits high shape recovery and fixity ratio above 97% even after 3 thermo-mechanical cycles. The simple approach employed in the present study is a feasible and effective method for synthesizing SM materials. Compared with the conventional method for SM epoxy preparation, the latex technology has great advantages, such as convenience and environmental friendliness. Moreover, this technology can be applied to both liquid and solid epoxy resins.

Reference

[1] J. S. Leng, X. Lan, Y. J. Liu, S. Y. Du, *Prog. Mater. Sci.*, 56(2011)1077.

[2] Y. B. Dong, J. Ding, and Y. Q. Fu, *Compos. Sci. Technol.*, 76(2013)8.

[3] Y. B. Dong, Q. Q. Ni, Y. Q. Fu, *Composites: Part A*, 72(2015)1.

[4] M. M. Ma, L. Guo, D. G. Anderson, R. Langer, *Science*, 339(2013)186.

[5] X. J. Han, Z. Q. Dong, and S. Zhang, *Macromol. Rapid. Commum.*, 33(2012)1055.

[6] A. Lendlein, H. Y. Jiang, and R. Langer, *Nature*, 434(2005)879.

[7] L, Viry, C, Merrcader, and P. Poulin, *J. Mater. Chem.*, 20(2010)3487.

[8] J. S. Leng, H. B. Lv, and S. Y. Du, *Appl. Phys. Lett.*, 91(2007)144105.

[9] Y. Cai, J. S. Jiang, and W. G. Zhang, *Composites: Part A*, 53(2013)16.

[10] I. K. Kuder, A. F. Arrieta, and P. Ermanni, *Prog. Aerosp. Sci.*, 63(2013)33.

[11] A. Lendlein, R. Langer, *Science*, 7(2002)1673.

[12] S. Sharifi, M. Behl, A. and Leddlein, *Biomaterials*, 34(2013)8105.

[13] H. B. Lu, J. S. Leng, and S. Y. Du, *Compos. Sci. Technol.*, 71(2011)1427.

[14] J. L. Hu, S. J. Chen, *J. Mater. Chem.*, 20(2010)3346.

[15] C. M. Chen, C. L. and T. Xie, *Adv. Funct. Mater.*, 23(2013)3813.

[16] Y. Li, S. S. Chen, and J. Q. Sun, *Adv. Mater.*, 24(2012)4578.

[17] Y. B. Dong, Q. Q. Ni, and Y. Q. Fu, *Mater. Lett.*, 132(2014)206.

[18] A. Wegmann, *Prog. Org. Coat.*, 32(1997)231.

[19] Y. C. Chern, S. M. Tseng, K. H. Hsieh, *J. App. Polym. Sci.*, 74(1999)328.

[20] D. R. Lu, Y. Wang, H. Wang, R. K. Bai, *Eur. Polym. J.*, 46(2010)1417.

[21] F. G. Garcia, B. G. Soares, *Polym. Test.*, 22(2003)51.

[22] M. Das, R. K. Mitra, *Colloid Polym. Sci.*, 292(2014)635.

[23] D. L. Xie, P. Arosio, H. Wu, *Langmuir*, 27(2011)7168.

[24] P. A. Gerin, Y. Grohens, and Y. Holl, *J. Adhes. Sci. Technol.*, 13(1999)217.

[25] C. Ricardo, P. Melina, and C. Bregni, *Int. J. Pharm.*, 356(2008)44.

[26] M. D. Prima, K. Gall, and S. C. Arzberger, *Mech. Mater.*, 42(2010)304.

[27] Q. Q. Ni, C. S. Zhang, and Y. Q. Fu, *Compos. Struct.*, 81(2007)176.

CHAPTER THREE

Preparation and properties of CNT/water-borne epoxy shape memory nanocomposites

3 Preparation and properties of CNT/WEP shape memory nanocomposites

3.1 CNT/WEP shape memory nanocomposites

Carbon nanotube (CNT)/WEP SM nanocomposites were successfully synthesized via freeze-drying and hot-press molding. CNTs were mixed directly with a WEP. WEP composites were obtained from these mixtures by freeze-drying and compressing under a pressure of 10 MPa at 120 °C for 2 h. The morphology and mechanical properties of the WEP composites were investigated by transmission electron microscopy (TEM), scanning electron microscopy (SEM), dynamic mechanical analysis and tensile testing. The shape memory (SM) properties of WEP composites were evaluated by fold-deploy SM testing. The effects of filler content and recovery temperature on the SM properties were revealed through systematic variation. Results confirmed that CNTs were homogenously dispersed and incorporated into the WEP matrices. Thus, significant improvements in the mechanical and SM properties of the composites were achieved.

3.1.1 Introduction

Shape memory polymers (SMPs) can be fixed into a stable temporary shape, and then revert to their permanent shape when triggered by an external stimulus [1-5]; this recovery process can be triggered by various stimuli, including heat [6-10], water [11, 12], pH [13], light [14, 15], electricity [16, 17], and magnetic fields [18, 19]. The most typical stimulus is direct heating, which leads to a temperature increase. Many excellent review papers have been published on various SMPs, especially thermal-responsive SMPs [20-22]. SMPs present several advantages over shape memory alloys (SMAs): (1)

variety of external stimuli able to promoting recovery; (2) highly flexible programming; (3) abundance of design approaches; (4) tunable properties; (5) suitability for biomedical applications; and (6) low weight and cost [6]. SMPs are widely used in applications such as aerospace structures [23], biomedical devices [24-27], sensors [28, 29], textiles [6, 30], dry adhesives [31, 32], self-crack-healing applications [33-35], and so on.

A stable polymer network and reversible switching transition of the polymer are two prerequisites leading to polymer shape memory effect (SME). A stable network of SMPs determines the original shape of the polymer, which network may be formed by an entangled molecule crystalline phase, chemical cross-linking or an interpenetrated network. The locking mechanism of the network is represented by reversible switching transition responsible for fixing a temporary shape [3]. Epoxies are widely used in many non-SM applications, such as coatings, adhesives, construction, and manufacturing, and exhibit high strength, good thermal stability, and excellent chemical resistance. Many recent studies have proven the favorable SM properties of epoxies [6, 36-39]. The shape recovery ratio and elastic modulus of epoxies range from 98% to 100% and from 2 GPa to 4.5 GPa, respectively [1]. The SME of epoxy is driven by entropy among the polymer chains between the cross-linked molecules. Below the SM transition temperature (T_{trans}), polymer chains between network points cannot undergo conformational changes and are locked into shape unless a suitably large mechanical force is applied. However, the chains can undergo rotational conformation changes at relatively lower stresses when heated to their T_{trans}. Above the T_{trans}, the polymer chains begin to align as the polymer deforms, thereby increasing the energy stored in the material as the entropy of the chains decreases. Upon cooling in the deformed shape, the polymer chains can no longer freely rotate. When the material is heated above its T_{trans} without constraint, the polymer chains recover the stored energy by returning to the initial high-entropy configuration, and return to their initial shape [40].

In our previous research, we found that WEP has excellent SM property, besides a mechanical strength and SM fixity ratio lower than those of common (solvent-based) SM epoxy. Fortunately, issues related to the processing and thermomechanical

properties of SMPs could be resolved by modifying the molecular structure of the applied polymer and adding functional fillers into the polymer [1]. Improvements in the thermal and mechanical properties of SMPs through incorporation of inorganic particles have been achieved. The most popular fillers for SMP matrices are carbon nanotubes (CNTs) [41, 42]. CNTs are used to reinforce the strength of the matrices and induce electricity and heating to enable shape recovery. CNTs have excellent mechanical properties, small diameters, and low density [43-45]. In the present study, CNTs were applied to improve the mechanical and SM properties of the CNT/WEP nanocomposites synthesized via freeze-drying, and hot-press molding. The effect of CNT addition on the mechanical and SM properties of the WEP was discussed.

3.1.2 Experimental

3.1.2.1 Materials

The WEP surfactant EP-g-TX100 and WEP emulsion (50% solid weight) with a particle size range of 50 nm to 300 nm, which have been successfully synthesized in our previous research [46]. CNTs (VGNF®, Showa Denko K. K., Japan) with an average diameter about 80 nm were fabricated via thermo-chemical vapor deposition [44]. A commercially available room-temperature curing agent (AB-HGF®, Zhejiang Anbang New Material Development Co., Ltd, China) was obtained from commercial sources and used as received.

3.1.2.2 Preparation of CNT/EP-g-TX100 dispersions

CNTs were dispersed in water by mixing with a calculated content of EP-g-TX100 followed by intensive stirring for 24 h with the water bath temperature maintained at around 25 °C. The ratios of EP-g-TX100/CNT are from 0.25:1 to 2:1 by weight. After stirring for 6 h, 35 mL of cold DI water was added to the flask and the mixture then was stirred for another 18 h. After the maximum dispersion was achieved, the CNTs dispersions were bottled.

3.1.2.3 Preparation of CNT/WEP SM nanocomposites

A three-step procedure was used to prepare the CNT/WEP SM nanocomposites. Firstly, CNTs were added to a beaker with diluted WEP (5% solid weight) and dispersed to homogeneity at room temperature using an intensive mixer. The WEP curing agent was then sequentially added to the mixture. The weight ratio of the WEP to the cuing agent was 4:1. Second, the mixture was frozen in liquid nitrogen for 5 min, and the aqueous solvent was removed using a Labconco Free Zone freeze-dryer operated at 0.1 mbar and -55 °C for 7 d. Finally, the resulting composite powder was compressed into films at 120 °C for 2 h under a pressure of 10 MPa.

3.1.2.4 Characterization

TEM images of the CNT/WEP SM nanocomposites were examined using a transmission electron microscope (JEM-2100F, JEOL, Japan) operated at 200 kV. TEM images of the composites were obtained from ultrathin sections that were cut with a glass knife on the Leica EM UC7 ultramicrotome (Leica, Germany). SEM observations of the specimens were conducted using a field emission scanning electron microscope (Ultra 55, Zeiss, Germany) at an operating voltage of 3 kV. Prior to testing, the samples were sputter-coated with gold to impart electrical conductivity and reduce charging artefacts. High vacuum conditions were applied and a secondary electron detector was used for image acquisition. Tensile test of the CNT/WEP nanocomposites were conducted using a testing machine (INSTRON 3367, USA) at a crosshead speed of 5 mm/min on dumbbell-shape specimens at room temperature. At least five effective specimens were tested for each sample. The CNT/WEP nanocomposites were determined via a DMA Q800 (TA Instrument, America) at a frequency of 1 Hz, and then heated from 0 to 100 °C at a rate of 5 °C/min. The test was conducted under engineering strain control, with a strain of 0.1% and a preload of 0.01 N.

SM fixity and recovery ratios are important parameters in evaluating SMP characteristics [1, 8]. SM properties of pristine WEP and the developed composites

were evaluated using the fold-deploy SM test. Specimens with an original length of L_o were heated to T_{high} above the T_g in hot water. The specimens were then bent into a "U" shape circling a central axis, this length is the distance between the two ends of the specimens (L_b). After heating, the specimens were cooled to 25 °C while being held with a constant external force for 10 min. The specimens shrank immediately after the release of the load at 25 °C. The length increased from L_b to L_f. As the specimens were heated from 25 °C to T_{high}, they underwent shape recovery and the length between the two ends increased to L_r. L_o is the original length, L_b is the length after bending at T_{high} (55, 65 and 75 °C) and cooling to 25 °C, L_f is the length at 25 °C after the release of the load, and L_r is the final recovered length. The values of the shape recovery ratio (R_r) and shape fixity ratio (R_f) are defined by Eq. (3.1).

$$R_f = \frac{L_o - L_f}{L_o - L_b} \times 100\%, \quad and \quad R_r = \frac{L_r - L_b}{L_o - L_b} \times 100\% \qquad (3.1)$$

3.1.3 Results and discussion

3.1.3.1 EP-g-TX100 as a dispersant for CNTs in aqueous

Fig. 3.1 shows the overall morphology of pristine CNTs using TEM (A) and the highly magnified structure of an individual CNT using HR-TEM. CNTs are used to reinforce the strength of the matrices and induce electricity and heating to enable shape recovery. However, the dispersion of CNTs into individual particles or small bundles has remained a vexing problem that limits the use of the excellent properties of CNTs in composite applications. Fig. 3.2 shows the results of a dipping test. The agglomerates of CNTs are visible on the glass rod in the absence of any dispersants (Fig. 3.2A). However, the glass rod appeared very uniformly coated with the CNT/EP-g-TX100 supernatant after dipping the supernatant. This result illustrates that EP-g-TX100 is a good potential dispersant for CNTs (Fig. 3.2B). Pristine CNTs completely floated on the water. The supernatant was transparent and colorless. The CNT/EP-g-TX100 solutions were stable and did not precipitate after at room temperature. The dispersion effect of

EP-g-TX100 was further confirmed via UV-vis spectroscopy.

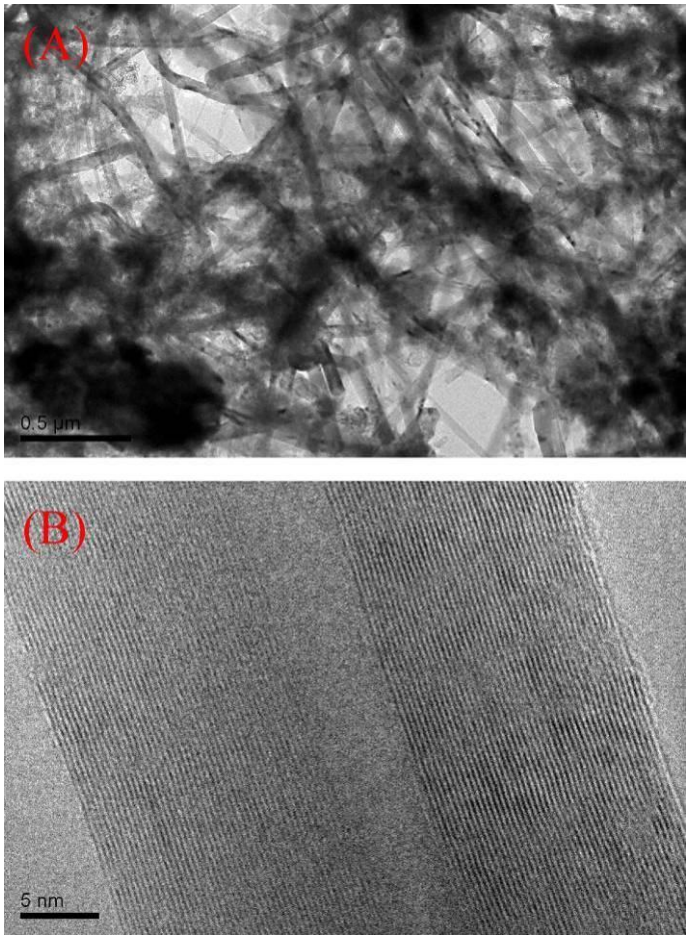

Figure 3.1 Overall morphology of pristine CNTs using TEM (A); and the highly magnified structure of an individual CNT using HR-TEM (B).

Fig. 3.3 shows the UV-vis spectra of the CNT solutions after the maximum dispersion were achieved. The corresponding spectra for the solution show two maximum peaks at 220 nm to 300 nm. These peaks gradually decrease from UV to near-IR, particularly in the longer wavelength range. For the sample without dispersant, almost no absorption is evident in the UV-vis spectrum, as shown in curve (B). The area under the UV-vis spectrum (A) is larger than the area below the spectrum line (B), implying a higher number of individual CNT particles in the solution with EP-g-TX100. These phenomena indicate that EP-g-TX100 significantly improves the CNT solubility in water. The EP-g-TX100 molecules or micelles that may have been adsorbed onto the CNT surface not only reduced the surface tension, but also separated the lager

agglomerates by overcoming the strong van der Waals interactions, to maintain good stability. These results suggest that EP-g-TX100 has a considerably dispersing capability for CNTs.

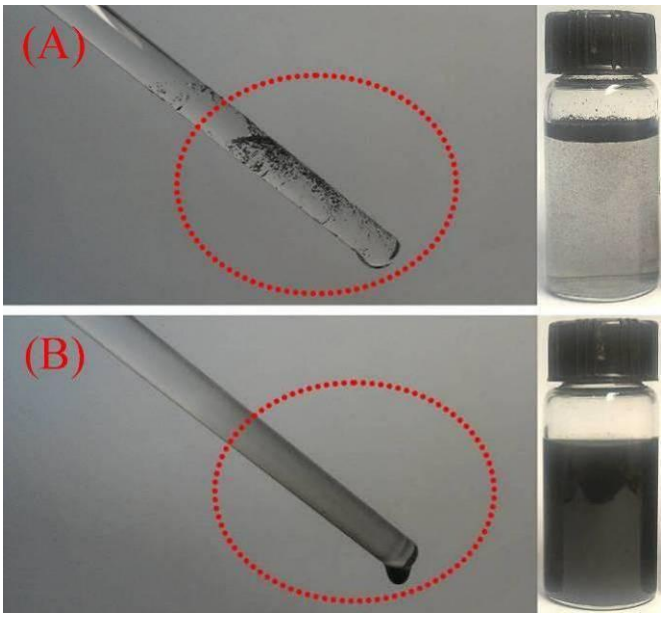

Figure 3.2 Dipping test to evaluate the dispersion of CNTs in water: (A) without any dispersant and (B) with EP-g-TX100.

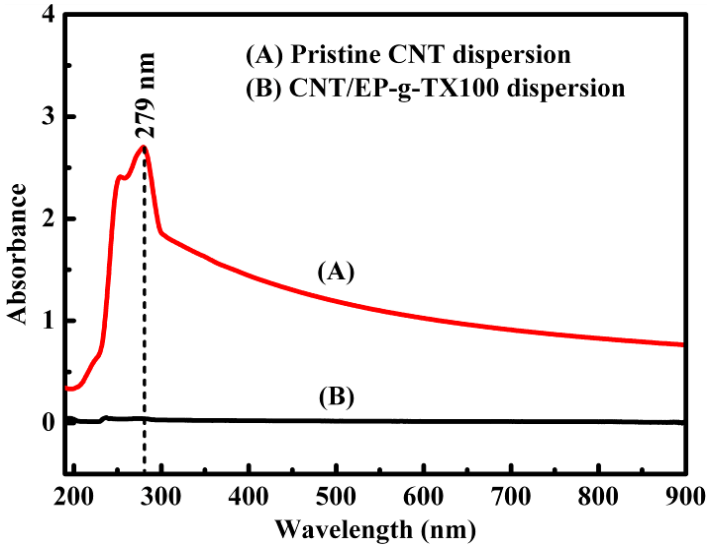

Figure 3.3 Evolution of the UV-vis spectra of aqueous 0.4 wt% CNT-0.8 wt% EP-g-TX100 solution.

The dispersion of CNTs and EP-g-TX100-functionalized CNTs in water was examined via TEM. Fig. 3.4 shows representative TEM images of CNTs and

EP-g-TX100 modified-CNTs. Before the modification, CNTs are aggregated, bundled, and closely packed (Fig. 3.4A). After EP-g-TX100 treating, the aqueous dispersibility of CNTs is significantly improved while retaining the CNT structure (Fig. 3.4B). The TEM images (Fig. 3.4B) clearly reveal that CNTs are covered with a coating layer, which is assumed to be EP-g-TX100 layered on the CNT surfaces. Moreover, the test results also show that the higher the EP-g-TX100/CNT mass ratio, the higher dispersion of EP-g-TX100 on the copper grids (Fig. 3.4C-F).

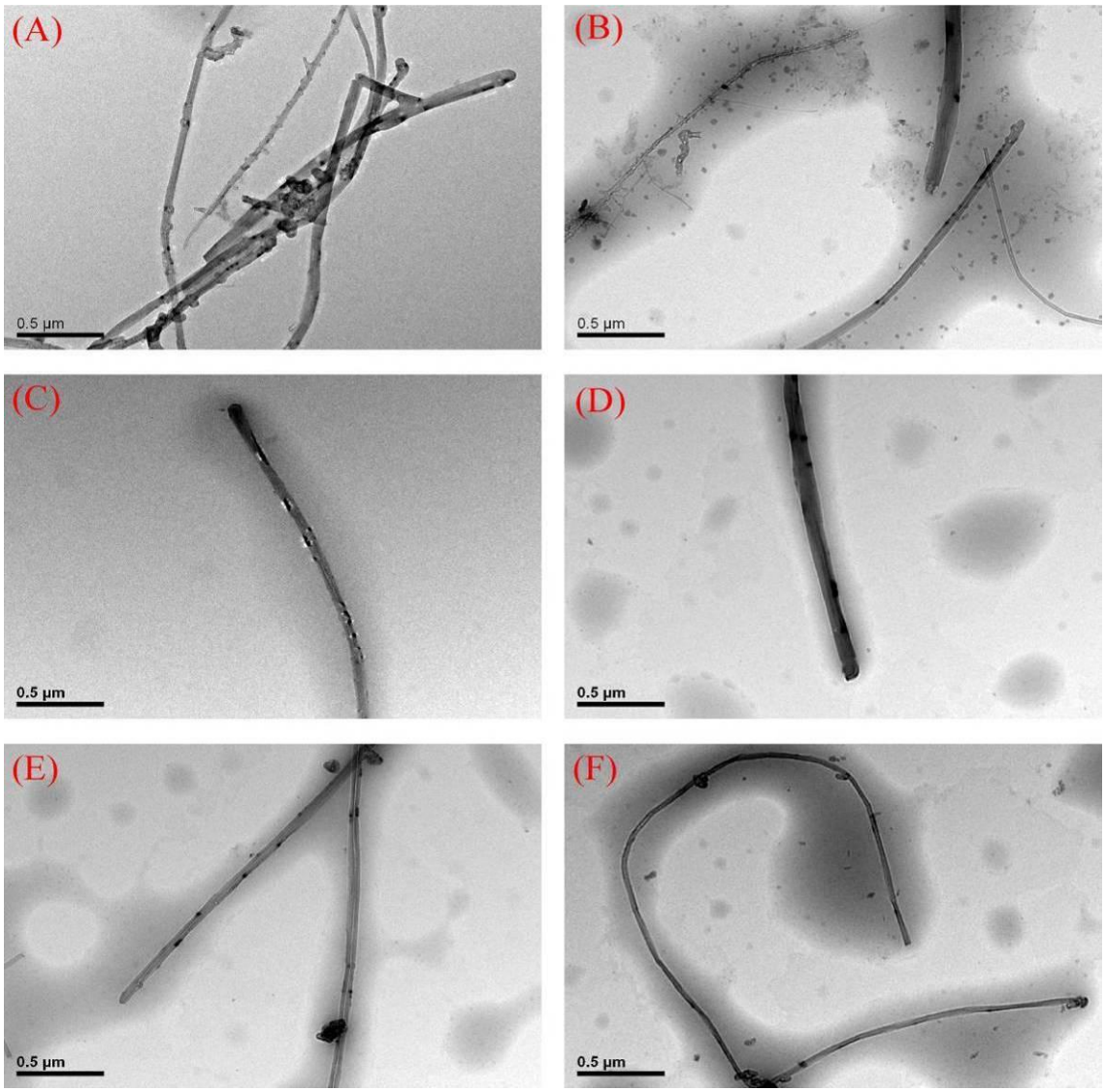

Figure 3.4 TEM images of (A) pristine CNTs; (B) EP-g-TX100 functionalized CNTs; and different EP-g-TX100/CNT mass ratio EP-g-TX100-functionalized CNTs: (C) 0.25:1; (D) 0.5:1; (E) 1:1; and (F) 2:1, respectively.

The interaction between the copolymers EP-g-TX100 and CNTs was investigated

via Raman spectroscopy. As shown in Fig. 3.5, shows no significant increase in the peak intensity of the D-band (represents disorder induced character of CNTs at approximately 1360 cm^{-1} [44]) in CNT/EP-g-TX100 (A) and pristine CNTs (B), indicating that the CNT graphene structure was well-protected after non-covalent functionalization with EP-g-TX100. Upshifts of approximately 5 cm^{-1} were observed when comparing the G-band (corresponds to the sound sp^2 carbon networks of CNTs at about 1580 cm^{-1} [44]) of CNT/EP-g-TX100 (A) with those of pristine CNTs (B). The 5 cm^{-1} upshift can be attributed to the lose electrons of CNTs [47], which suggests that a molecular level interaction (π-π stacking) occurred between CNTs and the EP-g-TX100 molecules. The higher efficiency of EP-g-TX100 in dispersing CNTs may be attributed to its distinct structure, wherein the benzene rings of the epoxy and TX100 may have a strong π-π interaction with the CNTs wall. As illustrated in Fig. 3.6, a copolymer for steric stabilization consists of lyophobic and lyophilic blocks. In an aqueous solvent, the alkyl chains of TX100 and epoxy backbone may strongly interact with CNTs via non-covalent interactions, whereas the PEO (CH_2CH_2O) chains of TX100 interact with water through hydrogen bonds. Afterward, the copolymer-coated CNTs remain dispersed.

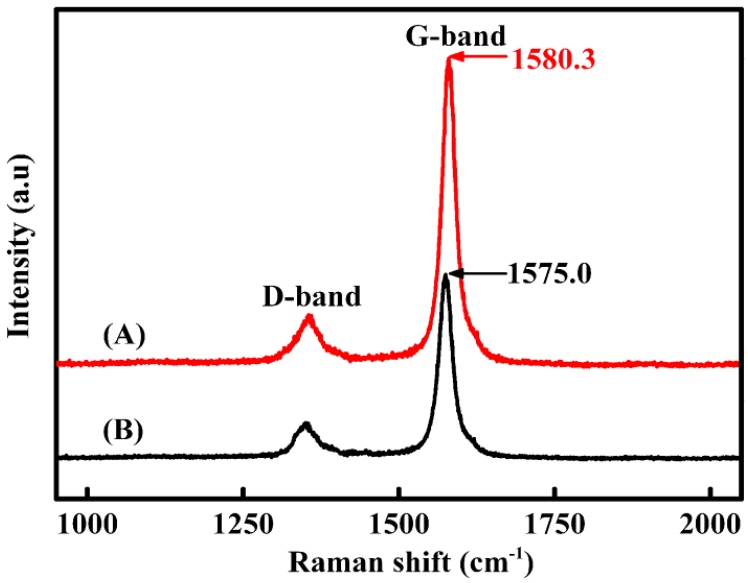

Figure 3.5 Raman spectra of (A) pristine CNTs and (B) EP-g-TX100 treated CNT.

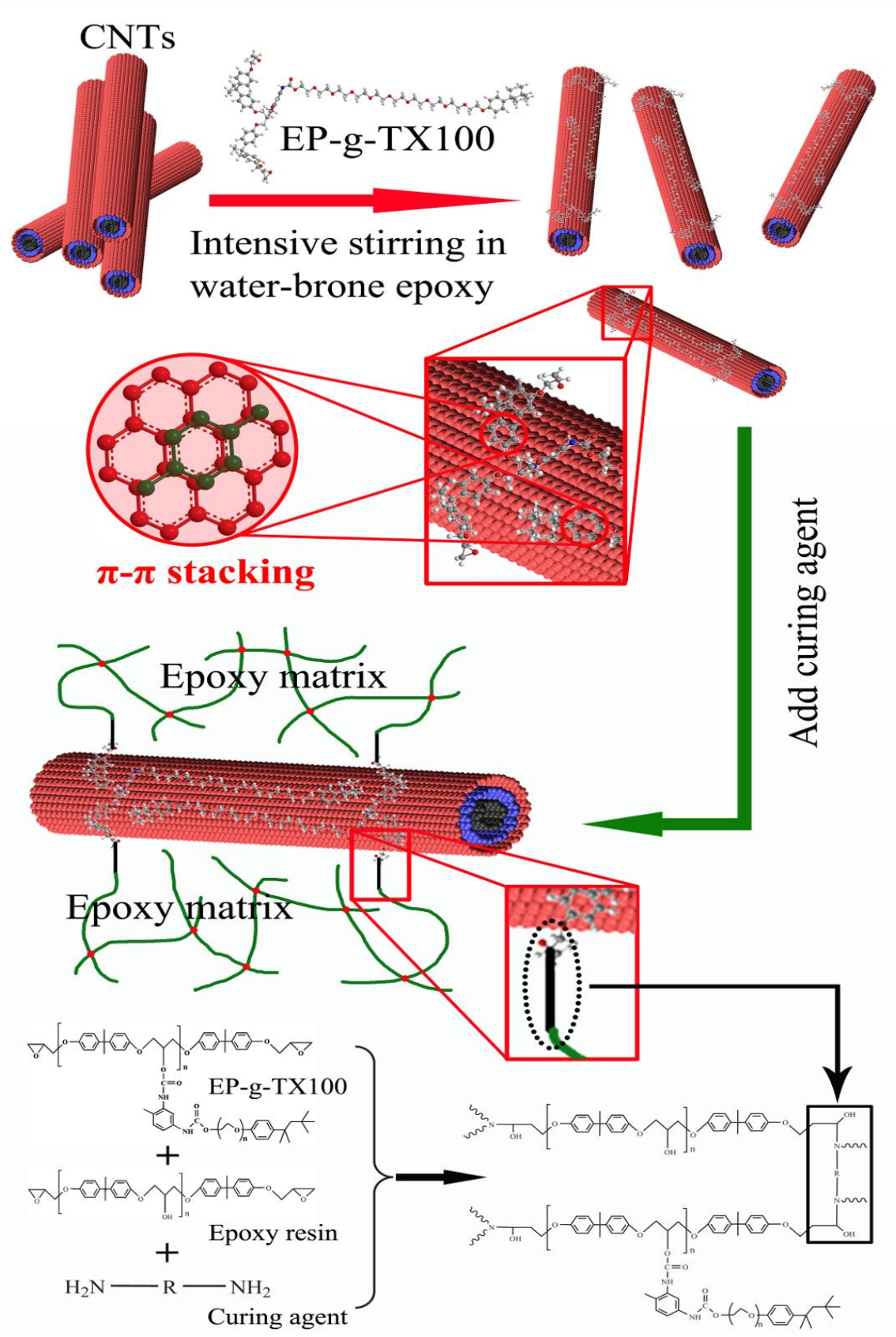

Figure 3.6 Schematic illustration of interface molecular engineering of the CNT/WEP SM nanocomposite by application of the EP-g-TX100.

3.1.3.2 Morphology and mechanical properties of CNT/WEP nanocomposites

In the WEP there are lots of free emulsifier and emulsifier micelles. In order to avoid the decreasing effect of EP-g-TX100 on the mechanical and SM properties of the final nanocomposites, we did not add the CNT/EP-g-TX100 solution to WEP, but added the CNT powder to the diluted WEP (5 % solid weight) directly and stirred at speed of 3000 r/min. Fig. 3.7A shows the images of WEP and its nanocomposites. The color of the samples is uniform and gradually become darker as the content of CNT increasing. Representative SEM and TEM micrographs of WEP and 2.5 wt% CNT/WEP composites are shown in Fig. 3.7B-E. The fractured section of pristine WEP exhibited a smooth surface characteristic of the brittle failure of a homogeneous material, as shown in Fig. 3.7B. By comparison, 2.5 wt% CNT/WEP nanocomposites showed much rougher fractured surfaces, as shown in Fig. 3.7C. CNTs in the samples were randomly and individually dispersed in the WEP as shown in Fig. 3.7C and Fig. 3.7E. These results can be attributed to non-covalent functionalization between the WEP surfactant EP-g-TX100 and CNTs. The fine dispersion and modified interfacial properties should be important to determine the mechanical and SM properties of the composites.

Table 3.1 Mechanical properties and T_g of CNT/WEP SM nanocomposites.

Sample	σ (MPa)	E (GPa)	ε (%)	T_g (°C)
Neat WEP	30.6±1.2	0.95±0.05	44.5±1.5	47.3
CNT(0.5 wt%)/WEP	37.6±1.3	1.36±0.08	42.0±1.0	50.9
CNT(1.0 wt%)/WEP	39.5±0.9	1.55±0.10	39.9±1.2	52.6
CNT(1.5 wt%)/WEP	37.2±1.1	1.39±0.12	37.0±1.6	51.6
CNT(2.0 wt%)/WEP	35.9±1.2	1.32±0.15	35.7±1.3	50.8
CNT(2.5 wt%)/WEP	34.0±0.8	1.22±0.10	34.2±1.4	49.6

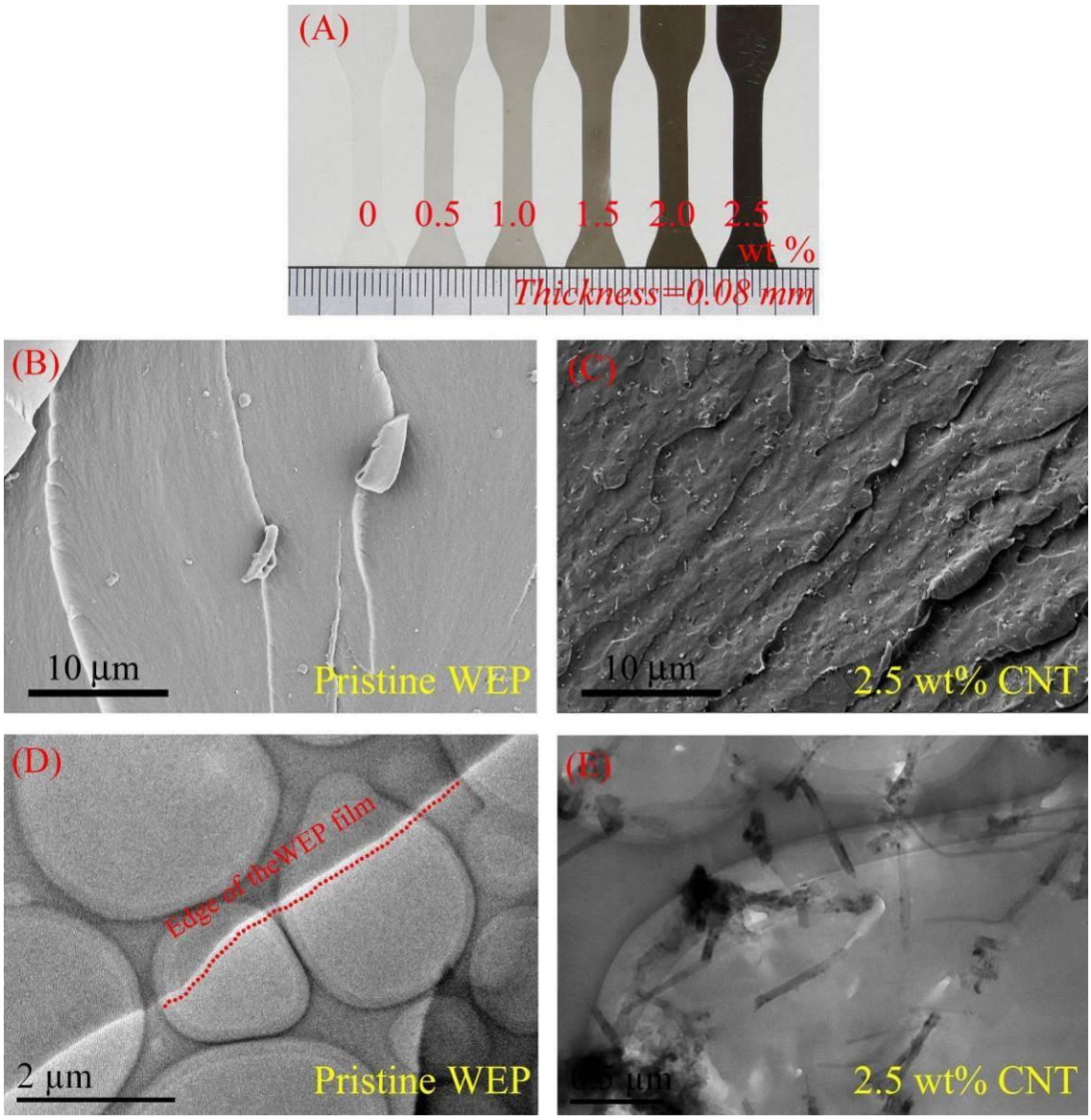

Figure 3.7 (A) Images of WEP and CNT/WEP nanocomposites; (B, D) SEM and TEM of the pristine WEP; (C, E) SEM and TEM of the 2.5 wt % CNT/WEP nanocomposite.

The effect of CNT loadings on the mechanical properties of the CNT/WEP nanocomposites are shown in Fig. 3.8 and Table 3.1. Pristine WEP exhibited nonlinear elastic behavior, a tensile strength of 30.1 MPa, and an elongation at break of approximately 43.2%. Added emulsifiers acted as plasticizers during the preparation of the WEP emulsion. The ultimate and yield strength of the CNT/WEP nanocomposites were higher than those of pristine WEP after CNT was added. The ultimate strength of the composite increased with the CNT content, and then reached the highest value of 39.5 MPa at 1.0 wt%. This finding can be attributed to the reinforcing effect of CNTs: (1) superior tensile modulus and strength; and (2) well-dispersed and well-incorporated

in the matrix. The surfactant of the WEP EP-g-TX100, as a non-covalent surfactant, can effectively improve CNT dispersion without damaging the CNTs by non-covalent functionalization, and can react with epoxy curing agent via epoxy groups. The non-covalently attached molecules can help form a better interface between the CNTs and the epoxy matrix, potentially improving the adhesion between the CNT and the surrounding epoxy matrix, as described in Fig. 3.6. As a result, an improvement in mechanical properties was achieved. The excess addition of CNT leads to compromise the tensile strength of the composites. The corresponding decrease in tensile strength that normally accompanies decreased the cross-link density of the composites. At high particle loading, the potential exist for the transport of amine and epoxy molecules to be significantly impeded by the large number of particles. Thus regions with very poor local stoichiometry and low cross-link density are created [48]. In addition, the possibility of particle aggregation had raised as the particle content increases, thus leading to degradation in the strength of the composites. Consequently, the tensile strengths of the composites with high CNT loadings showed serious decreases.

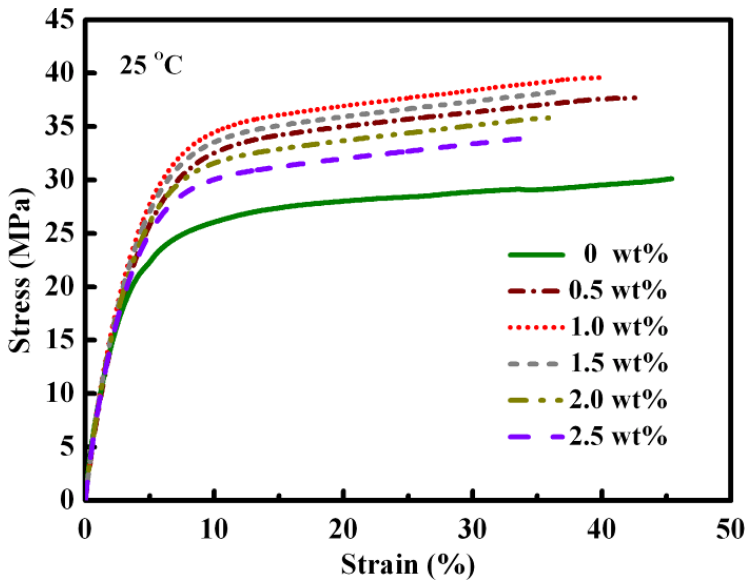

Figure 3.8 Stress–strain response of the CNT/WEP SM nanocomposites.

3.1.3.3 Dynamic mechanical properties

The storage moduli and tan delta values of neat WEP and its composites observed

from the DMA test are shown in Fig. 3.9.

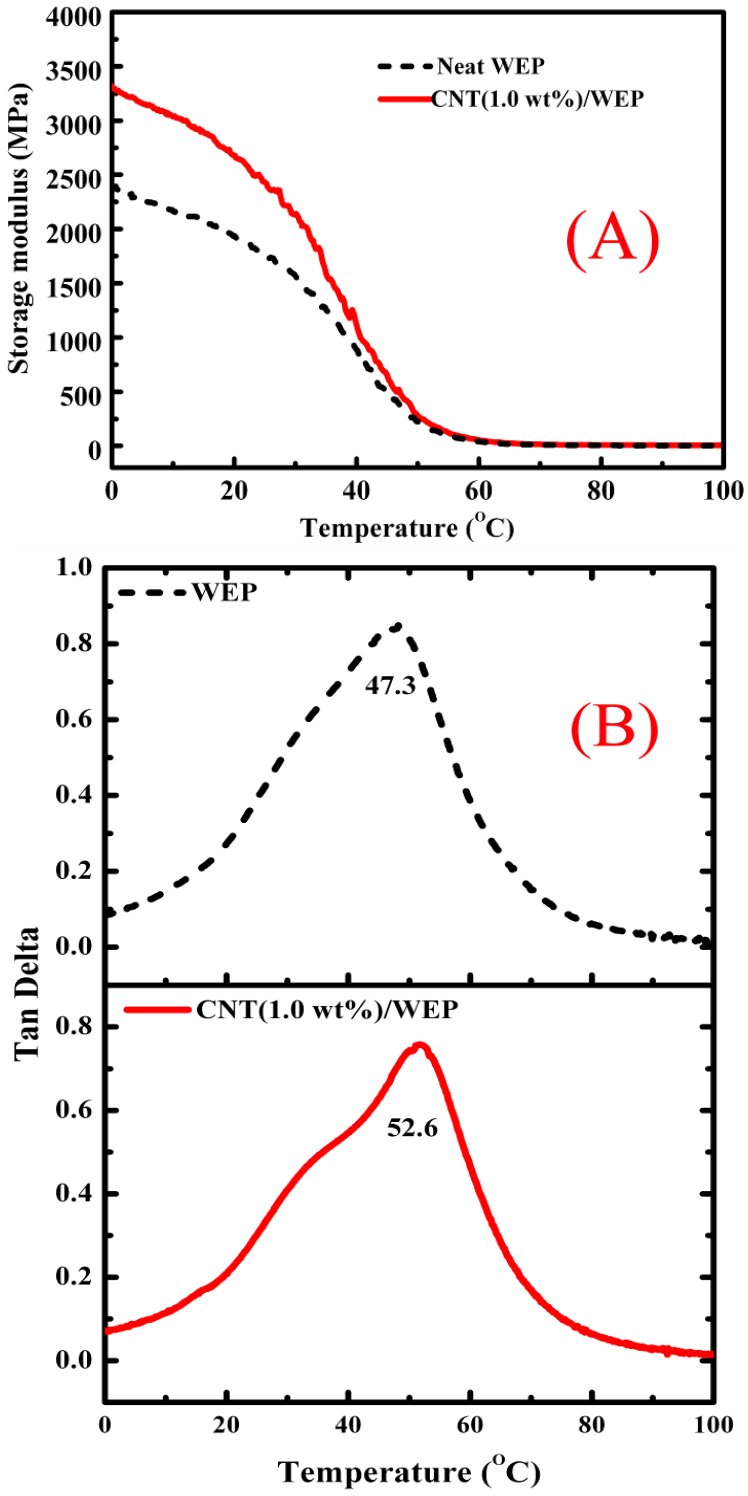

Figure 3.9 Storage moduli and tan delta values of neat WEP and CNT(1.0 wt%)/WEP nanocomposites obtained from DMA testing.

The samples underwent glass transition when the temperature was increased from 0 to 100 °C and exhibited similar temperature-dependent viscoelastic properties, as

shown in Fig. 3.9A. The storage modulus observed at temperatures far below the T_g was two orders of magnitude larger than that observed at temperatures above the T_g. For example, the 1.0 wt% CNT/WEP nanocomposite exhibited storage moduli of 3322.6 MPa at 15 °C and 8.7 MPa at 80 °C. For an excellent SMP, a large and sharp drop in the storage modulus around the glass transition is the most important. The storage modulus improved with the addition of fillers, as shown in Fig. 3.9A. The result suggests that filler incorporation reinforces the SM WEP. The T_g of the WEP composites increased with the filler weight fraction, as shown in Table 1. However, the T_g began to decrease, when the filler loading exceeded 1.0 wt%, likely because of the decreased effect of the cross-link density of the epoxy in the nanocomposites.

3.1.3.4 SM properties of CNT/WEP SM nanocomposites

The relationship between the shape recovery ratio and the filler content at 55, 65, and 75 °C is shown in Table 3.2 and Fig. 3.10A. No critical negative influence on the shape recovery ratio was observed with filler particles addition at different temperatures. The shape recovery ratio deteriorated at high weight fractions, which implies that fillers which had not been incorporated into the chain disturbed chain motion and impeded the elastic properties of the materials [8]. Besides the particle loading, the SM properties of particulate composites were markedly influenced by the particle/matrix interfacial adhesion [49]. Effective stress transfer is the most important factor which contributes to the SM properties of two-phase composite materials. The CNT/WEP interface is weak van der Walls attractive force as mention above. For poorly bonded CNT, the stress transfer at the CNT/WEP interface is inefficient especially at high filler content.

The shape fixity ratios of the composites at 25 °C are shown in Table 3.2 and Fig. 3.10B. Pristine WEP begins to recover several hours after the unloading of the constant external force. The fixity ratio of WEP was significantly improved by addition of fillers, which promote reduced polymer mobility. Advanced composites demonstrated excellent shape fixity even after 7 d at 25 °C. The high filler content in these composites contributes to the stiffness of the materials. A high storage modulus inhibits the

tendency of a material to return to its original shape after load releasing, thereby resulting in a high fixity ratio especially at low temperatures.

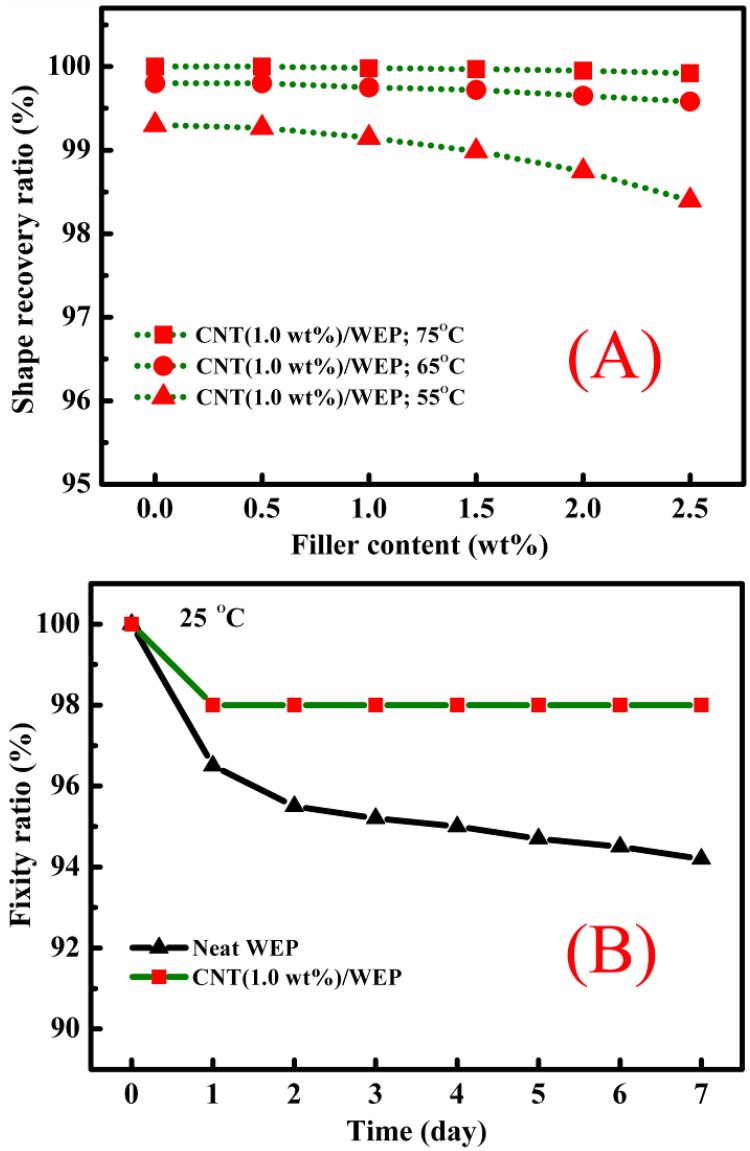

Figure 3.10 SM properties of the CNT/WEP SM nanocomposites.

The SM effect of the WEP composites is further demonstrated in Fig. 3.11. The SM effect allowed the samples to recover from tremendous strain. This effect is driven by the entropic behavior of the polymer chain between WEP cross-links. Therefore, the extremely high shape fixity and recovery ratios observed in the samples indicate the excellent SM functionality of the CNT/WEP nanocomposites prepared via latex technology.

Table 3.2 SM property of CNT/WEP nanocomposites.

Sample	Shape recovery ratio (%)			Fixity ratio (%)
	(55 °C)	(65 °C)	(75 °C)	(25 °C)
Neat WEP	99.30	99.90	100.0	95.55
0.5 wt% CNT	99.26	99.83	100.0	95.66
1.0 wt% CNT	99.15	99.75	99.98	97.62
1.5 wt% CNT	98.99	99.72	99.97	98.27
2.0 wt% CNT	98.75	99.65	99.95	99.15
2.5 wt% CNT	98.42	99.58	99.92	99.28

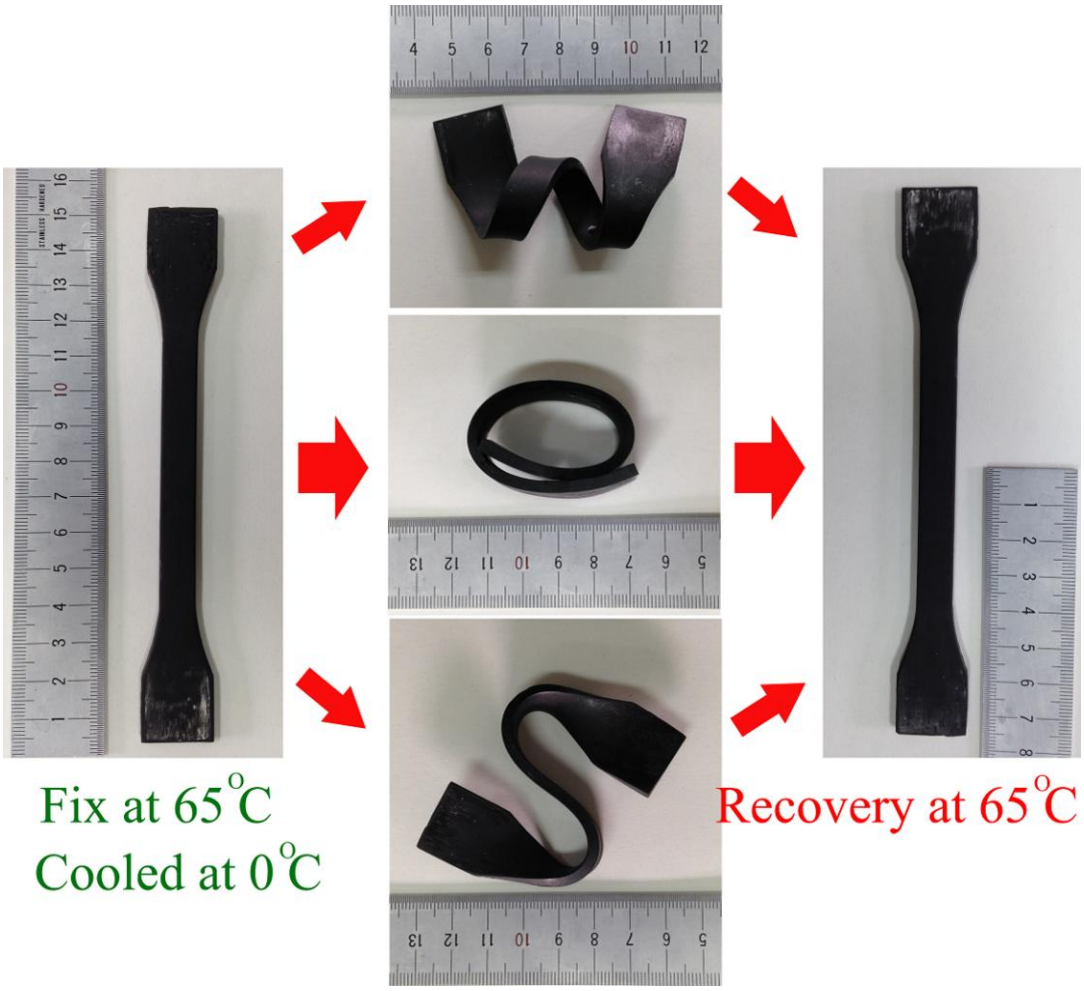

Figure 3.11 Illustration of the SME of CNT/WEP SM nanocomposites.

3.1.4 Conclusions

In the present study, CNT/WEP SM composites were designed and successfully prepared via freeze-drying and hot-press molding. The effects of CNT on the mechanical and SM properties of the WEP composites were investigated. The major findings are highlighted as follows:

1. WEP composites containing CNT exhibited better mechanical properties than pristine WEP. However, the strength of the composites began to decrease when the CNT contents reached 1.0 wt%.
2. The WEP composites exhibited a high shape recovery ratio of approximately 100% under different temperatures. The SM fixity ratio of pristine WEP was significantly ameliorated by addition of CNT.
3. CNT/WEP nanocomposites exhibited good SM functionality. The simple and environment-friendly approach employed in the present study is a feasible and effective method for synthesizing SM composites.

3.2 SM CNT/WEP composite foams

SM CNT/WEP composite foams were prepared. CNTs were first dispersed in WEP by intensive stirring and then mixed with curing agent and blowing agent at room temperature. SM CNT/WEP foams were obtained from these mixtures via freeze-drying and foaming under a vacuum at 100 °C. The SM properties of the epoxy foams were evaluated together with other physical properties. Compression and thermo-mechanical cycle tests were performed to measure the effects of the CNTs on the mechanical performance of the foams. The experimental results indicated that the SM CNT/WEP foams had high shape recovery and fixity ratios of more than 90% after several thermo-mechanical cycles with the addition of 1.0 wt% CNTs. The CNTs significantly enhanced the strength of the epoxy foams.

3.2.1 Introduction

SMP foams are attracting considerable interest worldwide [50-52]. SMP foams possess low density, high compressibility, and shape memory (SM) behavior. Thus, these foams have potential use in a wide range of applications that require a material to expand from a packaged shape to a much larger shape with minimal out-of-plane shape change [53-57]. SMP foams are also advantageous for applications that require extremely high volume recovery ratios. For example, SMP foams can be used as actuators that can be packaged on earth and recovered in space [58], thereby conserving the carried volume. Thus, SMP foams can also be used as a scaffold for cellular in-growth and combined with biological agents to promote biological integration [59, 60]. SMP foams are ideal candidates for multifunctional devices.

For heat-activated SMP foams, the SM effect is observed by performing a typical thermo-mechanical cycle. These foams are rigid below their glass transition temperature (T_g), and become spongy when heated above T_g. In this state, the foams can be packed into completely collapsed pores, without generating significant damage. This compact structure remains stable without constraining force, when cooled below T_g. When heated

above T_g, the foams recover their original shape. Heat-activated SMP foams can be divided into categories based on their chemical nature; the most common categories are polyurethane-based [61-63], polystyrene-based [64, 65], and epoxy-based [37, 40] foams. Epoxy resins, which are widely used in several non-SM applications, such as coatings, adhesives, construction, and manufacturing, exhibit the desirable properties of high strength, and good thermal stability, and chemical resistance. Conferring SM properties to these versatile resins has been the subject of several researchers, leading to some advances in the development of SM epoxy resin. Recent studies have shown the good SM properties of epoxies [58, 66]. Furthermore, SM epoxy has superior environmental durability, and is a good candidate for space application. Squeo and Quadrini [67] developed a new foaming technology for epoxies, namely, "solid-state foaming", which can produce foams without using any blowing agent or liquid-state process. The solid-state epoxy foams exhibit good SM properties. This new kind of material has been applied to the actuators of the International Space Station [58]. However, the solid-state foaming technique is only applicable only in solid epoxy resins, not in liquid epoxy resins.

In the present study, CNTs are used to enhance the mechanical and SM properties of epoxy foams which prepared from WEP. The effect of CNT addition and cell structure on the mechanical and SM properties of the WEP was discussed. In addition, the advantages of this technique include simplicity, versatility, reproducibility, and reliability.

3.2.2 Experimental

3.2.2.1 Materials

CNTs (VGNF®, Showa Denko K. K., Japan) were fabricated via thermo-chemical vapor deposition. WEP (50% solid weight) with a particle size range of 50 nm to 300 nm was synthesized by phase-inversion according to our previous research. A room-temperature cuing agent (AB-HGA®) was obtained from Zhejiang Anbang New

Material Development Co., Ltd. The blowing agent used was a tertiary butanol obtained from commercial sources.

3.2.2.2 Synthesis of SM CNT/WEP composite foams

A three-step procedure was used to prepare the epoxy foams. First, CNTs were added to a beaker with WEP and dispersed to homogeneity at room temperature using an intensive mixer. The blowing agent tertiary butanol (2.5 wt% of the mixture) and the curing agent were then sequentially added to the mixture. The weight ratio of the WEP to the cuing agent was 4:1. Second, the mixture was frozen in liquid nitrogen for 5 min, and the aqueous solvent was removed using a Labconco Free Zone freeze-dryer operated at 0.1 mbar and -20 °C for 48 h. The resulting powder was shaped via cold compaction in a 5 mm tall and 40 mm wide stainless steel mould at a packing pressure of 5 MPa for a holding time of 5 min. Third, the foaming process was performed by placing a single tablet in a 40 mm wide cylindrical stainless steel mould. The epoxy tablets were foamed in a vacuum oven at 100 °C and -0.1 MPa for 48 h.

3.2.2.3 Characterization

SEM observations of the specimens before and after compression were conducted using a field emission scanning electron microscope (Ultra 55, Zeiss, Germany) at an operating voltage of 3 kV. Prior to testing, the samples were sputter-coated with gold to impart electrical conductivity and reduce charging artefacts. High vacuum conditions were applied and a secondary electron detector was used for image acquisition. A compression test was conducted flat-wise, based on ASTM C 365 using a universal testing machine (INSTRON 8531) to evaluate the mechanical properties of the prepared foam. The specimens were polished to a size of 25 mm × 25 mm × 12.5 mm, and then tested. The loading rate was 1.3 mm/min at room temperature. A preload of 0.2 N was used to achieve full contact of the plate on the sample. At least five effective specimens were tested. For four-point measurements, the flat surfaces of the foam samples were firmly pasted with conductive coating around their circumference at a spacing of

approximately 1 mm. Conductive coating leads were attached to these electrodes for testing.

A thermo-mechanical cycle test was conducted to investigate the shape recovery property of the epoxy foams. The specimens were compressed to the maximum strain of 80% (ε_m) at a constant compression speed at 65 °C above T_g (step 1). Maintaining the strain at 80%, the specimen was cooled down to 25 °C below T_g (at the glass state) and held for 10 min (step 2). The specimen was unloaded at 25 °C at a small unloading strain ε_u (step 3), completing the three-step shape fixity process. The specimen was heated from 25 to 65 °C without load and held for 10 min to examine the shape recovery capacity. The strain of the specimen was then recovered. When this cycle finished, a residual strain remained. The heating or cooling speed was 5 °C/min, and the loading and unloading speed was 1.3 mm/min. The test was repeated four times.

3.2.3 Results and discussion

3.2.3.1 Epoxy foam Micrograph

The microstructures of the epoxy foam are shown in Fig. 3.12A. The SEM image shows that the cells with a diameter up of to 650 μm were evenly distributed in the epoxy resin. Furthermore, the shape of the cells is polyhedral rather than spherical because of the compression among the cells. The epoxy foam density was dependent on the blowing agent (tertiary butanol) content. At the end of the production stage, the epoxy foam density was approximately 0.29 g/cm^3. The maximum (Max_d) and minimum diameter (Min_d) of every cell in Fig. 3.12A was measured using the ImageJ imaging processing software. The average cell diameter distribution of the [(Max_d + Min_d)/2] is illustrated in Fig. 3.12B.

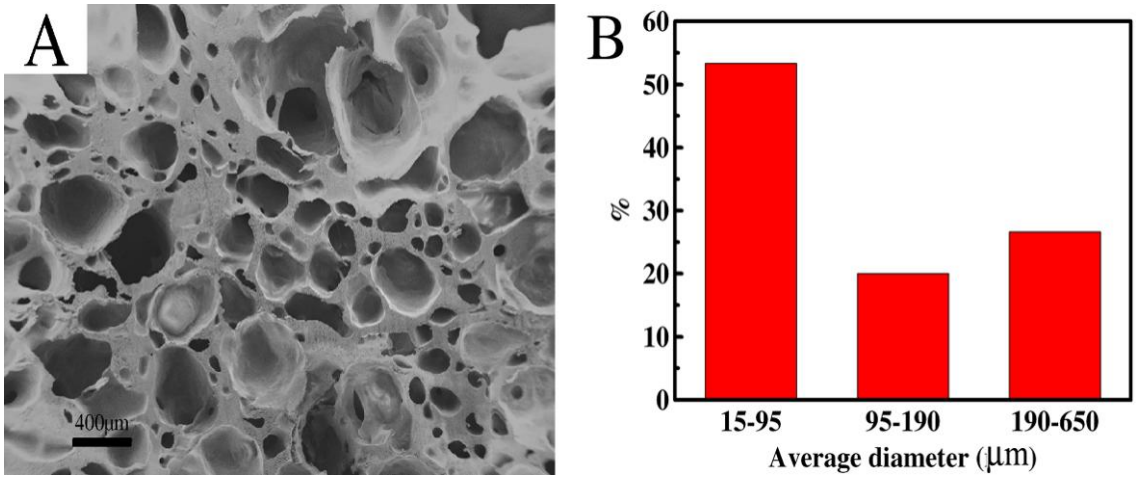

Figure 3.12 (A) Micrograph of the CNT/WEP foam; (B) the average cell diameter distribution.

3.2.3.2 Compression results

Fig. 3.13A shows the compressive stress-strain curve of the epoxy foam, which exhibits similar regimes to the stress-strain curve of regular syntactic foams. The stress-strain curve can be clearly characterized by three distinct regions. In the initial elastic regime and during early yield, the stress almost linearly increases as the foam becomes rigid. Subsequently, a wide plateau region corresponding to the rubbery deformation of the foam matrix is observed. In the end, the cell collapses and becomes compact with further increase in strain, and the stress-strain curve is directed upward to higher stress, at a larger strain. Compared with regular syntactic foam, the deformation in the rubbery region is obviously much higher [40, 65]. This finding suggests that the foam can absorb more energy without disintegration. Furthermore, the 10 s free shape recovery rate of the epoxy foam at 65 °C is 94.5% at 93.35% pre-deformation strain.

The compression test results of the epoxy and CNT/WEP foams are shown Fig. 3.13B. The strengths of the CNT/WEP foams at 80% deformation strain were higher than that of the pure WEP foam. The foam strength initially increases with the weight fraction of CNT and then decreases when the weight fraction reaches 0.8 [inset in Fig. 3.13B]. The mechanical behavior of the CNT/WEP foam improved with respect to the unreinforced foam.

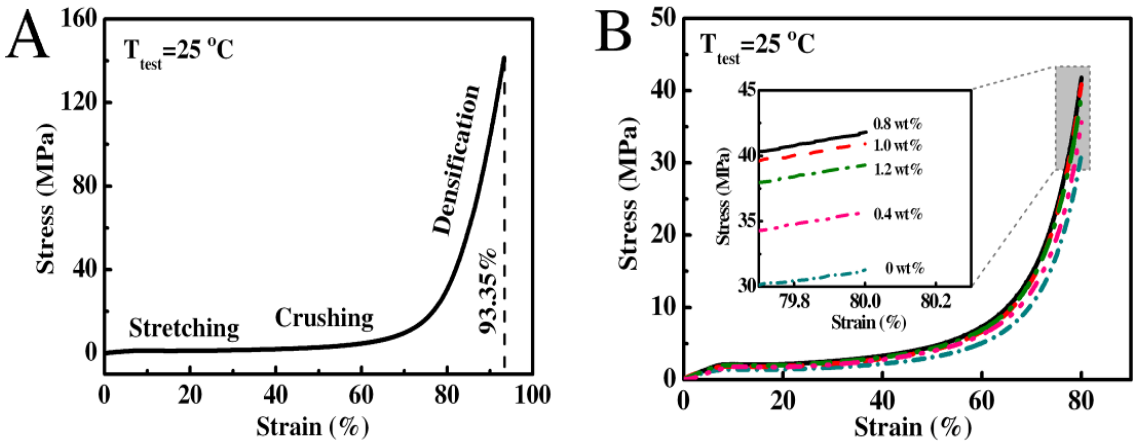

Figure 3.13 (A) Compressive stress-strain curves of WEP foam, and (B) Stress-strain response of the epoxy and CNT/WEP foams at room temperature.

3.2.3.3 Thermo-mechanical cycle test

The stress-strain-temperature curves of WEP (the red line) and CNT/WEP (the green line) foams obtained in the thermo-mechanical cycle test using the maximum strain (ε_m = 80%) are shown in Fig. 3.14. The four steps associated with the shape fixity and recovery is highlighted. Shape fixity and recovery ratios are two important parameters for determing, and evaluating SMP characteristics, as defined by Eq. (3.2). The shape recovery and fixity ratios are determined in terms of the strain [8, 64], where N is the number of thermo-mechanical cycles (N=1 in Fig. 3.14), R_f is the shape fixity ratio, R_r is the shape recovery ratio, ε_m is the pre-deformation strain (strain at the end of step 2), ε_u is the temporary strain fixed (strain at the end of step 3) and ε_p is the permanent strain (strain at the end of step 4).

$$R_f(N) = \frac{\varepsilon_u(N)}{\varepsilon_m}, \quad and \quad R_r(N) = \frac{\varepsilon_m - \varepsilon_p(N)}{\varepsilon_m - \varepsilon_p(N-1)} \qquad \text{Eq.(3.2)}$$

The relationship of the shape fixity and recovery ratios to the cycle number is shown in Fig. 3.15. The shape fixity ratios are clearly very high (approximately 94% R_f for the two foams), suggesting a good shape fixity of the smart foams. In the first cycle, the shape recovery ratios are approximately 95% for the WEP foam and 98% for the WEP foam reinforced with 1.0 wt% CNTs. This result suggests that the incorporation of

CNTs enhances the shape recovery ratio of the WEP foam. However, both foams have a shape recovery ratio of more than 98% after the second cycle. The ratio tends to be a constant 99% with increased cycle numbers. This phenomenon is called "training" effect [8].

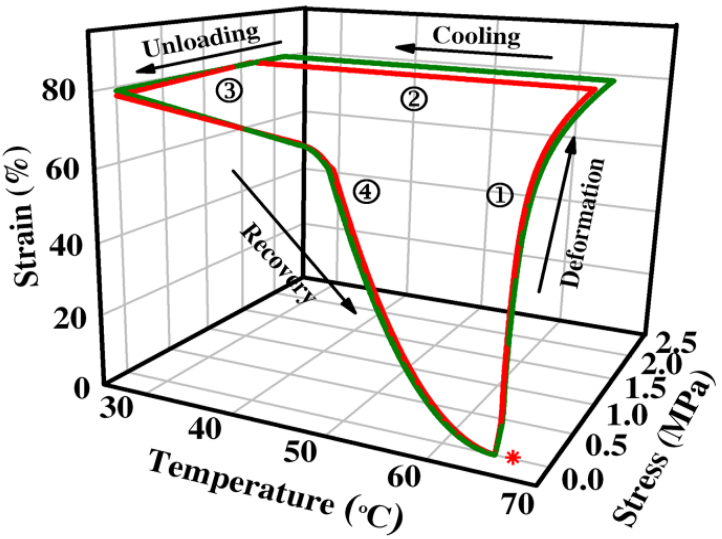

Figure 3.14 Four-step thermo-mechanical cycle: (1) compression to a maximum strain of 80% at 65 °C, (2) cooling to 25 °C with ε_m kept constant, (3) holding for 10 min at 25 °C under no load, and (4) heating to 65 °C under no load. The red and green lines are the stress-strain-temperature curves of WEP and CNT/WEP foams, respectively, obtained in the thermo-mechanical cycle test under the maximum strain of 80%.

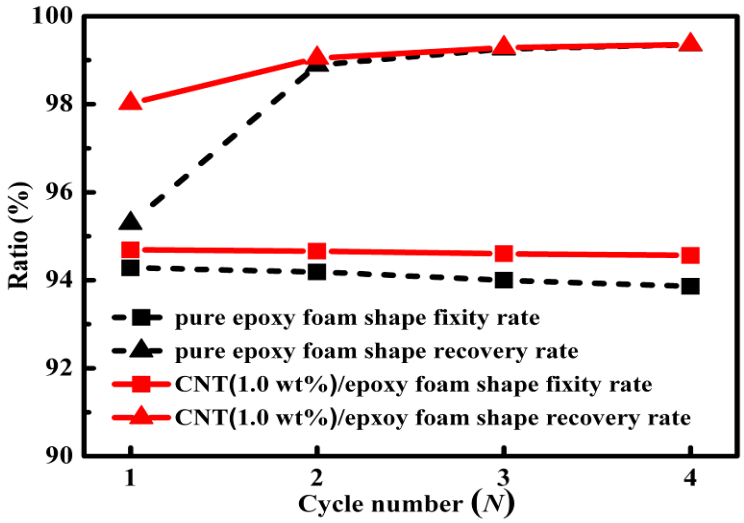

Figure 3.15 Relationship of the shape recovery and fixity ratios to the cycle number of the CNT/WEP foams.

Fig. 3.16 shows that approximately 10 s is required for shape recovery at 65 °C, which is relatively quick considering a size of 18 mm × 13 mm × 13 mm and a bulk density of 0.29 g/cm^3. The shape memory effect allows the foam to recover from a large strain after being packed in a temporary shape. This effect is driven by the entropic behavior in the polymer chains between the cross-links of the epoxy. Below T_g, the polymer chains between the network points cannot undergo any conformational changes and are locked into shape unless a suitably large mechanical force is applied. The chains can undergo rotational conformation changes at relatively lower stresses when heated to T_g. As the polymer deforms above T_g, the polymer chains begin to align, increasing the stored energy in the material as the entropy of the chains decreases. Upon cooling in the deformed shape, the polymer chains can no longer freely rotate. The polymer chains then recovered this stored energy by returning to the initial high entropy configuration when the material is heated above T_g without constraint, returning to the initial shape [40]. Therefore, the very high shape fixity and recovery ratios suggest the good SM functionality of CNT/WEP foam prepared via latex technology. The stable recovery of CNT/epoxy foams is achieved after several training cycles.

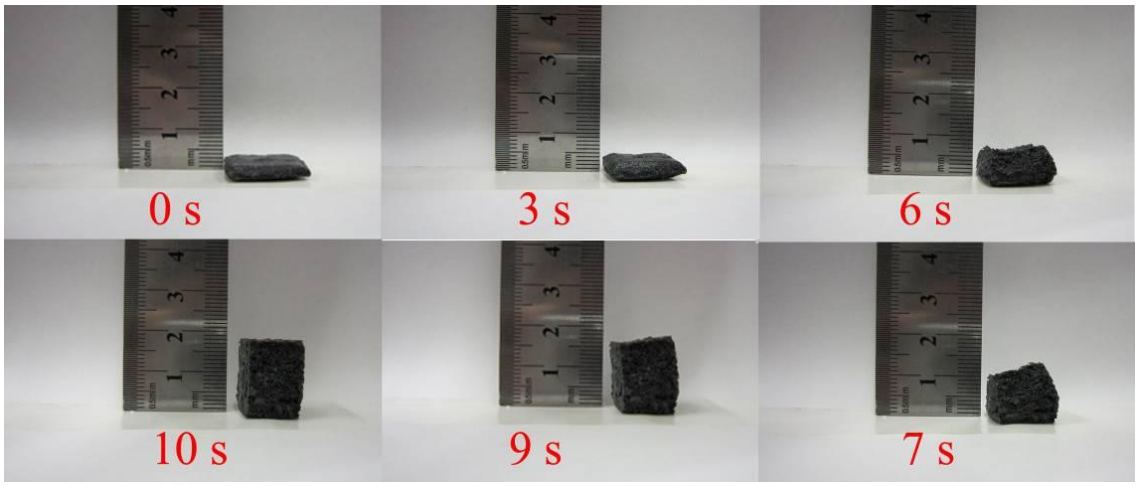

Figure 3.16 Shape recovery behaviour of CNT/WEP foam at 65 °C.

3.2.3.4 Electrical conductivity of the CNT/WEP foams

Fig. 3 shows the effect of CNT concentration on the electrical conductivity of the CNT/WEP foams. The electrical conductivity of the foam significantly increased when the CNT content is approximately 0.6 wt%, indicating that the percolation threshold for the formation of a conductive CNT network in the epoxy matrix is achieved. The conductivity of pure WEP is in the order of 10^{-13} S/m. For a CNT concentration of 1.0 wt%, the conductivity is 10^{-3} S/m. For higher CNT concentrations, no pronounced increase in conductivity could be observed. CNTs are excellent and favorable fillers for synthesizing conductive polymer composites because of their high electrical conductivity, which can remarkably decrease the electrical resistivity of the composite at low weight or volume content.

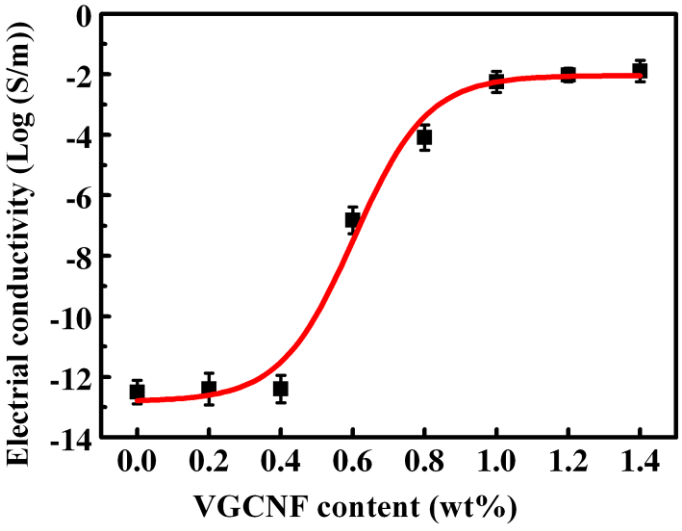

Figure 3.17 Electrical conductivity of the CNT/WEP foams as a function of CNT concentration.

3.2.4 Conclusions

Epoxy foams composed of CNTs and SMP foams were prepared via latex technology. Their mechanical properties and shape recovery behaviors were investigated. Based on a comprehensive test, the following conclusions are obtained:

1. The strengths of the CNT/WEP foams under the deformation strain of 80% were higher than that of the pure WEP foam.
2. The epoxy foams had good SM functionality and can maintain their high shape recovery and fixity ratio at more than 90% after several thermo-mechanical cycles.
3. Compared with the conventional method for epoxy based foam preparation, the latex technology has great advantages, such as convenience and environmental friendliness. Moreover, this technology can be applied to both liquid and solid epoxy resins.
4. For the CNT/WEP foam, the percolation threshold for conduction was approximately 0.6 wt% and the electrical conductivity was approximately 10 orders of magnitude larger than that of pristine epoxy foam.

Reference

[1] J. S. Leng, X. Lan, and S. Y. Du, *Prog. Mater. Sci.*, 56(2011)1077.

[2] Y. J. Liu, H. B. Lv, and J. S. Leng, *Compo. Sci. Technol.*, 69(2009) 2064.

[3] H. Meng, and G. Q. Li, *Polymer*, 54(2013)2199.

[4] H. Meng, and G. Q. Li, *J. Mater. Chem.*, 1(2013)7838.

[5] J. L. Hu, H. H. Huang, and J. Lu, *Prog. Polym. Sci.*, 37(2012)1720.

[6] Y. B. Dong, J. Ding, and Y. Q. Fu, *Compos. Sci. Technol.*, 76(2013)8.

[7] L. B. Xu, Y. Q. Fu, and M. L. Du, *Chinese J. Chem.*, 29(2011)703.

[8] Q. Q. Ni, C. S. Zhang, and Y. Q. Fu, *Compos. Struct.*, 81(2006)176.

[9] C. S. Zhang, Q. Q. Ni, and S. Y. Fu, *Compo. Sci. Technol.*, 67(2007)2973.

[10] C. S. Zhang, and Q. Q. Ni, *Compos. Struct.*, 78(2007)153.

[11] W. M. Huang, B. Yang, and Y. S. Chan, *Appl. Phys. Lett.*, 86(2005)114105.

[12] M. M. Ma, L. Guo, and R. Langer, *Science*, 339(2013)186.

[13] X. J. Han, and M. M. Fan, *Macromol. Rapid. Commum.*, 33(2012)1055.

[14] A. Lendlein, H. Y. Jiang, and R. Langer, *Nature*, 434(2005)879.

[15] D. Habault, H. J. Zhang, and Y. Zhao, *Chem. Soc. Rev.*, 42(2013)7244.

[16] L. Viry, C. Merrcader, and P. Miaudet, *J. Mater. Chem.*, 20(2010)3487.

[17] Y. C. Jung, H. J. Yoo, and M. Endo, *Carbon*, 48(2010)1598.

[18] Y. Cai, J. S. Jiang, and W. G. Zhang, *Composites: Part A*, 53(2013)16.

[19] J. Thevenot, H. Olicira, and O. Sandre, *Chem. Soc. Rev.*, 42(2013)7099.

[20] W. M. Huang, B. Yang, and Z. Ding, *J. Mater. Chem.*, 20(2010)3368.

[21] A. Lendlein, *J. Mater. Chem.*, 20(2010)3332.

[22] J. L. Hu, Y. Zhu, and H. H. Huang, *Prog. Polym. Sci.*, 37(2012)1720.

[23] X. Lan, X. H. Wang, and J. S. Leng, *Smart Mater. Struct.*, 18(2009)24002.

[24] A. Lendlein, and R. Langer, *Science*, 296(2002)1673.

[25] W. Small, P. Singhal, and D. J. Maitland, *J. Mater. Chem.*, 20(2010)3356.

[26] M. C. Serrano, and G. A. Ameer, *Macromol. Biosci.*, 12(2012)1156.

[27] S. Sharifi, T. G. V. Kooten, and D. W. Grijpma, *Biomaterials*, 34(2013)8105.

[28] J. Kunzelman, T. Chung, and P. T. Mater, *J. Mater. Chem.*, 18(2008)1082.

[29] A. M. Diorio, X. F. Luo, and P. T. Mather, *Soft Matter*, 7(2011)68.

[30] Q. L. Zhang, and J. C. Feng, Sol. Energ. *Mat. Sol. C.*, 117(2013)259.

[31] L. F. Boesel, C. Greiner, and A. D. Campo, *Adv. Mater.*, 22(2010)2125.

[32]C. M. Chen, C. L. Chiang, and T. Xie, *Adv. Funct. Mater.*, 23(2013)3813.

[33] Y. Li, S. S. Chen, and J. Q. Sun, *Adv. Mater.*, 24(2012)4578.

[34] X. F. Luo, and P. T. Mather, *ACS Macro. Lett.*, 2(2013)152.

[35] L. Yao, M. Z. Rong, and M. Q. Zhang, *J. Mater. Chem.*, 21(2011)9060.

[36] T. Xie, X. and Y. T. Cheng, *Macromol. Rapid. Commun.*, 30(2009)1823.

[37] I. A. Rousseau, and T. Xie, *J. Mater. Chem.*, 20(2010)3431.

[38] C. M. Chen, C. L. Chiang, and S. Yang, *Adv. Funct. Mater.*, 23(2013)3813.

[39] K. S. S. Kumar, and N.Reghunadhan, *React. Funct. Polym.*, 73(2013)421.

[40] M. D. Prima, K. Gall, and S. C. Arzberger, *Mech. Mater.*, 42(2010)304.

[41] Z. H. Tang, D. Q. Sun, and D. Yang, *Compos. Sci. Technol.*, 75(2013)15.

[42] Y. Kai, Y. J. Liu, and J. S. Leng, *RSC Adv.*, 4(2014)2961.

[43] M. H. Al-Saleh, U. Sundararaj, *Carbon*, 47(2009)2.

[44] M. Endo, Y. J. Kim, and M. S. Dresselhaus, *Appl. Phys. A*, 82(2006)559.

[45] M. A. Raza, A. Westwood, C. Stirling, *Carbon*, 50(2012)84.

[46] Y. B. Dong, R. Wang, and Y. Q. Fu, *J. Colloid Interf. Sci.*, 391(2013)8.

[47] J. H. Zou, L. W. Liu, and L. Zhai, *Adv. Mater.*, 20(2008)2055.

[48] L. Mascia, L. Prezzi, B. Haworth, *J. Mater. Sci.*, 41(2006)1145.

[49] J. Ding, Y. F. Zhu, and Y. Q. Fu, *Polym. Composite*, 35(2014)412.

[50] D. Ratna, J. K. Kocsis, *J. Mater. Sci.*, 43(2008)254.

[51] L. Sun, W. M. Huang, and Z. Ding, *Mater. Des.*, 33(2012)577.

[52] G. Q. Li, N. Uppu, *Compos. Sci. Technol.*, 70(2010)1419.

[53] G. Vialle, K. Gall, and T. Sanderson, *Smart. Mater. Struct.*, 18(2009)115014.

[54] M. D. Prima, K. Gall, and T. Sanderson, *Mech. Mater.*, 42(2010)405.

[55] T. Pretsch, *Polymers*, 2(2010)120.

[56] J. F. Patrick, N. R. Sottos, and S. R. White, *Polymer*, 53(2012)4231.

[57] X. C. Gui, J. Q. Wei, and Y. Jia, *Adv. Mater.*, 22(2010)617.

[58] E. A. Squeo, F. Quadrini, *Mater. Lett.*, 20(2012)20.

[59] C. M. Yakacki, K. Gall, *Adv. Polym. Sci.*, 226(2010)147.

[60] W. Small, P. Singhal, and D. J. Maitland, *J. Mater. Chem.*, 20(2010)3356.

[61] S. E. Chung, C. H. Park, *J. App. Polym. Sci.*, 117(2010)2265.

[62] Y. J. Yu, K. Hearon, and T. S. Wilson, *Smart Mater. Struct.*, 20(2011)85010.

[63] S. M. Kang, S. J. Lee, B. K. Kim, *Express Polym. Lett.*, 6(2012)63.

[64] G. Q. Li, M. John, *Compos. Sci. Technol.*, 68(2008)3337.

[65] G. Q. Li, D. Nettles, *Polymer*, 51(2010)755.

[66] D. M. Feldkamp, I. A. Rousseau, Macromol. *Mater. Eng.*, 296(2011)1128.

[67] E. A. Squeo, F. Quadrini, *Smart. Mater. Struct.*, 19(2010)105002.

CHAPTER FOUR

Preparation and properties of silica/water-borne epoxy shape memory nanocomposites

4 Preparation and properties of silica/WEP shape memory nanocomposites

4.1 Silica/WEP shape memory nanocomposites

Silica/WEP SM nanocomposites were successfully prepared by hydrolysis of tetraethoxysilane (TEOS) within the epoxy matrix via freeze-drying and hot-press molding method. The silane coupling agent 3-triethoxysilylpropylamine (KH550) was introduced to improve the interfacial properties between the in-situ generated silica particle and epoxy matrix. The morphology structure and the effect of the content of the in-situ formed silica on the mechanical and SM properties of the silica/WEP composites were studied. The experimental results indicated that the silica particles were homogenously dispersed and well incorporated into the epoxy matrix. Significant improvements were achieved in the mechanical property of the organic-inorganic hybrid materials. The silica/WEP composites exhibited high shape recovery and fixity ratio approximately 100% even after 10 thermo-mechanical cycles.

4.1.1 Introduction

SMPs can be fixed into a stable temporary shape, and then revert to their permanent shape when triggered by an external stimulus [1-4], including heat [5-7], water [8], pH [9], light [10], electricity [11, 12], and magnetic fields [13]. SMPs are widely used in applications such as aerospace structures [14], biomedical devices [15, 16], sensors [17], textiles [18], dry adhesives [19], self-crack-healing applications [20].

Many recent studies have proven the favorable SM properties of epoxies [21, 22]. A vast majority of these products are still formulated with organic solvents. Water-borne

epoxies (WEPs), as novel versatile environmentally-friendly materials, which are being attached great importance in engineering field and mainly used in concrete coatings, metal primers, epoxy cement concrete, glass fiber sizing, and wood adhesives [23]. In our previous research, we found that WEP has excellent SM effect [24], besides an inferior mechanical strength and a lower SM fixity ratio compared to the conventional solvent-based epoxy. Fortunately, problems related to the processing and thermo-mechanical properties of SMPs can largely be resolved by modifying the molecular structure of the applied polymer and adding functional fillers into the polymer [1].

Improvements in the mechanical and SM properties of SMPs through incorporation of inorganic particles have been achieved. The most popular fillers for the SMP matrices are CNTs [25]. CNTs are applied to reinforcing the strength of the matrices and induce electricity and heating to enable shape recovery. The recently incorporation of nanoparticels and ferromagnetic nanoparticles in SMP matrices was used to actuate the shape recovery in different ways. For example, epoxy filled with Ni-nanopowder can be actuated well in electromagnetic fields [26]. The electrospun Fe_3O_4-loaded multi-walled nanotube/polycaprolactone (PCL) composite nanofibres exhibited excellent SM effect triggered by an alternating magnetic field [27]. Among the numerous additives currently, silica particles are another commonly used because of them chemical stability, favorable morphology, availability, and low price. However, as other nanosize particles, nanosilica particles are prone to cluster in the polymer and cannot form excellent composites owing to the poor interfacial compatibility between the polymer matrix and the silica. Therefore, modifying the surface structure of silica to enhance its dispersibility into raw materials and interfacial adhesion is essential. Improving the interfacial property of the silica particle is also important. Wang [28] and Lee [29] used polycaprolactone grafted-silica and allylisocynate modified-silica, respectively, to improve polycaprolactone and water-borne polyurethane SM effects. The resultant silica/SMP composites exhibited excellent mechanical and SM properties. In addition, Jang [30] reported that the SM effect is retained in reinforced SMPU/silica hybrids. The effective utilization of the silica in composite applications strongly

depends on the ability of the silica to disperse homogeneously throughout the matrix and exhibit excellent interfacial adhesion.

In the present study, WEP composite reinforced with in-situ generated silica were successfully prepared via freeze-drying and hot-press molding process. This approach assumes both homogeneous dispersion of the silica particles within a continuous polymer matrix and improvement of the mechanical and SM properties of the WEP. The effects of the in-situ formed silica on the mechanical and SM properties of epoxy were characterized from the aspects of morphology, mechanical properties, dynamic mechanical properties, and SM behaviors. Moreover, this work provides a useful and environment-friendly method in designing and improving the mechanical and SM properties of the SMPs.

4.1.2 Experimental

4.1.2.1 Materials

WEP (50% solid weight) with a particle size range of 50 nm to 300 nm was synthesized by phase-inversion according to our previous research. A commercially available room-temperature curing agent (AB-HGF®, Zhejiang Anbang New Material Development Co., Ltd, China), tetraethoxysilane (TEOS), 3-triethoxysilylpropylamine (KH550), and absolute ethanol were obtained from commercial sources and used as received.

4.1.2.2 Synthesis of the silica/WEP composites

A four-step procedure was conducted to prepare silica/WEP composites, as shown in Fig. 4.1. Firstly, TEOS (20.00 g) and absolute ethanol (40.00 g) were added into a three necked-flask and stirred (300 r/min) under a nitrogen atmosphere for 30 min. A total of 44.000 g KH 550-ethanol solution (4.00 g of KH550) was then added drop-wise into the TEOS-ethanol solution under a nitrogen atmosphere and mixed vigorously at speed of 300 r/min for 30 min. Secondly, the curing agent was added to the WEP and

dispersed to homogeneity at room temperature by intensive mixing in a beaker at speed of 500 r/min for 30 min. The weight ratio of the epoxy to the curing agent was 4:1. Then, a known volume of silica sol prepared in the first step was poured into the WEP and curing agent mixture. The resulting mixture was mixed at speed of 1000 r/min for 15 min, and then frozen in liquid nitrogen. The aqueous solvent and ethanol were removed using a Labconco Free Zone freeze-drier operated at 0.1 mbar and -55 °C for 7 d. Finally, the resulting composite powder was compressed into films at 120 °C for 2 h under a pressure of 10 MPa.

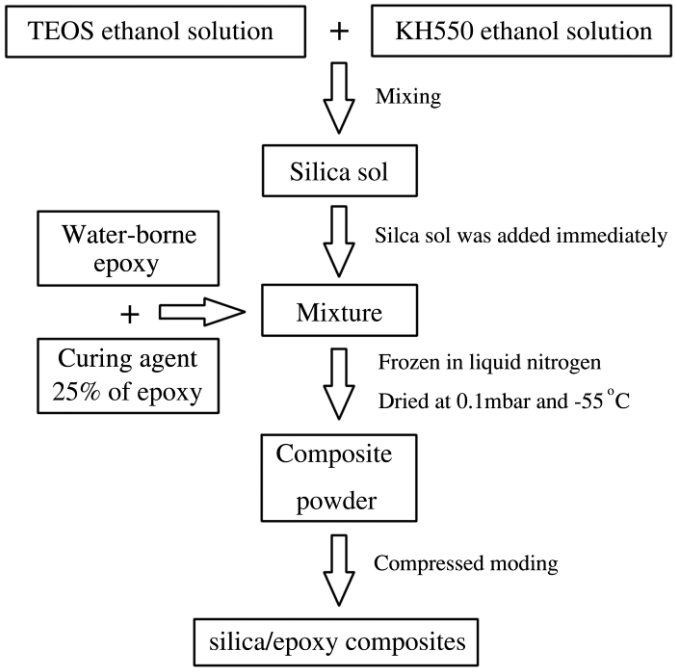

Figure 4.1 Schematic of the process for preparing of the silica/WEP nanocomposites.

4.1.2.3 Characterization

TEM images of the silica/WEP composites were obtained from ultrathin sections that were cut with a glass knife on the Leica EM UC7 ultramicrotome (Leica, Germany). Fractured surface of the silica/WEP composites were observed under a field emission scanning electron microscope (FE-SEM; Ultra 55, Zeiss, Germany) at an operating voltage of 3 kV. The Fourier transform infrared (FTIR) spectra of the silica/WEP composites were recorded on a Nicolet 5700 attenuated total reflection Fourier

transform infrared (ATR-FTIR) instrument (Thermo Electron Corp., USA) with a resolution of 4 cm^{-1}. Tensile test of the silica/WEP composites were conducted using a testing machine (INSTRON 3367, USA) at a crosshead speed of 5 mm/min on dumbbell-shape specimens at room temperature. At least five effective specimens were tested for each sample. The composites samples were determined via a DMA Q800 (TA Instrument, America) at a frequency of 1 Hz, and then heated from 0 to 100 °C at a rate of 5 °C/min. The test was conducted under engineering strain control, with a strain of 0.1% and a preload of 0.01 N.

To investigate the shape recovery property of the silica/WEP composites, a thermo-mechanical cycle test was conducted via the DMA Q800 (TA Instrument, America) in the tension mode and frequency of 1 Hz. The specimens were pulled up to the maximum strain of 30% (ε_m) at a constant tensile speed at 65 °C above T_g (step 1). While maintaining the strain at 30%, the specimen was cooled down to 25 °C below T_g (at the glass state) and held for 10 min (step 2). The specimen was unloaded at 25 °C, at a small unloading strain ε_u (step 3), completing the three-step shape fixity process. To examine the shape recovery capacity, the specimen was heated form 25 °C to 65 °C under no load and held for 10 min, and the strain of the specimen was recovered. When this cycle finished, a residual strain remained. The heating or cooling speed was 5 °C/min, and the loading and unloading speed was 0.05 N/min. The test was repeated 10 times to check the reproducibility of SM effect.

4.1.3 Results and discussion

4.1.3.1 Morphology and structure

The representative SEM micrographs obtained from fractured surface of the silica/WEP composites are shown in Fig. 4.2. The fractured section of the pristine WEP exhibits a smooth surface representing brittle failure of a homogeneous material, as shown in Fig. 4.2A**.**

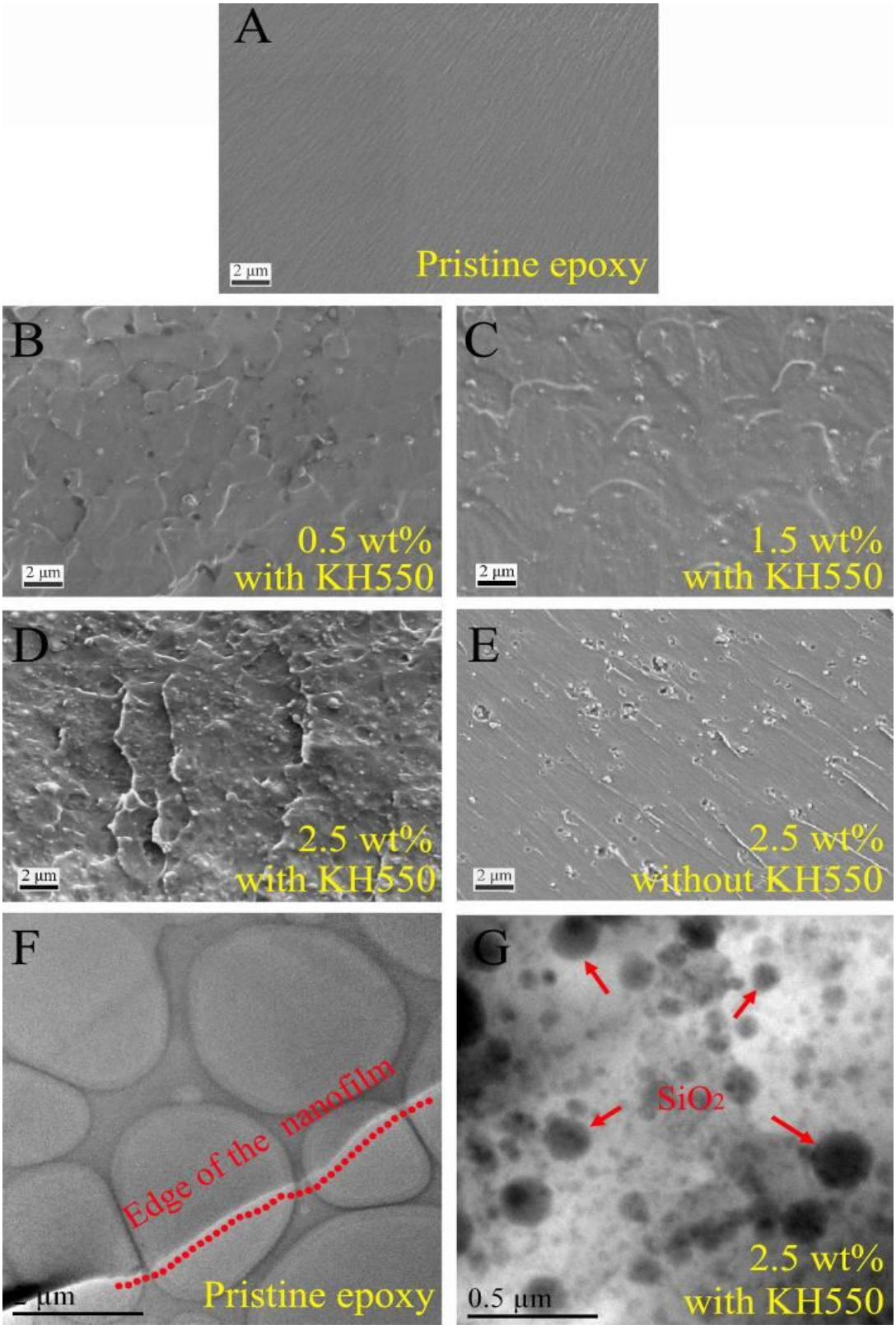

Figure 4.2 SEM micrographs of the fractured surfaces of the silica/WEP nanocomposite: (A) 0 wt%, (B) 0.5 wt%, (C) 1.5 wt%, (D) 2.5 wt%, and (E) 2.5 wt% untreated with silane coupling agent KH550, respectively. (F) TEM micrographs of the pristine WEP, and (G) TEM micrographs of the 2.5 wt% silica/WEP nanocomposite.

Compared with the pristine WEP, the silica/WEP composites have much rougher fractured surface, as shown in Fig. 4.2B to Fig. 4.2D. The bright dots show that the embedded silica particles are randomly and individually dispersed in the epoxy matrix. The well-dispersed dots increased with the silica loading. Interfacial boundary also becomes indistinct, thus indicating a robust interfacial interaction between the silica practices and the epoxy matrix. Uniform distribution and efficient incorporation of the silica particles into the matrix could have an important role in improving the mechanical and SM properties of the resulting composites. However, silica particles were observed clearly on the feature surface of the silica/WEP composites untreated with silane coupling agent KH550. Most silica particles were pulled from the matrix and left hemisphere holes, as shown in Fig. 4.2E. The dispersion of the silica particle was further confirmed via TEM. Fig. 4.2F shows the TEM photographs of the 2.5 wt% silica/WEP composite treated with KH550. The silica particles were uniformly dispersed in the epoxy matrix.

The formation of organic and inorganic networks in silica/WEP composites were further determined from the ATR-FTIR spectra, as shown in Fig. 4.3. The absorption peak of Si-O-Si asymmetric stretching varies in the range of 1050-1130 cm^{-1} depending upon the density of silica [31]. Higher the content of silica, higher the wave number showing the Si-O-Si band. The presence of a distinct absorption peak at 1090 cm^{-1} with a shoulder around 1100 cm^{-1}, as shown in Fig. 4.3. This absorption peak confirmed the formation of silica network in the composites. For the comparison with the unmodified silica-epoxy system (curve E), it was obviously observed that, after addition of the silane coupling agent KH550, the intensity of the Si-OH stretching band at 3387 cm^{-1} on the surface of the silica particles decreased definitely. This phenomenon was due to the polycondensation reaction between Si-OH of KH550 and Si-OH of the silica which consumed the groups and thereby formed Si-O-Si bonding [32]. The characteristic -OH stretching, appeared as peaks closer to 3400 cm^{-1} in curve B, C and D which gradually broaden with the introduction of KH550, might well be assigned to the second to secondary hydroxyl groups formed as a result of epoxy ring opening during the cross-linking reaction with the amine group of KH550 [33]. The absence of the

stretching vibration absorption peak of the epoxy group at 915 cm^{-1} can also suggested the fact. These results indicated that KH550 was successfully grafted on the surface of the silica particle and the silica-KH550-epoxy structure was achieved. A good dispersion and interfacial cooperation of the silane-silica in epoxy matrix was obtained. The formation of inorganic and organic networks with the silane coupling agent is depicted in Fig. 4.4**.**

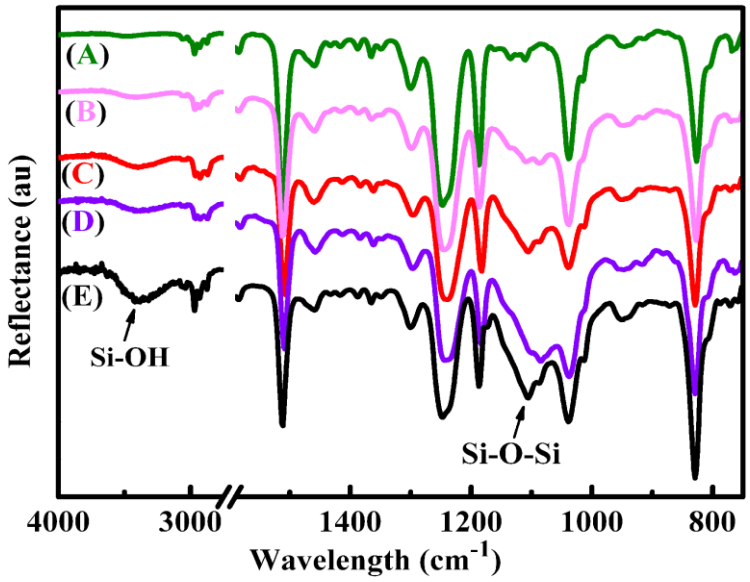

Figure 4.3 ATR-FTIR curves of the silica/WEP nanocomposite: (A) 0 wt%; (B) 0.5 wt%; (C) 1.5 wt%; (D) 2.5 wt%; and (E) 2.5 wt% untreated with silane coupling agent KH550, respectively.

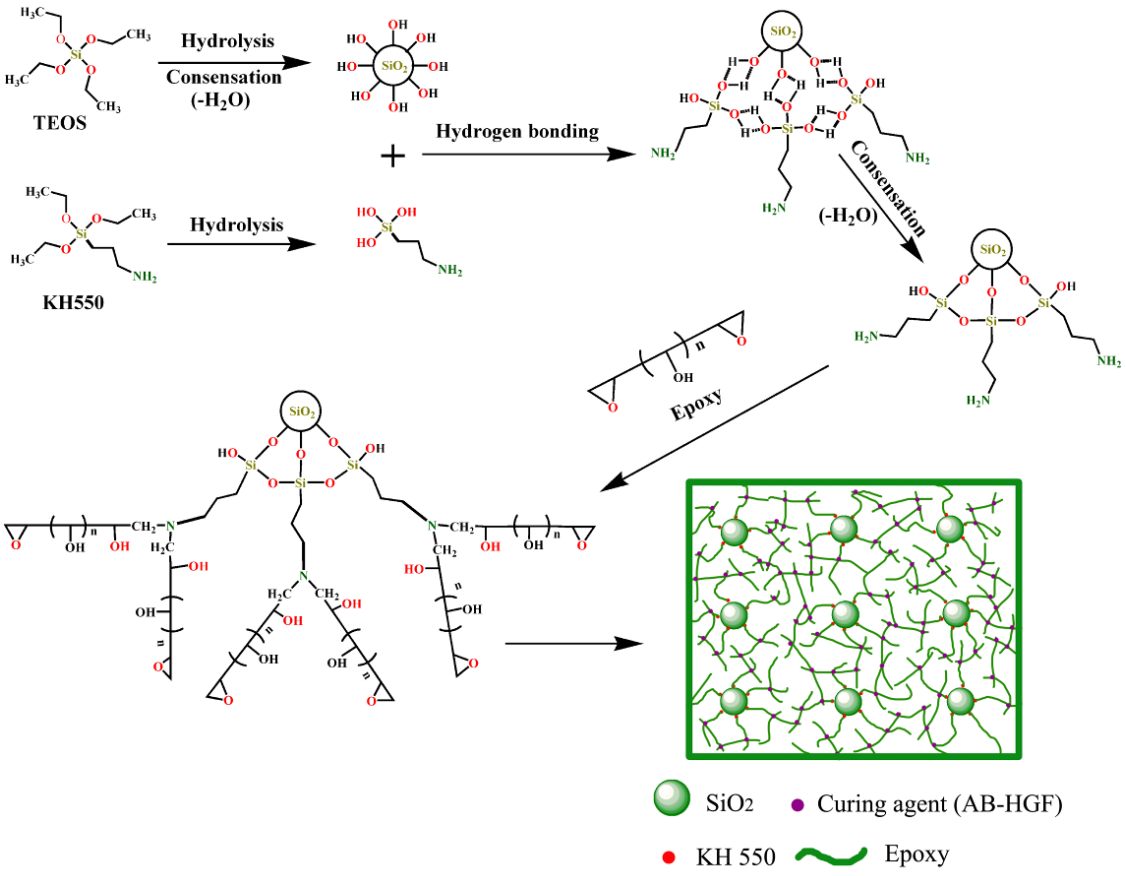

Figure 4.4 Schematics illustration of silica/WEP nanocomposites synthesis.

4.1.3.2 Dynamic mechanical properties

The storage moduli and tan delta values of the pristine WEP and its composites observed from the DMA test are shown in Fig. 4.5. All samples underwent glass transition when the temperature was increased from 0 to 100 °C and exhibited similar temperature-dependent viscoelastic properties, as shown in Fig. 4.5A. The storage modulus observed at temperatures far below the T_g was two orders of magnitude larger than that observed at temperatures above the T_g. For example, the 1.5 wt% silica/WEP composite exhibited storage modulus of 3191.2 MPa at 15 °C and 8.7 MPa at 80 °C. This result suggests that the composites are excellent SM materials. The storage modulus improved with the addition of fillers, as shown in Fig. 4.5A.

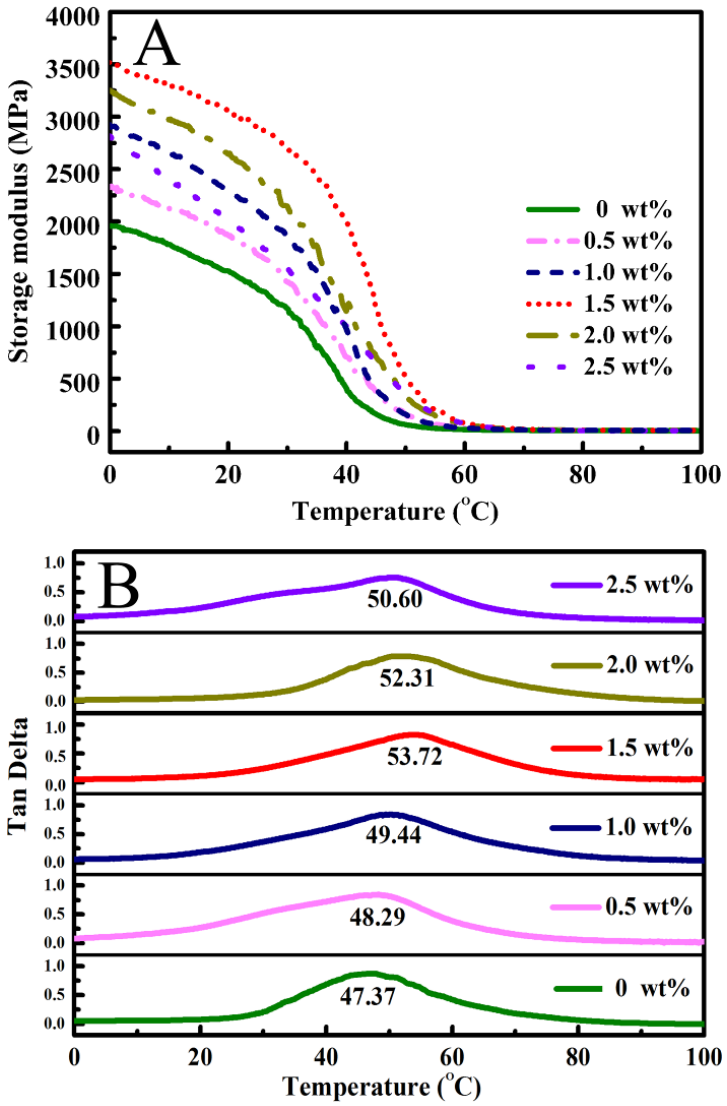

Figure 4.5 Storage modulus (A) and tan delta (B) of the silica/WEP nanocomposites from DMA testing.

The T_g of the composites increases with the silica content (amount of silica theoretically calculated from the reaction stoichiometry), and then the T_g began to decrease, when the filler loading exceeded 1.5 wt%, as shown in Fig. 4.5B. An increase in T_g is believed to be due to the formation of highly immobilized and interface layer that is developed near the surface of the silica particles with the help of the silane coupling agent. The conformational entropy and the chain kinetics are greatly altered within the interface region, and the polymer chains experience sufficient constrains [34, 35]. It is these constraining forces which in consequence shift T_g to higher temperature. On the contrast, the T_g of the composites decreases at higher silica loading, which could be described on different accounts. The increase in the filler content may also increase

the free-volume owing to the much loosened packing of the polymer chains, which in consequence assists the segmental motion of the polymer on the large scale [36]. In addition, at very high particle loading, the potential exist for the transport of amine and epoxy molecules to be significantly impeded by the large number of particles. Thus regions with very poor local stoichiometry and low cross-link density are created [37]. This would result in a lower T_g. Mascia [38] and Afzal [33] reported that amine curing agents have a tendency to adsorb on the surface silica particles and as a result epoxy monomer homopolymerize, which eventually reduced crosslink density and T_g. A decline in T_g at higher filler concentration has been recorded in the silica/epoxy composite as well as in other polymers [39, 40]. Nonetheless, a decrease in T_g of a hybrid SMP is inevitable at higher filler loadings due to several opposing factors [41].

4.1.3.3 Mechanical properties

The effect of the silica loadings on the mechanical properties of the silica-epoxy hybrid materials are shown in Fig. 4.6. The pristine WEP exhibited nonlinear elastic behavior, a tensile strength of 30.1 MPa, and an elongation at break of approximately 43.2%. The strength and elongation at break of the pristine epoxy were lower and higher, respectively, than those of the solvent-based epoxy resin [30, 42]. Added emulsifiers acted as plasticizers during the preparation of the WEP [24]. Compared with the pristine WEP, the tensile strength of the composites enhanced with the addition of silica. The results could be attributed that the nanosize particles are homogeneously dispersed in matrix, so when an external stress acted on the composites, it is easy to produce stress concentration, which causing crazing in the surrounding matrix and absorbing more deformation energy [1, 43]. In addition, the existence of nanometer rigid particles makes expansion blocked. It prevents the crack extending and finally stop cracking, which improves the mechanical properties of the hybrid materials. Moreover, the interfacial adhesion between the silica particles and epoxy matrix could be enhanced through opening the epoxy rings and linked with the silane coupling agent KH550. Therefore, the composite strength is increased.

It can be seen that the tensile strength of the silica-modified composites are remarkably increased with the increase of the silica content when the content of silica is less than initially 1.5 wt%, and then decreased gradually with the increase of the silica content. The excess addition of silica leads to compromise the tensile strength of the composites. The corresponding decrease in tensile strength that normally accompanies decreased the cross-link density of the composites which had discussed in Section 4.1.3.2. In addition, the possibility of particle aggregation had raised as the particle content increases, thus leading to degradation in the strength of the composites. Furthermore, the composites may have some residual ethanol which introduced for sol-gel process and produced during TEOS hydrolysis and greatly impaired the mechanical properties of the final thermosetting of the material. Consequently, the tensile strengths of the composites with high filler loadings showed serious decreases.

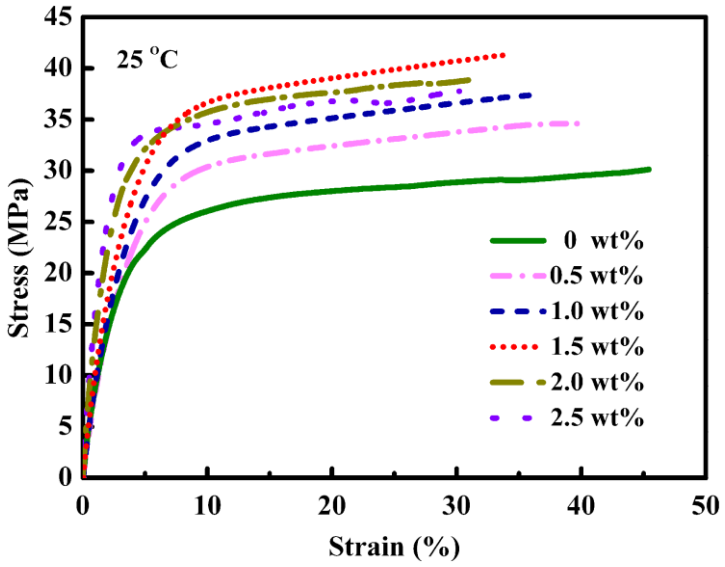

Figure 4.6 Stress-stain responses of the silica/WEP nanocomposites at 25 °C.

4.1.3.4 Shaper memory properties

A sample measuring 150 mm× 5 mm × 4 mm requires approximately 24 s for shape recovery in a 65 °C water bath, as shown in Fig. 4.7. The SM effect allows the sample to recover from the tremendous strain. The SM effect of the sample is driven by entropy among the polymer chains between the cross-linked molecules. Below the SM

transition temperature (T_g), polymer chains between network points cannot undergo conformational changes and are locked into shape unless a suitably large mechanical force is applied. However, the chains can undergo rotational conformation changes at relatively lower stresses when heated to their T_g. Above T_g, the polymer chains begin to align as the polymer deforms, thereby increasing the energy stored in the material as the entropy of the chains decreases. Upon cooling in the deformed shape, the polymer chains can no longer freely rotate. When the material is heated above its T_g without constraint, the polymer chains recover the stored energy by returning to the initial high-entropy configuration, and return to their initial shape [44].

The stress-strain-temperature curves of the silica/WEP composites obtained in the thermo-mechanical cycle test using the maximum strain (ε_m = 30%) are shown in Fig. 4.8. The four steps associated with the shape fixity and shape recovery are highlighted. Shape fixity and recovery ratios are two important parameters for determing, and evaluating SMP characteristics, as defined by Eq. (4.1). The shape fixity and recovery ratios are determined in terms of the strain [45, 46], where N is the number of thermo-mechanical cycles (N=1 in Fig. 4.8), R_f is the shape fixity ratio, R_r is the shape recovery ratio, ε_m is the pre-deformation strain (strain at the end of step 2), ε_u is the temporary strain fixed (strain at the end of step 3) and ε_p is the permanent strain (strain at the end of step 4).

$$R_f(N) = \frac{\varepsilon_u(N)}{\varepsilon_m}, \quad and \quad R_r(N) = \frac{\varepsilon_m - \varepsilon_p(N)}{\varepsilon_m - \varepsilon_p(N-1)} \qquad \text{Eq.(4.1)}$$

The relationship of the shape recovery and fixity ratios to the cycle number is shown in Table 4.1. In the first cycle, the shape recovery ratios over 90% of the epoxy reinforced with silica. Furthermore, the composites have a shape recovery ratio of more than 99% after the second cycle. The ratio tends to be a constant 100% with increased cycle numbers. This phenomenon is called “training” effect [45]. Moreover, the samples have relatively low recovery rate at the incipient and terminal stage of the step 4 in the thermo-mechanical cycle (these phenomena also can be seen in Fig. 4.7). The low recovery rate can be attributed to the heavy friction among the molecules at incipient

stage. Most constrained forces have been released at the terminal stage, thus slowing down the recovery rate. However, no negative influence is observed with the addition of the silica particles to the shape recovery ratio. This finding can be attributed to the inorganic-organic networks formatted by the epoxy and silica particles with the silane coupling agent KH550.

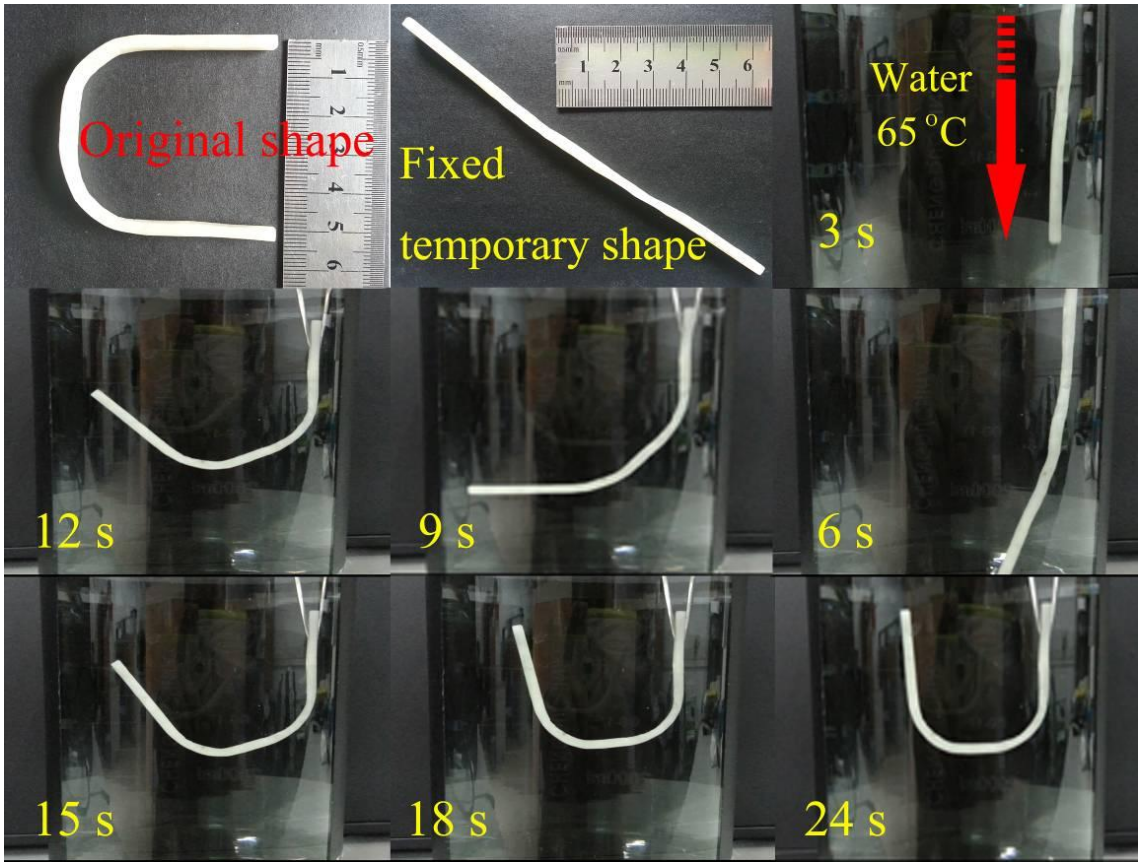

Figure 4.7 Shape recovery behaviour of the 1.5 wt% silica/WEP nanocomposite.

The shape fixity ratios are clearly very high (approximately 96% R_f for the composites), suggesting a good shape fixity of the smart materials. The fixity of the pristine WEP is significantly improved by the addition of silica, as shown in Table 4.1. The higher filler content generally makes the materials stiffer, and the fixed temporary shape is lower tendency to return to their original shape after the release of the loading [30]. In addition, the stress-strain curves obtained in the thermo-mechanical cycle test of the maximum strain ε_m = 30% at 65 °C of the silica/WEP composite are shown in Fig. 4.9. The shape of the stress-strain curves are almost exactly the same after 10 cycles. Furthermore, the in-situ generated silica particles will not only make rise of the

mechanical property of the WEP but also keep the SM property similar to the pristine bulk. Therefore, the silica/WEP composites with extremely high shape fixity and recovery ratios, and excellence thermo-mechanical properties were achieved in this work.

Table 4.1 Relationships between cycle number and shape memory property of the nanocomposites.

N [a]	Fixity ratio (%) at 25 °C						Shape recovery ratio (%) at 65 °C					
	0[b]	0.5	1.0	1.5	2.0	2.5	0	0.5	1.0	1.5	2.0	2.5
1	96.2	96.8	98.1	98.7	99.2	99.6	98.3	98.0	97.2	96.6	95.2	93.1
2	96.2	96.8	98.1	98.6	99.2	99.7	99.5	99.8	99.8	99.5	99.6	99.7
3	96.0	96.7	98.0	98.6	99.5	99.8	100	99.7	99.9	99.7	99.9	99.8
4	96.1	96.7	98.2	98.6	99.3	99.6	99.9	99.8	99.9	99.6	99.8	99.9
5	96.2	96.8	98.2	98.5	99.3	99.6	100	100	99.7	99.8	99.7	99.9
6	96.2	96.8	98.1	98.6	99.4	99.8	100	99.8	99.8	99.7	99.9	100
7	96.2	96.8	98.1	98.7	99.3	99.7	99.8	100	99.8	99.8	100	99.7
8	96.1	96.8	98.3	98.6	99.4	99.6	100	99.9	100	99.8	100	99.8
9	96.2	96.8	98.1	98.6	99.3	99.6	100	100	99.8	100	99.7	100
10	96.2	96.8	98.1	98.7	99.2	99.8	99.7	100	99.8	100	99.9	99.8

[a] Thermo-mechanical cycle number.

[b] 0, 0.5, 1.0, 1.5, 2.0, and 2.5 are the silica content (wt%) of the silica/WEP nanocomposites.

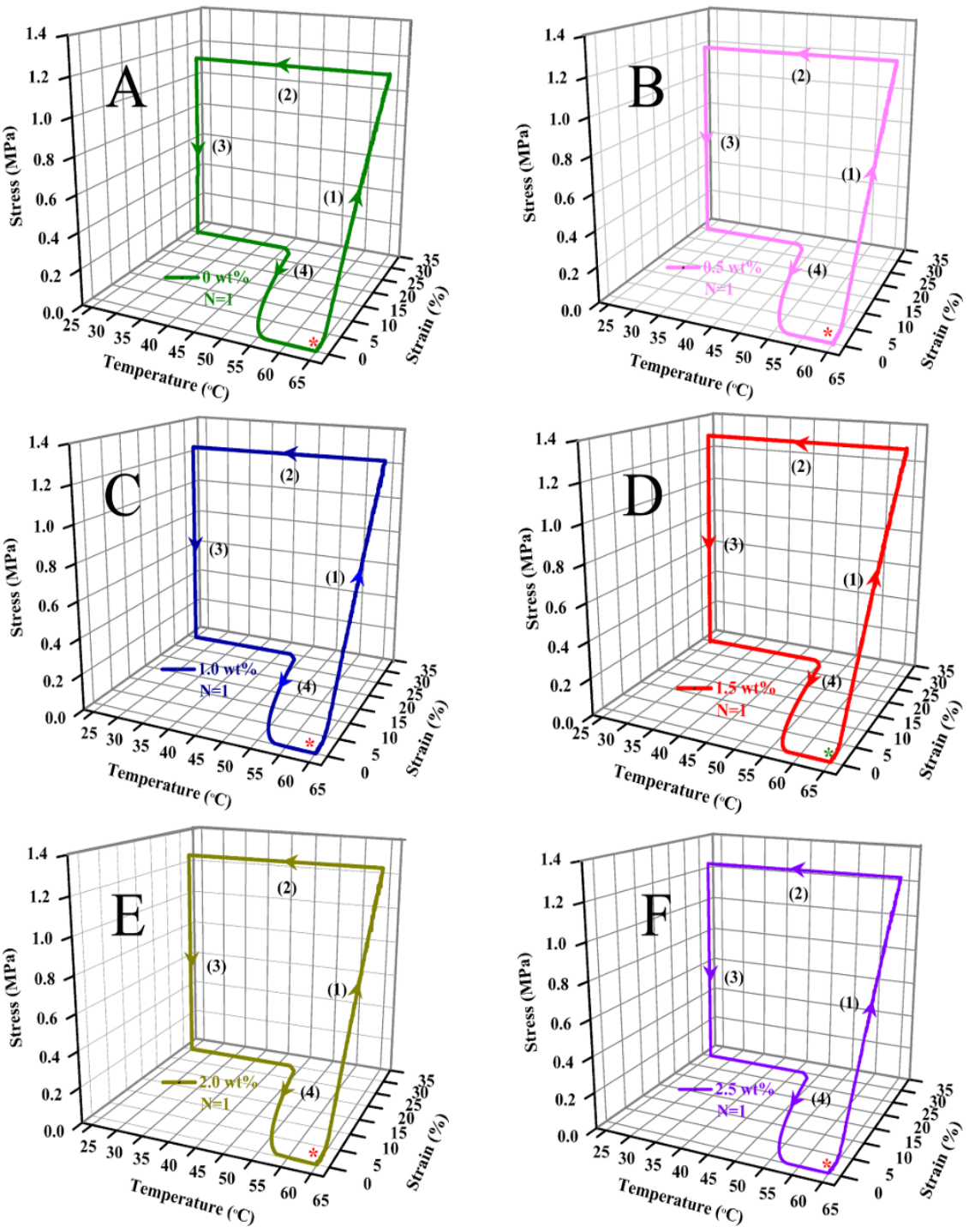

Figure 4.8 Thermo-mechanical properties of the silica/WEP nanocomposite: (A) 0 wt%, (B) 0.5 wt%, (C) 1.0 wt%, (D) 1.5 wt%, (E) 2.0 wt%, and (F) 2.5 wt%, respectively.

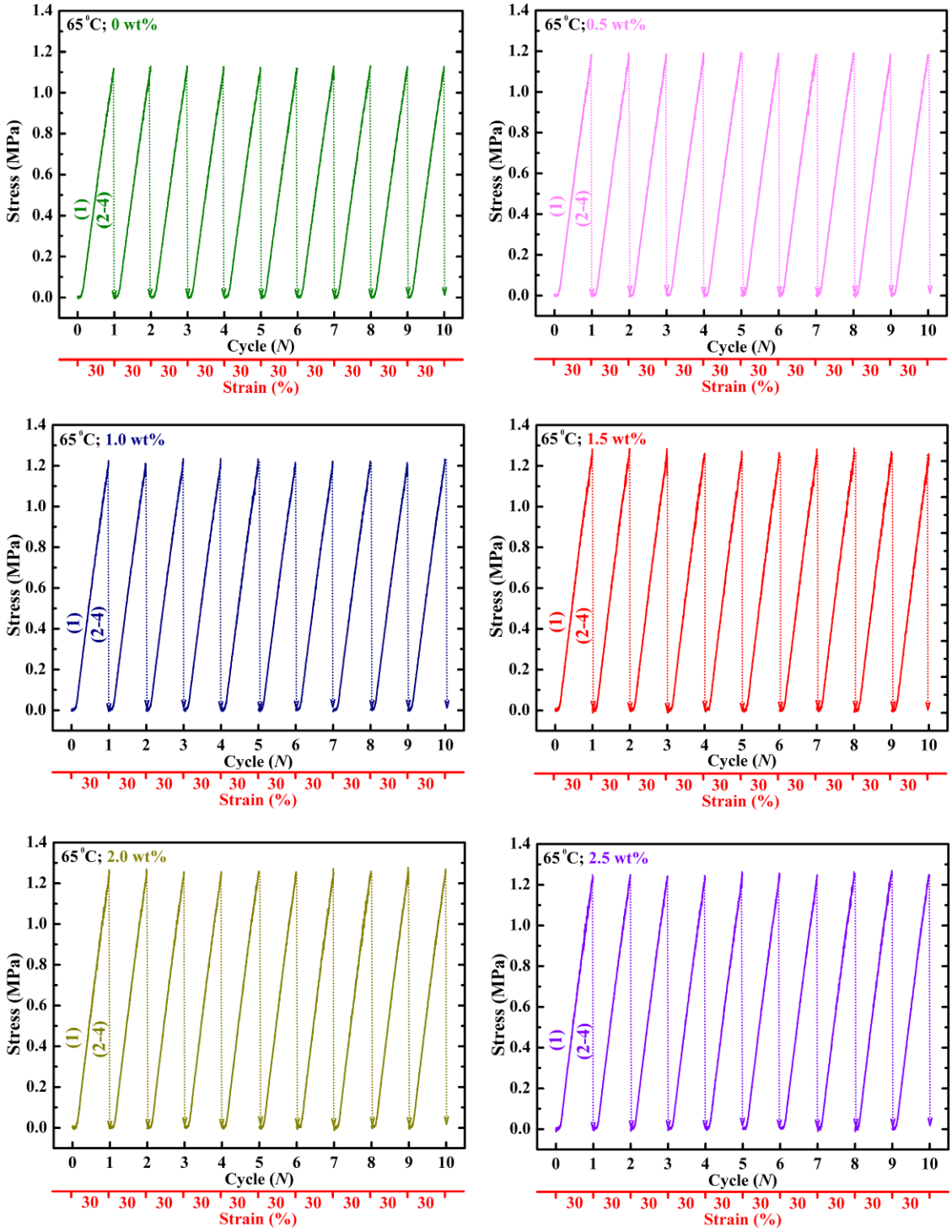

Figure 4.9 Stress-stain curves of the silica/WEP nanocomposite under 10 thermo-mechanical cycles: (A) 0 wt%, (B) 0.5 wt%, (C) 1.0 wt%, (D) 1.5 wt%, (E) 2.0 wt%, and (F) 2.5 wt%, respectively.

4.1.4 Conclusions

This study designed and synthesized the in-situ generated silica/WEP SM nanocomposites via freeze-drying and hot-press molding methods. The structure and the effect of the silica on the mechanical and SM properties of the inorganic-organic hybrid materials were investigated. The major findings are highlighted as follows:

1. Silica was successfully synthesized by in-situ generated within the WEP. The interface properties among the silica particle and epoxy, as well as the dispersion of the silica particles were significantly improved.
2. The mechanical properties of the WEP were improved with the in-situ generated and silian-founctionalized silica. However, the strength of the composites started to decrease when the silica content reached 1.5 wt%.
3. In-situ silica enhanced WEP composites had good SM functionality. The SM fixity ratio of the WEP was significantly ameliorated by the in-situ generated silica. The composites exhibited high shape recovery and can maintain their high shape recovery and fixity ratios at more than 90% even after 10 thermo-mechanical cycles.

4.2 SM silica/WEP composite foams

SM silica/epoxy composite foams were successfully synthesized via latex technology and prepared without blowing agent addition. Silica was synthesized via tetraethoxysilane (TEOS) hydrolysis. Silica/epoxy foams were obtained from the TEOS solution and WEP mixtures after freeze-drying and foaming in the presence of residual moisture as the blowing agent under a vacuum at 110 °C. The morphologies of the resulting foams were evaluated using scanning electron microscopy (SEM) and transmission electron microscopy (TEM). Compression and thermo-mechanical cycle tests were performed to measure the mechanical and SM properties of the foams. Experimental results indicated that the micrographs and mechanical properties of the foams were closely related to freeze-drying time. The final composite foams exhibited high shape recovery and fixity ratios and could maintain both properties at more than 90% even after five thermo-mechanical cycles. The properties obtained in the epoxy foams may offer new opportunities for their use in future structural applications.

4.2.1 Introduction

SMPs can be fixed into a stable temporary shape, and then revert to their permanent shape when triggered by an external stimulus [1, 7, 47, 48]. These stimuli, include heat [49, 50], water [8], pH [9], light [10], electricity [51, 52], and magnetic fields [53, 54]. Increasingly demanding industry requirements in terms of developing polymer-based foams with shape memory (SM) properties have recently attracted considerable interest worldwide [1, 7]. Compared with fully dense SMPs, SMP foams possess lower density, and higher compressibility, can achieve higher temporary deformations and exhibit higher deformations when they recover their permanent shape. Thus, SMP foams have the potential use in a wide range of applications, such as biomedical devices [55], aerospace structures [56], and self-healing application [57].

Thermo-responsive SMP foams, are commonly categorized into polyurethane-based [58, 59], polystyrene-based [60, 61], and epoxy-based [62-64]

foams. SM epoxy foam has superior environmental durability, and is a good candidate for space application. However, the processes involved in developing epoxy foam are very environmentally unfriendly, complex, and expensive. A vast majority of the foam products are still formulated with organic blowing agents, such as, p, p-oxybis(benzenesulfonyl hydrazide) [65], azodicarbonamide [66], and supercritical carbon dioxide [67, 68]. However, as environmental regulation becomes stricter, the requirement for the industries to switch to more ecological and safer systems is constantly increasing.

Our previous research found that environmentally-friendly water-borne epoxy (WEP) has excellent SM effect [24]. However, WEP possesses an inferior mechanical strength and a lower SM fixity ratio compared with conventional solvent-based epoxies. Improvements in the mechanical and SM properties of SMPs have been achieved by incorporating inorganic particles [25, 26]. The resultant silica/SMP composites exhibited excellent mechanical strength and SM properties. In the present study, nano-silicas are used to enhance the mechanical and SM properties of epoxy foams which prepared from WEP. The effect of nano-silica addition and cell structure on the mechanical and SM properties of the foam was discussed. The mechanical and SM properties of the silica/WEP foams were evaluated along with other physical properties. The final composite foams exhibited high shape recovery and fixity ratios and could maintain both properties at more than 90% even after five thermo-mechanical cycles.

4.2.2 Experimental

4.2.2.1 Materials

WEP (50% solid weight) with a particle size range of 50 nm to 300 nm was synthesized by phase-inversion according to our previous research. A commercially available curing agent (AB-HGF®, Zhejiang Anbang New Material Development Co., Ltd, China), tetraethoxysilane (TEOS), tetraethoxysilane (TEOS), 3-triethoxysilylpropylamine (KH550), and absolute ethanol were obtained from

commercial sources and used as received. All experiments were performed using deionized (DI) water.

4.2.2.2 Synthesis of SM silica/WEP composite foams

First, a curing agent was initially added to the WEP and dispersed to homogeneity at room temperature by intensive mixing in a beaker at 500 rpm for 15 min. The weight ratio of the epoxy to the curing agent was 4:1. Subsequently, a known volume of silica sol (KH550: TEOS: ethanol=1: 5: 20, w/w/w) was poured into the WEP and curing agent mixture. Second, the resulting mixture was mixed at 1000 rpm for 15 min, and then frozen in liquid nitrogen. The aqueous solvent and ethanol were removed using a Labconco Free Zone freeze-dry operated system at 0.1 mbar and -55 °C for 3, 4, and 5 days (d). The resulting powder was shaped via cold compaction in a 15 mm tall and 35 mm wide cylindrical stainless steel mold at a packing pressure of 5 MPa for a holding time of 5 min. Third, the epoxy tablets were foamed in a vacuum oven at 110 °C and -0.1 MPa for 4 h and post-cured at 120 °C for 12 h. Fig. 4.10 illustrates the fabrication procedure of the silica/WEP foams.

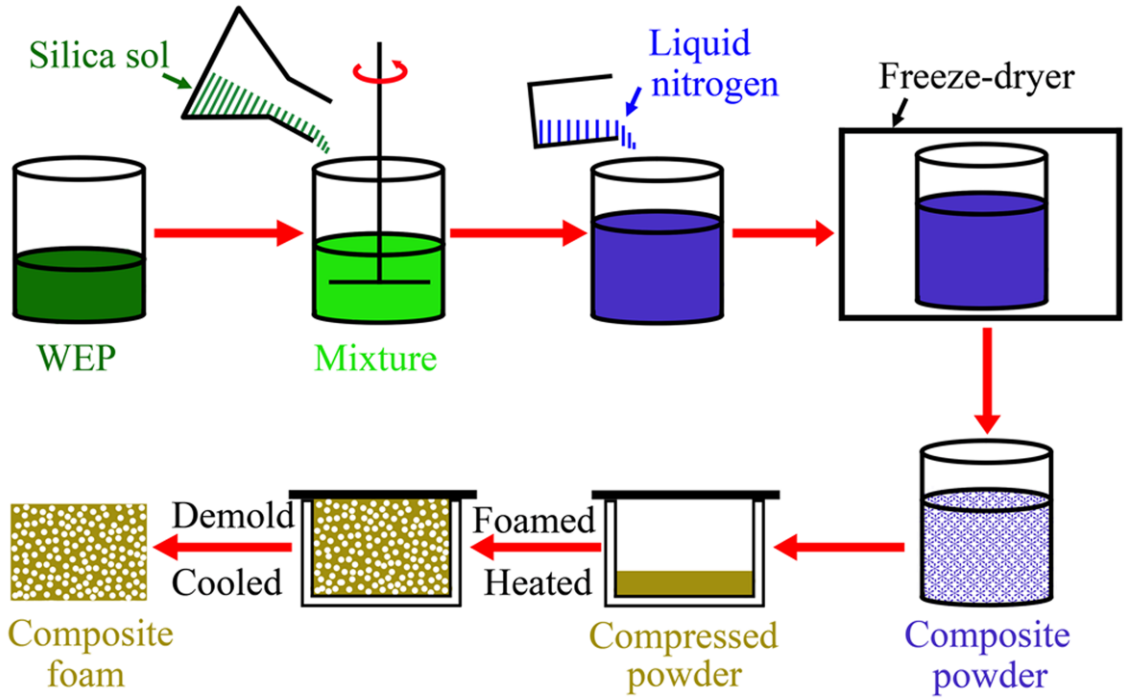

Figure 4.10 Schematic of the process for preparing silica/WEP composite foams.

4.2.2.3 Characterization

Scanning electron microscopy (SEM) observations of the specimens before and after compression were conducted using a field emission scanning electron microscope (Ultra 55; Zeiss, Germany) at an operating voltage of 3 kV. Prior to testing, samples were sputter-coated with gold to impart electrical conductivity and reduce charging artefacts. High vacuum conditions were applied and a secondary electron detector was used for image acquisition. The average cell size and cell density of the silica/WEP foam were obtained by image analysis on the SEM images using ImageJ software. Cell density (N_f) was determined by the number of cells per unit volume of foam, which was calculated by Eq. (4.2), where n and A are the number of bubbles and the area of the micrograph (cm^2), respectively. Transmission electron microscopy (TEM) images of the silica/WEP foams were obtained from ultrathin sections that were cut with a glass knife on the Leica EM UC7 ultramicrotome (Leica, Germany) and examined using a transmission electron microscope (JEM-2100F; JEOL, Japan) operated at 200 kV. All density measurements of the foams were performed by dividing the sample weight by the sample volume, by using an analytical balance and a caliper. Foam density was calculated on 20.0 mm long cylindrical specimens extracted by sawing from the foams. The top and bottom of the foams were not considered for density measurements.

$$N_f = \left(\frac{(n)}{A} \right)^{3/2} \qquad \text{Eq.(4.2)}$$

Compression tests were conducted flat-wise by using a universal testing machine (INSTRON 8531) to evaluate the mechanical properties of the prepared foams. The specimens were polished to a size of 10.0 mm × 10.0 mm × 25.0 mm and then tested. The loading rate was 1.0 mm/min at room temperature. A preload of 0.2 N was used to achieve full contact of the plate on the sample. At least five effective specimens were tested.

The thermo-mechanical properties of the foams were studied using a DMA Q800 (TA Instrument, USA). Rectangular foams with a typical dimension of 9.0 mm × 5.0 mm × 2.0 mm were loaded under tension and oscillatory deformation with an amplitude of 10

μm, at a frequency of 1 Hz. Samples were heated from 0 to 100 °C at a rate of 5 °C/min and run under engineering strain control, with 0.1% strain and 0.01 N preload. The ends of the samples were wrapped with aluminum foil to avoid fracture in the grips.

To visually demonstrate the SM behavior, we equilibrated a rectangular foam in an isothermal oven at 55 °C for 5 min to soften it well. The foam was compressed to a temporary shape and then immediately placed in a freezer at 0 °C, while holding the compressive force for 5 min to fix the temporary shape. Subsequently, the already compressed specimen was heated at 55 °C, and the original shape was obtained.

The SM properties of the foams were characterized with the same DMA Q800 mentioned above, but in "Force Control" mode. Cylindrical foam samples with typical dimensions of 10.0 mm (high) × 10.0 mm (diameter) were compressed to the maximum strain of 70% (ε_m) at a constant compression speed at 55 °C above T_g (step 1). The specimen was cooled down to 15 °C below T_g (at the glass state) and held for 10 min while maintaining the strain at 70% (step 2). The specimen was then unloaded at 15 °C at a small unloading strain ε_u (step 3), completing the three-step shape fixity process. The shape recovery capacity was examined by heating the specimen from 15 to 55 °C without load and held for 10 min. The strain of the specimen was then recovered. When this cycle is finished, a residual strain remained. The heating or cooling speed was 5 °C/min, and the loading and unloading speed was 1.0 mm/min. This test was repeated five times.

4.2.3 Results and discussion

4.2.3.1 Micrograph of the silica/WEP foams

Fig. 4.11 shows representative images of cross-sectional surfaces of the silica/WEP foams with the same filler content (in previous research, the mechanical and SM properties of WEP were significantly improved by adding silica, and the optimal mass ratio is 1.5% [69]). The effect of freeze-drying time on the foam morphology and cell size distribution is shown in Fig. 4.11A-C. The average cell sizes of the foams prepared

after 3, 4, and 5 d freeze-drying were about 198.8, 181.7, and 146.8 μm, respectively. In Fig. 4.11A and B, windows are shown within the cells where neighboring cells met. In the higher density foam (Fig. 3C), the average cell size is finer. Few of these windows and some unfoamed areas are also shown in the image. The phenomena can be attributed to the small amount of water (blowing agent) in ice form remaining in the composite powder and the greater amount of solid polymer available to fill between the cells because of the long freeze-drying time. Fig. 4.11D to 4.11F show the cell, window, and strut of the composite foam, respectively. The cell wall thinning with decreasing density and the foaming mechanism of the silica/WEP foam at different stages are shown in Fig. 4.12. The representative SEM image of the cell wall clearly shows the in-situ generated silica particles homogeneously distributed in the polymer matrix, as shown in Fig. 4.13. The TEM image confirms the existence of the silica particles uniformly distributed and embedded in the epoxy matrix, as shown in SEM. The silica/WEP foam parameters evaluated in the study are shown in Table 4.2.

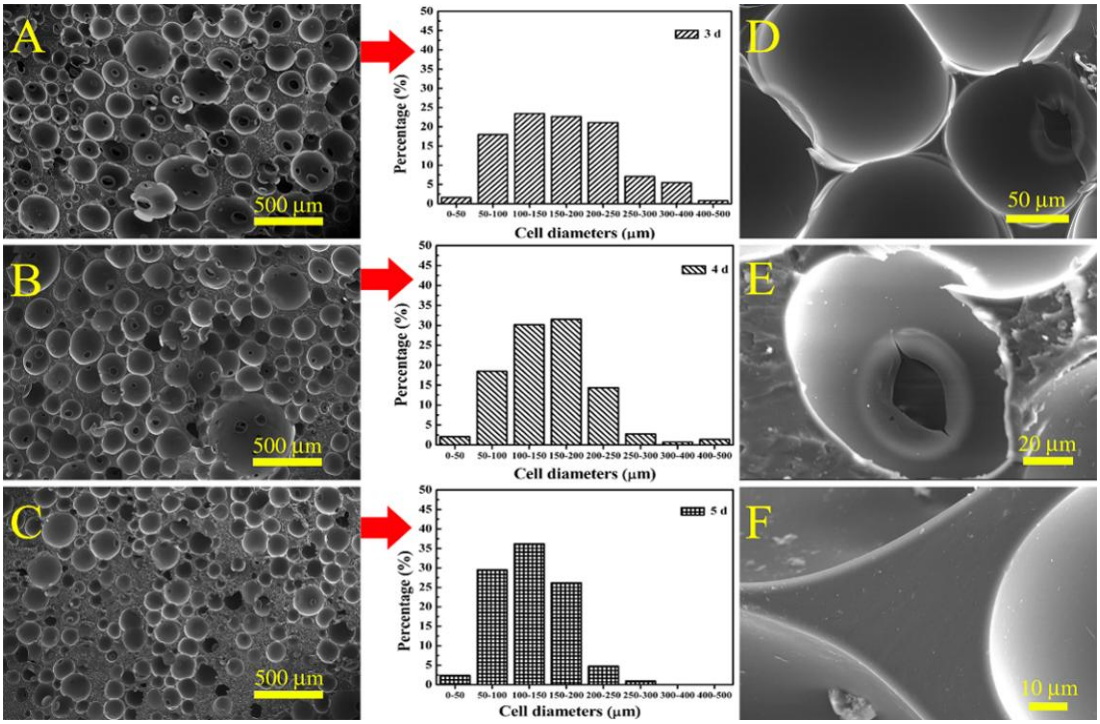

Figure 4.11 SEM images of silica/WEP foams and cell size distributions with different freeze-drying time: (A) SMF1 (3 d), (B) SMF2 (4 d), and (C) SMF3 (5 d). (D-F) The cell, window, and cell strut of the foam, respectively.

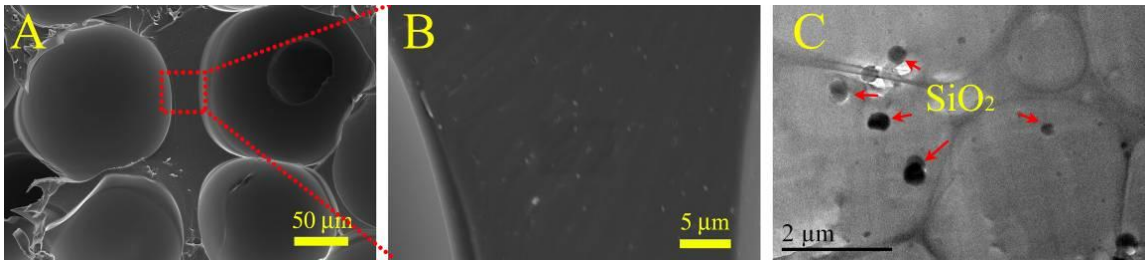

Figure 4.12 (A-B) SEM micrograph of the silica particles in the foam cell wall, (C) TEM micrograph of the silica/WEP foam.

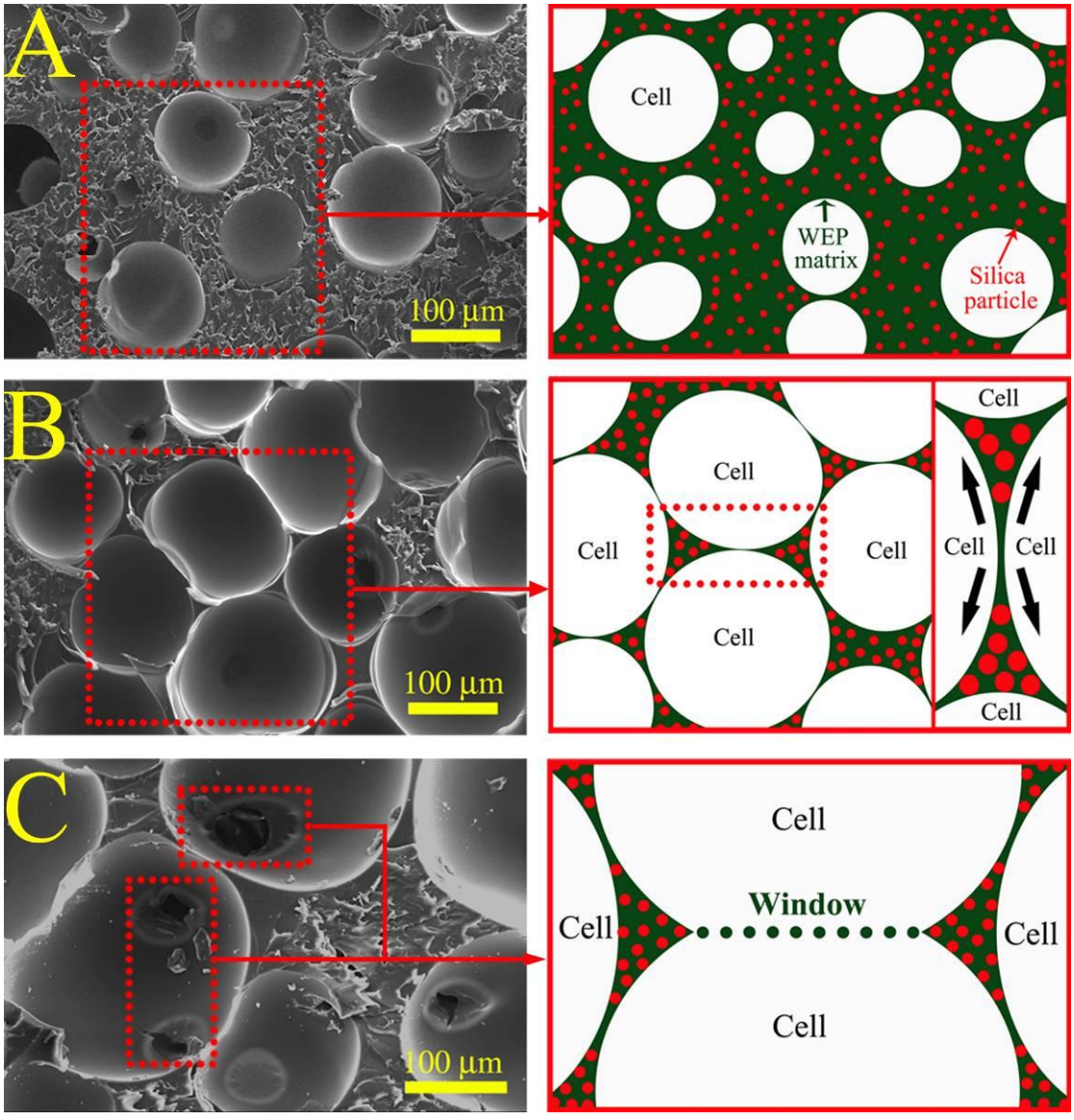

Figure 4.13 Foaming mechanism of the silica/WEP foam at the different stage.

4.2.3.2 DMA tests

The storage modulus and tan delta values of the silica/WEP foams observed from the

DMA test are shown in Fig. 4.14. All samples underwent glass transition when the temperature was increased from 0 to 100 °C and exhibited similar temperature dependent viscoelastic properties, as shown in Fig. 6. Freeze-drying time did not significantly affect the T_g values, and as a consequence, no significant change in the cross-linking density was expected. The storage modulus observed at temperatures far below the T_g was two orders of magnitude larger than that observed at temperatures above the T_g (Fig. 4.14). For example, the sample SMF1 exhibited storage modulus of 815.6 MPa at 10 °C and 1.9 MPa at 90 °C. For an excellent SMP, a large and sharp drop in the storage modulus around the glass transition is the most important [37].

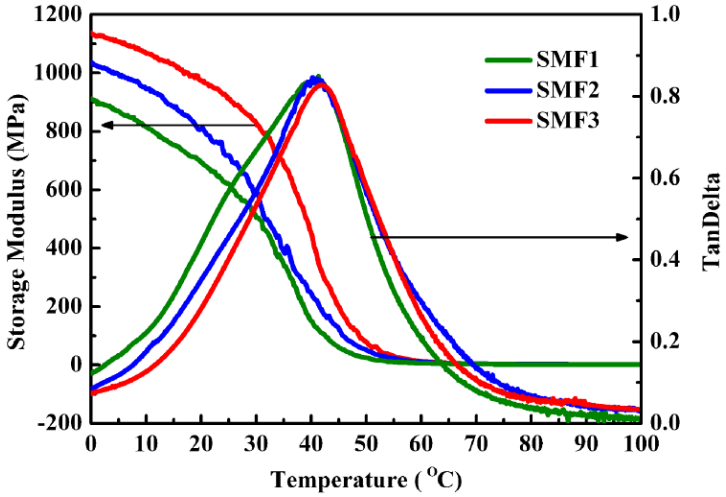

Figure 4.14 Storage modulus and tan delta of the silica/WEP foams from DMA testing.

Table 4.2 Summary of processing conditions and foam parameters.

Properties	SMF1	SMF2	SMF3
Freeze-drying Time (d)	3	4	5
Foam Density (g/cm^3)	0.328	0.352	0.386
Average Cell Size (μm)	198	182	147
Cell Density (cells/cm^3)	1.67×10^5	2.03×10^5	3.35×10^5
Compressive Strength at strain of 70% (MPa)	27.6	29.1	35.2
Modulus of Compression (MPa)	44.3	55.2	73.9
T_g (°C)	41.5	41.6	42.0

4.2.3.3 Compression characterization

The modulus and compressive strengths of the silica/WEP foams as function of the freeze-drying time are shown in Fig. 4.15 and Table 4.2. The compressive stress-strain curves of the silica/WEP foams exhibited similar regimes to the stress-strain curve of regular syntactic foams. The stress-strain curve can be clearly characterized by three distinct regions, as shown in Fig. 4.15. In the initial elastic region and during early yield, the stress almost linearly increased as the foam became rigid. Subsequently, a wide plateau region mainly corresponding to the rubbery and cell deformation of the foam matrix was observed. Finally, the cell collapsed and became compact with further increase in strain, and the stress-strain curve was directed upward toward higher stress, at a larger strain. Compared with regular syntactic foam, the deformation in the rubbery region was obviously higher [62, 63]. This finding suggests that the foams can absorb more energy without disintegration. Notably, the mechanical properties also increased with increasing freeze-drying time. These results can be contributed the increased in freeze-drying time, which decreased the amount of foaming agent (water), and increased the foam density. The short freeze-drying time foam (low foam density) could collapse because of the bending of the cell wall. For the long freeze-drying time foam (high foam density), the cell wall exhibited high rigidity and thickness, and depended on the matrix properties.

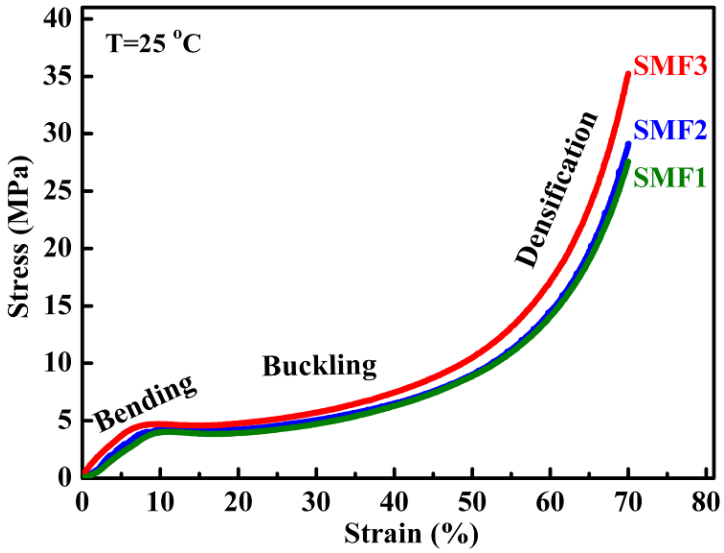

Figure 4.15 Compressive curve of the silica/WEP foams with the different freeze-drying time: 3 d (SMF1), 4 d (SMF2), and 5 d (SMF3).

4.2.3.4 SM behaviors of the silica/WEP composite foams

The shape recovery behavior of the foam is shown in Fig. 4.16. From the shape recovery process, we found that an initial shape can be recovered in 30 s at 55 C. The foam also had the ability to undergo and recover large strains. For the thermally activated cross linked epoxy system, the SM effect is entropic in nature [70]. The foam was heated above the transition temperature (T_g), deformed, and subsequently cooled below T_g to fix the temporary geometry. This geometry was maintained because thermodynamic barriers prevent the polymer chains from relaxing and returning to their original state of higher entropy, which the chains automatically assumed during initial polymerization and processing. The stored energy in the material, as the configurational entropy of the chain decreased, was subsequently locked into the polymer chains, and the chains were restricted from freely rotating. After heating above T_g without constraint, an increase of entropy caused the deformed SM foam to return to its high-entropy state, which is the original geometry. At the molecular level, the covalent cross-linked net-points of the SM foam keep the polymer chains from sliding past one another while heated above T_g [71]. Heating these foams to 55 °C, deforming them to a temporary shape, and cooling to 0 °C under deformation “freezes-in” the new shape and produces

changes in the porous structure. Moreover, the “freezes-in” porous structures in SMF2 with compressive strains of 50% and 70% are shown in Fig. 4.17A and B. The voids, which are spherical in the as-synthesized SMF2, became oval on compression to the strain of 50% (Fig. 4.17A). Upon compression to the strain of 70% the porous structure became highly flattened, as shown in Fig. 4.17B.The thermo-mechanical deformation sequence and recovery process are illustrated in Fig. 4.18.

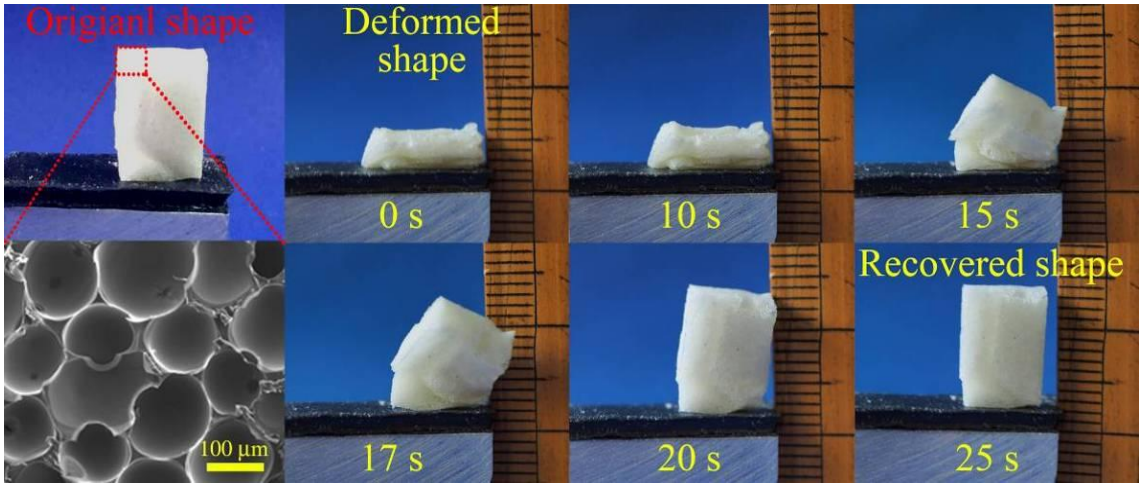

Figure 4.16 Series of photographs showing the macroscopic SM effect of the foam.

The stress-strain-temperature curve of the silica/WEP foam (SMF2) obtained in the thermo-mechanical cycle test using the maximum strain (ε_m=70%) is shown in Fig. 4.19. The stress-strain-temperature curves of the other samples are similar and therefore not shown in present study. The compressive fixity ratio (R_f) and recovery ratio (R_r) over a total of five cycles of the silica/WEP foams are listed in Table 4.3. R_f is defined as the ability of the SM material to maintain its temporary shape after cooling when the applied stress is removed. R_r is the ability of the SM material to recover its initial shape upon heating and measured as the ratio of strain variation during recovery over strain variation during the preceding deformation. R_f and R_r are two important parameters for determining and evaluating SM material characteristics, as defined by Eq. (4.3) [45, 60]. The four steps associated with the shape fixity and shape recovery are highlighted. R_f and R_r are determined in terms of the strain, where N is the number of thermo-mechanical cycles (N=1, 2, 3, 4, and 5 in Fig. 4.19), ε_m is the pre-deformation strain (strain at the end of step 2), ε_u is the temporary strain fixed (strain at the end of

step 3) and ε_p is the permanent strain (strain at the end of step 4).

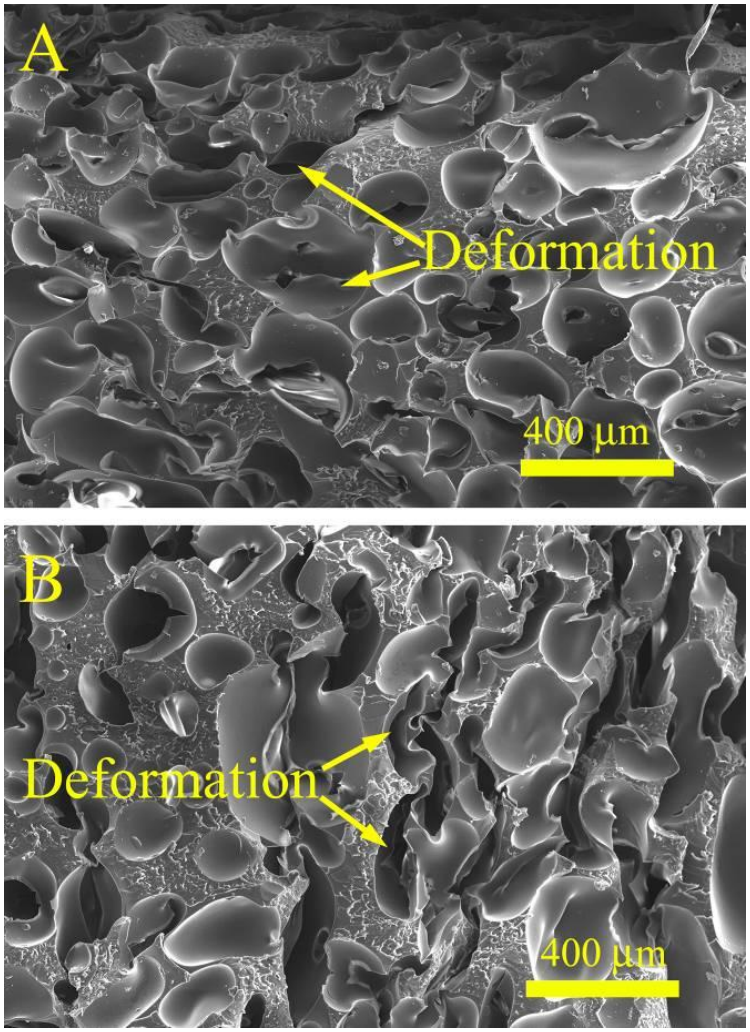

Figure 4.17 SEM micrographs of the silica/WEP foam fracture surface: (A) frozen-in strain of 50%, and (B) frozen-in strain of 70%.

After the first cycle (N=1), R_r values reached >~87% during the subsequent cycle for all foams. An increase in R_r (>~95%) after the first SM cycle (N≥2) can be observed in Table 4.3. This phenomenon is called "training" effect [45]: the first SM cycle removes the residual strain that originates from processing such that subsequent shape recovery is improved. R_f was clearly high (approximately 100%) after five thermo-mechanical cycles for all samples. This result suggests that high performance smart materials with excellent SM properties were achieved. The shape fixity ratio of the foams decreased from about 99.9 (SMF3) to 99.7% (SMF1), whereas the shape recovery ratio increased from 87.5 (SMF3) to 91.3% (SMF1) with increasing freeze-drying time. These results

indicate that the shape fixity and shape recovery ratio depended on the glassy state and the rubbery state modulus of the foams, respectively [41]. Fig. 4.20 shows the effect of the five thermo-mechanical cycles on the surface morphology of the silica/WEP foams. The foams maintained their original spherical void structures following five cycles. These results suggest that the silica/WEP foam with excellent SM functionality were successfully prepared from WEP via an eco-friendly technology. In addition, some black holes (marked with yellow arrow) were observed in the cross-section of the foams and were filled by the internal cell wall of the foam after the thermal-mechanical cycle, as shown in Fig. 4.20.

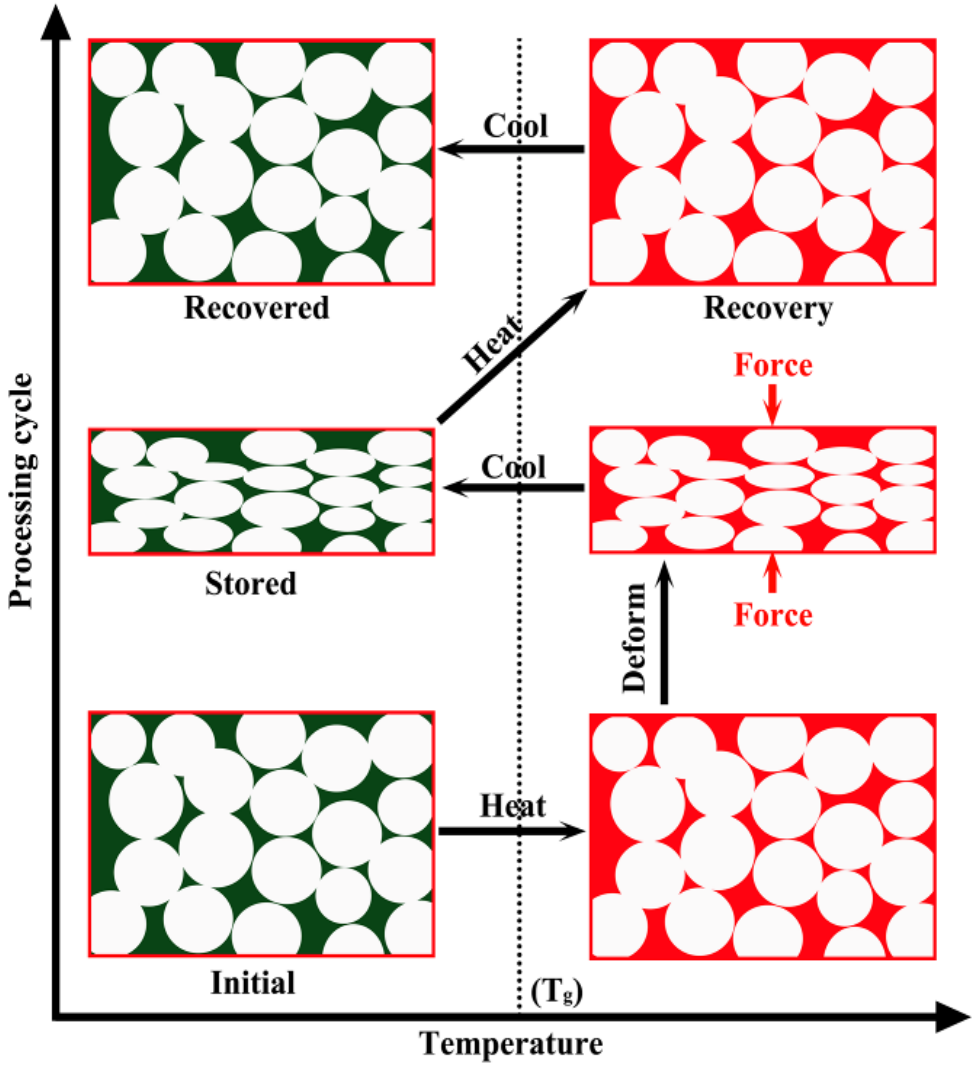

Figure 4.18 Schematic of the thermo-mechanical deformation and recovery cycle used to investigate the SMP behavior of these materials.

Table 4.3 Effect of thermo-mechanical cycle on R_r and R_f.

N[a]	SMF1		SMF2		SMF3	
	R_r (%)	R_f (%)	R_r (%)	R_f (%)	R_r (%)	R_f (%)
1	91.3	99.7	90.4	99.8	87.5	99.9
2	96.0	99.7	95.8	99.7	95.2	100
3	99.1	99.7	98.5	99.8	96.8	100
4	99.3	99.8	99.2	99.8	98.6	99.9
5	99.6	99.7	99.5	99.7	99.0	100

[a] Thermo-mechanical cycle number.

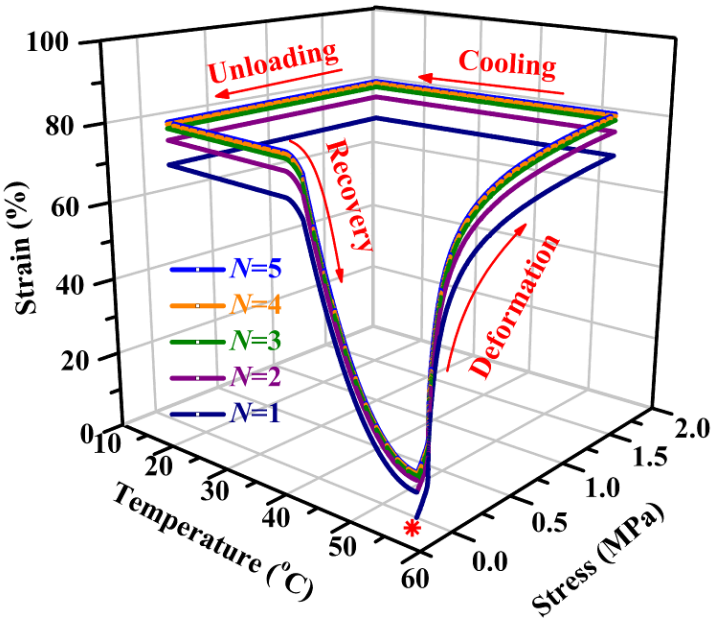

Figure 4.19 Shape memory properties of the silica/WEP foam SMF2 evaluated by four-step thermo-mechanical cycle.

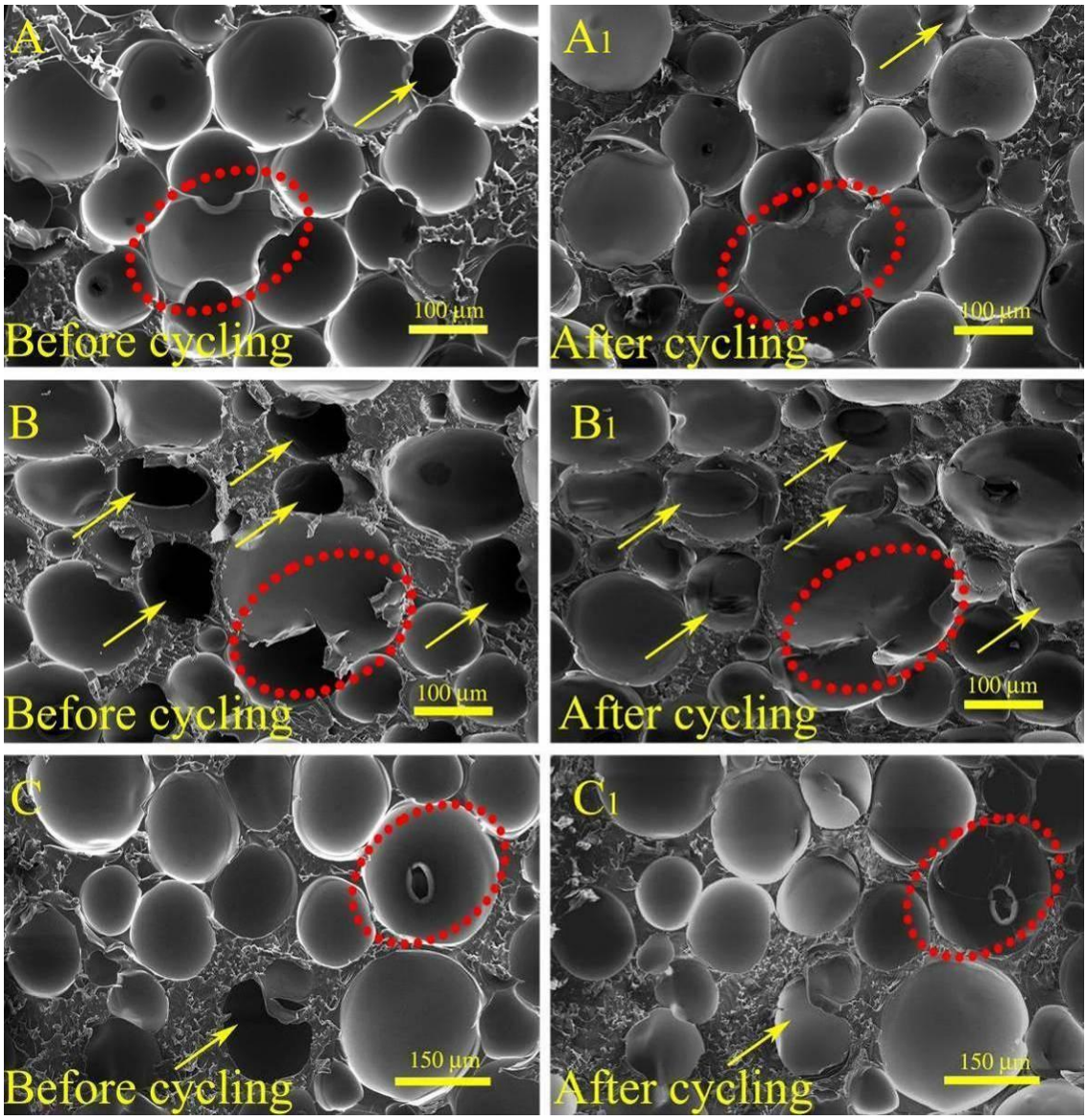

Figure 4.20 SEM micrographs of foam fracture surfaces following five deformation and recovery cycles: (A and A1) SMF1, (B and B1) SMF2, and (C and C1) SMF3.

4.2.4 Conclusions

In this study, novel silica/WEP SM composite foams were prepared without adding a foaming agent. The effect of freeze-drying time on the morphological, mechanical, and SM properties of the silica/WEP foams were investigated. When the freeze-drying time increased, the density, cell density, T_g, compression strength and modulus of the foams increased, whereas the size of the cell decreased. The composite foams possessed excellent SM properties. The shape fixity ratio of the foams decreased from 99.9 (SMF3) to 99.7% (SMF1), whereas the shape recovery ratio increased from 87.5 (SMF3) to 91.3% (SMF1) with increasing freeze-drying time. The composite foams could maintain their high shape recovery and fixity ratios at more than 90% even after five thermo-mechanical cycles. In this study, we proposed an environmentally friendly foaming technique (without organic foaming agent) that avoids the risks of safety production and environmental problems, such as workers' health, flammability, ozone depletion, and global warming. Moreover, this work contributes to the field of WEP composite foam with SM property. Further developments are in progress and mainly focused on obtaining composite foams with excellent SM properties, along with satisfactory mechanical properties.

Reference

[1] J. S. Leng, X. Lan, and S. Y. Du, *Prog. Mater. Sci.*, 56(2011)1077.

[2] Y. J. Liu, H. B. Lv, and J. S. Leng, *Compos. Sci. Technol.*, 69(2009)2064.

[3] Q. H. Meng, J. L. Hu, *Composites: Part A*, 40(2009)1661.

[4] H. B. Lv, J. S. Leng, and S. Y. Du, *Adv. Eng. Mater.*, 10(2008)592.

[5] Y. B. Dong, J. Ding, and Y. Q. Fu, *Compos. Sci. Technol.*, 76(2013)8.

[6] M. Nishkawa, K. Wakatsuki, and N. Takeda, *Composites: Part A*, 43(2012)165.

[7] J. Ding, Y. F. Zhu, Y. Q. Fu, *Polym. Compos.*, 35(2014)412.

[8] M. M. Ma, L. Guo, and R. Langer, *Science*, 339(2013)186.

[9] X. J. Han, Z. Q. Dong, and Liu Y, *Macromol. Rapid Commum.*, 33(2012)1055.

[10] A. Lendlein, O. Junger, R. Langer, *Nature*, 434(2005)879.

[11] L. Viry, C. Merrcader, and A. Kuhn, *J. Mater. Chem.*, 20(2010)3487.

[12] J. S. Leng, H. B. Lv, and Y. J. Liu, *Appl. Phys. Lett.*, 91(2007)144105.

[13] Y. Cai, J. S. Jiang, Y. Zeng, *Composites: Part A*, 53(2013)16.

[14] I. K. Kuder, A. F. Arrieta, and P. Ermanni, *Prog. Aerosp. Sci.*, 63(2013)33.

[15] A. Lendlein, R. Langer, *Science*, 7(2002)1673.

[16] S. Sharifi, M. Behl, and A. Leddlein, *Biomaterials*, 34(2013)8105.

[17] H. B. Lu, Y. J. Liu, and J. S. Leng, *Compos. Sci. Technol.*, 71(2011)1427.

[18] J. L. Hu, S. J. Chen, *J. Mater. Chem.*, 20(2010)3346.

[19] C. M. Chen, C. L. Chiang, and T. Xie, *Adv. Funct. Mater.*, 23(2013)3813.

[20] Y. Li, S. S. Chen, and J. Q. Sun, *Adv. Mater.*, 24(2012)4578.

[21] T. Xie, X. C. Xiao, Y. T. Cheng, *Macromol. Rapid Commun.*, 30(2009)1823.

[22] Z. W. He, N. Satarkar, and T. Xie, *Adv. Mater.*, 23(2011)3192.

[23] A. Wegmann, *Prog. Org. Coat.*, 32(1997)231.

[24] Y. B. Dong, Q. Q. Ni, and Y. Q. Fu, *Mater Lett.*, 132(2014)206.

[25] Z. H. Tang, D. Q. Sun, and B. C. Guo, *Compos. Sci. Technol.*, 75(2013)15.

[26] J. M. Park, Z. J. Wang, and J. H. Jang, *Smart Mater. Struct.*, 19(2010)124006.

[27] T. Gong, E. B. Li, and L. Wang, *Acta Biomater.*, 8(2012)1248.

[28] Y. M. Zhang, Q. H. Wang, and C. Wang, *J. Mater. Chem.*, 21(2011)9073.

[29] S. K. Lee, S. H. Yoon, and I. Chung, *J. Polym. Sci. Pol. Chem.*, 49(2010)634.

[30] M. K. Jang, A. Hartwig, B. K. Kim, *J. Mater. Chem.*, 19(2009)1166.

[31] Y. Q. Fu, Q. Q. Ni, M. Iwamoto, *J. Non-Cryst. Solids*, 351(2005)760.

[32] J. Lin, X. Wu, and C. Zheng, *Appl. Surf. Sci.*, 303(2014)67.

[33] A. Afzal, H. M. Siddiqi, *Polymer*, 52(2011)1345.

[34] B. J. Ash, L. S. Schadler, R. W. Siegel, *Mater. Lett.*, 55(2002)83.

[35] V. A. Bershtein, P. Pissis, and P. Sysel, *J. Polym. Sci. Pol. Phys.*, 40(2002)1056.

[36] Y. L. Liu, C. Y. Hsu, and W. L. Wei, *Polymer*, 44(2003)5159.

[37] L. Mascia, L. Prezzi, B. Haworth, *J. Mater. Sci.*, 41(2006)1145.

[38] M. Preghenella, A. Pegoretti, C. Migliaresi, *Polymer*, 46(2005)12065.

[39] C. G. Chen, R. S. Justice, and J. W. Baur, *Polymer*, 49(2008)3805.

[40] W. X. Wang, H. B. Lv, and J. S. Leng, *J. Mater. Chem. A*, 2(2014)5441.

[41] X. L. Lan, Y. J. Liu, and J. S. Leng, *Smart Mater. Struct.*, 18(2009)24002.

[42] J. H. Kang, E. J. Siochi, and T. L. Turner, *Compos. Sci. Technol.*, 96(2014)23.

[43] Q. Tan, L. W. Liu, and J. S. Leng, *Composites: Part A*, 64(2014)132.

[44] M. D. Prima, K. Gall, and A. Lin, *Mech. Mater.*, 42(2010)304.

[45]Q. Q. Ni, C. S. Zhang, and Y. Q. Fu, *Compos. Struct.*, 81(2007)176.

[46] T. Ohki, Q. Q. Ni, and N. Ohsako, *Composites: Part A*, 35(2004)1065.

[47] Y. K. Bai, Y. M. Zhang, Q. H. Wang, *J. Mater. Sci.*, 48(2013)2207.

[48] T. Gurunathan, R. Chepuri, R. Narayan, *J. Mater. Sci.*, 48(2013)67.

[49] W. S. Guo, Z. L. Shen, B. C. Guo, *Polymer*, 55(2014)4324.

[50] T. Tsujimot, K. Toshimitsu, H. Uyama, *Polymer*, 55(2014)6488.

[51] Z. H. Tang, H. L. Kang, Q. Y. Wei, *Carbon*, 64(2013)487.

[52] W. Wang, X. Liu, and Y. J. Liu, *Compos. Sci. Technol.*, 106(2015)20.

[53] A. Mohammadi, M. M. Barikani, *J. Mater. Sci.*, 48(2013)7493.

[54] Y. Cai, J. S. Jiang, Z. W. Liu, *Composites: Part A.*, 53(2013)16.

[55] P. Sighal, W. Small, H. E. Cosgriff, *Acta Biomaterialia*, 10(2014)67.

[56] Q. Fabrizio, S. Loredana, S. E. Anna, *Mater. Lett.*, 20(2012)20.

[57]Li, G. Q. N. Uppu, *Compos. Sci. Technol.*, 70(2010)1419.

[58] S. E. Chung, C. H. Park, *J. Appl. Polym. Sci.*, 117(2012)2265.

[59] S. M. Kang, S. J. Lee, B. K. Kim, *Express. Polym. Lett.*, 6(2012)63.

[60] G. Q. Li, M. John, *Compos. Sci. Technol.*, 68(2008)3337.

[61] G. Q. Li, D. Nettles, *Polymer*, 51(2010)755.

[62] I. A. Rousseau, T. Xie, *J. Mater. Chem.*, 20(2010)3431.

[63] M. D. Prima, K. Gall, D. L. Mcdowell, *Mech. Mater.*, 42(2010)304.

[64] E. A. Squeo, F. Quadrini, *Smart. Mater. Struct.*, 19(2010)105002.

[65] L. J. Wang, X. Yang, T. H. Jiang, *J. Appl. Polym. Sci.*, 131(2014)41175.

[66] L. J. Wang, X. Yang, T. H. Jiang, *Composites Part B.*, 56(2014)724.

[67] H. M. Guo, V. Kumar, *Polymer*, 57(2015)157.

[68] Y. Z. Long, L. F. Zheng, Y. J. Gu, *Polymer*, 55(2014)6494.

[69] Y. B. Dong, Q. Q. Ni, Y. Q. Fu, *Composites: Part A.*, 72(2015)1.

[70] M. Behl, I. Bellin, S. Kelch, A. Lendlein, *Adv. Funct. Mater.*, 19(2009)102.

[71] W. Small, P. Singhal, D. Maitland, J. *J. Mater. Chem.*, 20(2010)3356.

[72] E. Smela, *Adv. Mater.*, 15(2003)481.

CHAPTER FIVE

Conclusions

5 Conclusions

This thesis has investigated the preparation and properties of SM epoxy materials and their nanocomposites.

In chapter 1, I reviewed references and provided brief summary of shape memory polymers (SMPs), and SMP composites (SMPCs) and their applications.

In chapter 2, a facile and environmental-friendly method to prepare epoxy-based SM materials was reported. We successfully synthesized new reactive copolymer emulsifier epoxy-graft-polyoxyethylene octyl phenyl ether (EP-g-TX100) for preparing of water-borne epoxy (WEP). The chemical structure and emulsifying ability of EP-g-TX100 were systematically characterized. The as-synthesized emulsifier EP-g-TX100 exhibits the expected structure, can covalently react with the curing agent through the side chains, and have excellent emulsifying ability for epoxy. On the base of the emulsifier, we synthesized WEP via phase-inversion technology. The WEP particles had an average diameter of 137 nm, with particles ranging from 50 nm to 300 nm. Then, the epoxy material was prepared via freeze-drying and hot-press molding technology. The final epoxy product shows excellent SM property.

In chapter 3, SM CNT/WEP nanocomposites were designed and successfully prepared via freeze-drying and hot-press molding. WEP composites containing CNT exhibited better mechanical properties than pristine WEP. However, the strength of the composites began to decrease when the CNT contents reached 1.0 wt%. The WEP composites exhibited a high shape recovery ratio of approximately 100% under different temperatures. The SM fixity ratio of pristine WEP was significantly ameliorated by addition of CNT. Moreover, Epoxy foams composed of CNTs and WEP were prepared. The compression strengths of the CNT/WEP composite foams under the deformation strain of 80% were higher than that of the pure epoxy foam. The epoxy foams had good SM functionality and can maintain their high shape recovery and fixity

ratio at more than 90% after several thermo-mechanical cycles.

In chapter 4, in-situ generated silica/WEP SM nanocomposites via freeze-drying and hot-press molding methods were designed and synthesized. Silica was successfully synthesized by in-situ generated within WEP. The interface properties among the silica particle and epoxy, as well as the dispersion of the silica particles were significantly improved. The mechanical properties of WEP were improved with the in-situ generated and silian-founctionalized silica. However, the strength of the composites started to decrease when the silica content reached 1.5 wt%. In-situ silica enhanced WEP composites had excellent SM functionality. The SM fixity ratio of the WEP was significantly ameliorated by the in-situ generated silica. The composites exhibited high shape recovery and can maintain their high shape recovery and fixity ratios at more than 90% even after 10 thermo-mechanical cycles. On the other hand, silica/WEP SM foams were prepared without foaming agent addition. An environmental friendliness foaming technique (no extra organic foaming agent) avoids the risks of safety production and environmental problems, such as workers' health, flammability, ozone depletion, global warming. It was observed that the freeze-drying time profoundly influenced the foam morphology, mechanical and SM properties: this effect contributed to longer freeze-drying time leads to less foaming agent (water) remained. The hybrid foams showed excellent SM properties. This work represents a contribution in the field of WEP hybrid foam with SM property. Further developments are in progress and mainly focused on the obtainment of composite foams with excellent SM properties alongside with satisfactory mechanical properties.

In all, the synthesized WEP, as a novel versatile environmentally-friendly materials, are being attached great importance in engineering field and mainly used in coatings, metal primers, epoxy cement concrete, glass fiber sizing, and wood adhesives, etc., and additional function of SM will be a good aspect for extending their further applications. Furthermore, our strategy for obtaining SM epoxy materials will pave the way for designing and developing the functional shape memory effect polymers. The proposed method is applicable to various host polymers and does not require organic solvents.